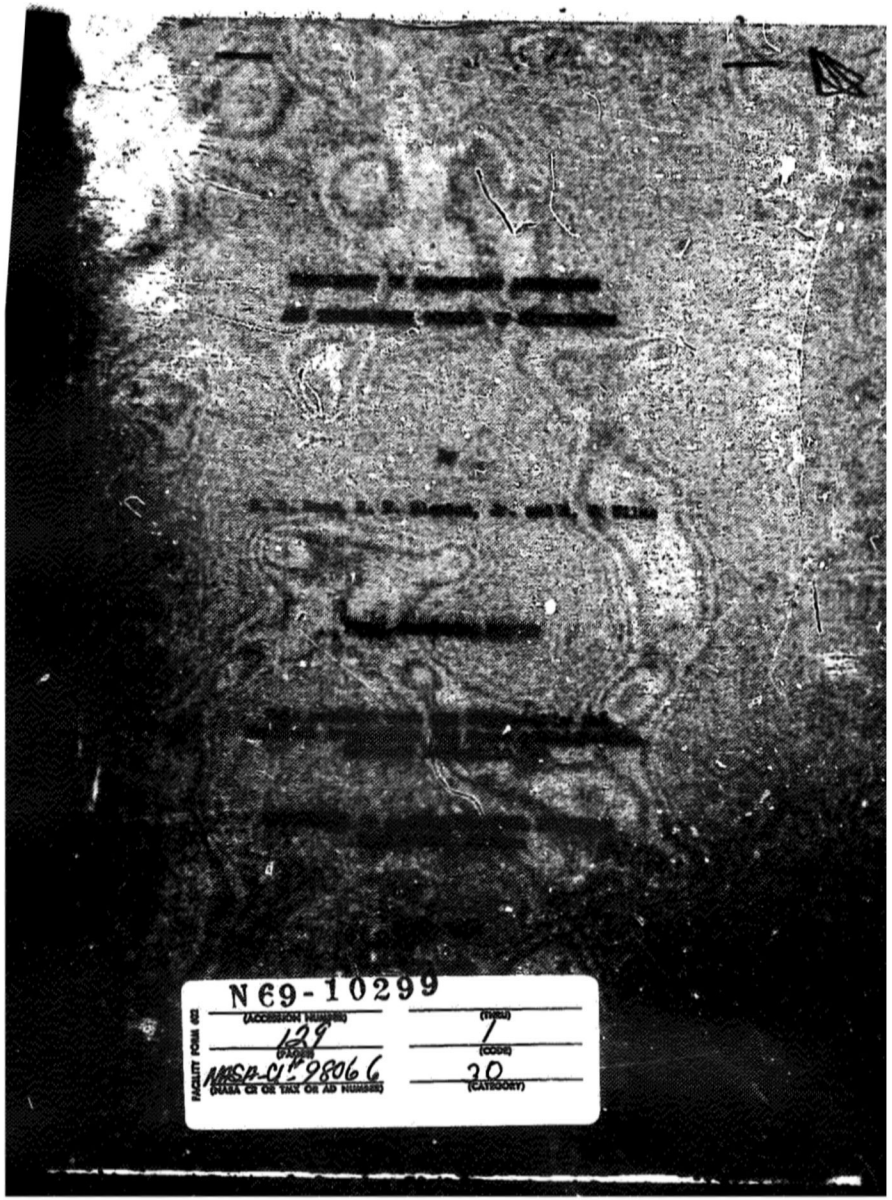
N69-10299
(ACCESSION NUMBER)
129
(PAGES)
NASA-CR-98066
(NASA CR OR TMX OR AD NUMBER)
1
(THRU)
(CODE)
30
(CATEGORY)
FACILITY FORM 602

DEPLOYMENT OF SPACECRAFT APPENDAGES AND TEMPERATURE CONTROL OF EXPERIMENTS

By

R. R. Reed, R. W. Blanton, Jr. and E. V. Wilms

FINAL TECHNICAL REPORT

This research work was supported by the National Aeronautics and Space Administration Contract NAS8-21110 "A"

UNIVERSITY OF ALABAMA RESEARCH INSTITUTE
Huntsville, Alabama

April 1968

https://ntrs.nasa.gov/search.jsp?R=19690000968 2020-03-12T05:28:07+00:00Z

DEPLOYMENT OF SPACECRAFT APPENDAGES

AND TEMPERATURE CONTROL OF EXPERIMENTS

TABLE OF CONTENTS

Chapter I

INTRODUCTION AND SUMMARY

1. STATEMENT OF THE PROBLEM

Two of the most urgently needed analytical investigations of near future space flights are concerned with (1) the deployment of appendages necessary for experimentation and (2) the temperature control of the experimental apparatus. The first is essentially a problem in dynamics and kinematics where the second is a problem in thermodynamics and heat transfer. Those participating in this study have the background to handle both of these problems of urgent interest. Thus, the two problems are combined into a single investigation.

These investigations involved actual hardware for experimentation aboard vehicles of the near future. Thus, close association with the sponsor was necessary. The sponsor had complete access to studies as they were in process, and directed the investigators to study specific aspects of the problems, within the manpower and time limits.

In particular, the deployment of the solar panel array aboard the ATM vehicle was investigated. The study involved not only the conceptual design of the mechanism but also theoretical investigations involving its degrees of freedom, natural frequencies, damping, rates of deployment, forces during deployment and maneuvering, and so on. These studies are documented in Chapter II and Chapter III and were conducted by Dr. R. R. Reed and Dr. E. V. Wilms, respectively.

The particular temperature control of experiments study was centered around the temperature control of the X-Ray telescope on the ATM vehicle.

Design factors which were considered included the thermal conductivity of telescope and supports, location and control of external heaters, nature and location of heat sources and sinks, environmental conditions, and so on. A theoretical solution of the one-dimensional model with a radiating boundary condition was solved using the digital computer. These studies were conducted by Dr. R. W. Blanton and are documented in Chapter IV.

2. RESULTS AND RECOMMENDATIONS

The solar panel array had stringent space requirements which governed the deployment mechanism design. The initial requirement of a retraction capability also rendered some mechanisms undesirable. After due consideration, the scissor mechanism was selected for its simplicity, controlability, retraction capability, and small space requirements. The analysis of the scissor mechanism, including deployment accelerations and forces as well as dynamic response studies, show significant results. The deployment joint forces in the scissor mechanism are not excessive for one and two minute deployment times and reasonable accelerations of the driving link. The 4-bar driving link causes a dip in the motion of panel array being deployed, while the chain driver support, when properly dimensioned, does not dip. The validity of a lumped parameter dynamic study was considered. The bending frequency was calculated and for the first mode it takes from 5 to 7 seconds per cycle. The amplification factor for dynamically applied loads such as a docking load (.1g) was significant and for this load a 48 in. deflection occurred when the load stayed on for a half-cycle. The approximate torsional response for the first mode shows an amplitude less than 0.10 radian. The damping of the deployed array was determined to be very small. That is, about 0.50 per cent of critical damping occurred, requiring approximately 7 minutes to reduce the amplitude by 90 per cent.

Other results are apparent in Chapters II and III.

In the design of the X-Ray telescope it is necessary to stabilize the average temperature of the casing so that the focal length and film location will be accurate during operation. It was determined that the insulation applied directly to the telescope case would essentially eliminate radial heat losses and circumferential gradients. This is particularly true when the case is insulated from the supporting spar member or case and spar are approximately at the same temperature. Thus, a one-dimensional mathematical model of the telescope was obtained with solar heat input at the exterior end and radiation to the vehicle interior environment from the other end. A method of solving the conduction equations, recently developed at UAH, was utilized. The time delay for an input at the exterior end to be felt at the interior end was on the order of 75 minutes. Further information on this, and other supporting studies are given in Chapter IV.

It is recommended that further study be given to the higher modes of vibration of the solar panel array. One should have information on natural frequencies, damping, and mode shapes in bending and torsion so that the control system will not excite resonant conditions. It is further recommended that additional studies should be performed with the mathematical model for heat conduction in the X-Ray telescope. Different heat inputs along its length, environmental conditions, and orbital conditions can be studied with the model developed.

Chapter II

METHODS AND ANALYSIS FOR DEPLOYMENT OF SOLAR PANELS

1. INTRODUCTION

The various methods for deployment of the solar panels are shown. An evaluation table is then used to select the most appropriate method based on criteria desirable to obtain. Thus, the scissor mechanism is shown to be most appropriate. This mechanism is investigated in much greater detail in the remainder of this chapter. Certain problem areas were anticipated with the scissor so simple analytical and graphical studies are made to investigate these problems. The forces on the mechanism are due to accelerations of maneuvering and deployment. The deployment accelerations are obtained from the kinematics of the mechanism for idealized driving link motion. These results are used in the equations of kinetics to determine joint forces as well as driving forces and torques. Numerical results for displacement, velocity, and acceleration are plotted and equations for the joint forces are given, assuming rigid members. Computer programs are available for an arbitrary geometry on request.

A vibration study of the scissor mechanism is necessary to determine modal frequencies, joint forces, and damping characteristics. The investigation of a lumped mass system with six masses is shown. The energy loss per cycle due to joint friction is determined for the first vibration mode. This is used to determine a modal equation of motion for the first mode.

2. METHODS FOR PANEL DEPLOYMENT

The following illustrates three mechanisms considered to be possible

solutions for the deployment mechanism. It does not show all mechanisms that were considered as many were eliminated because of complexity or space requirements.

A. Collapsible Frame Mechanism

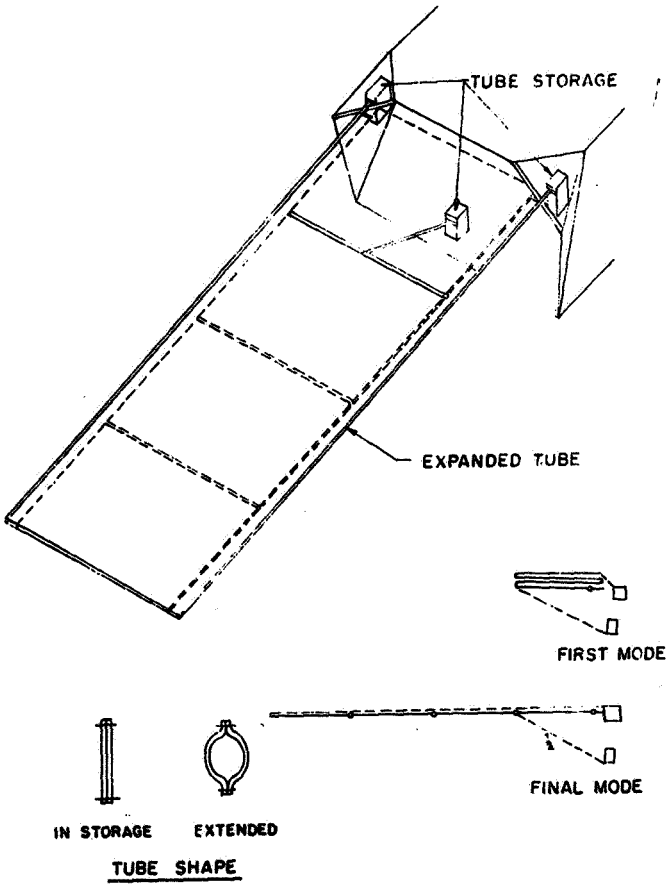

B. Scissor Mechanism

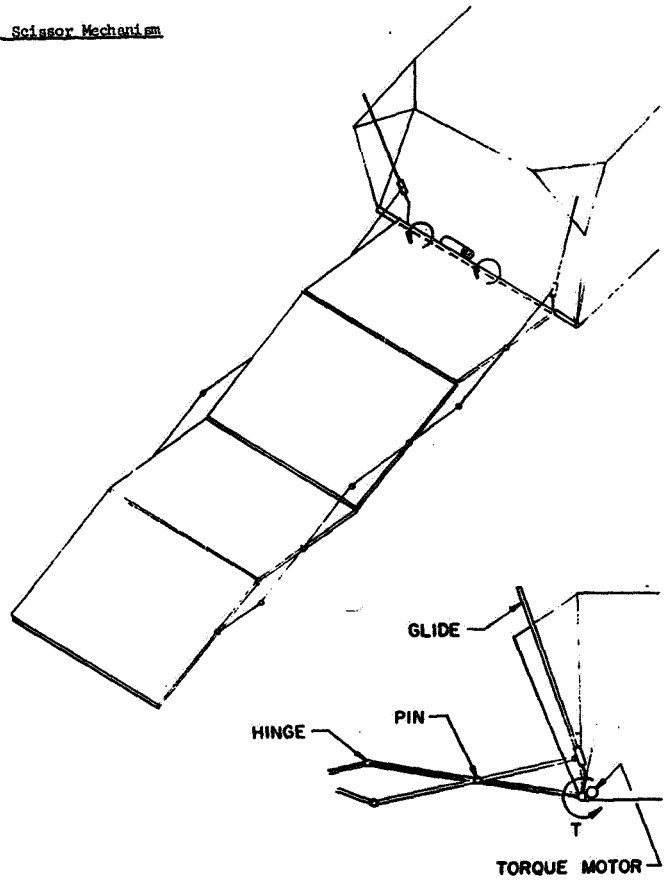

C. Torsion Bar Mechanism

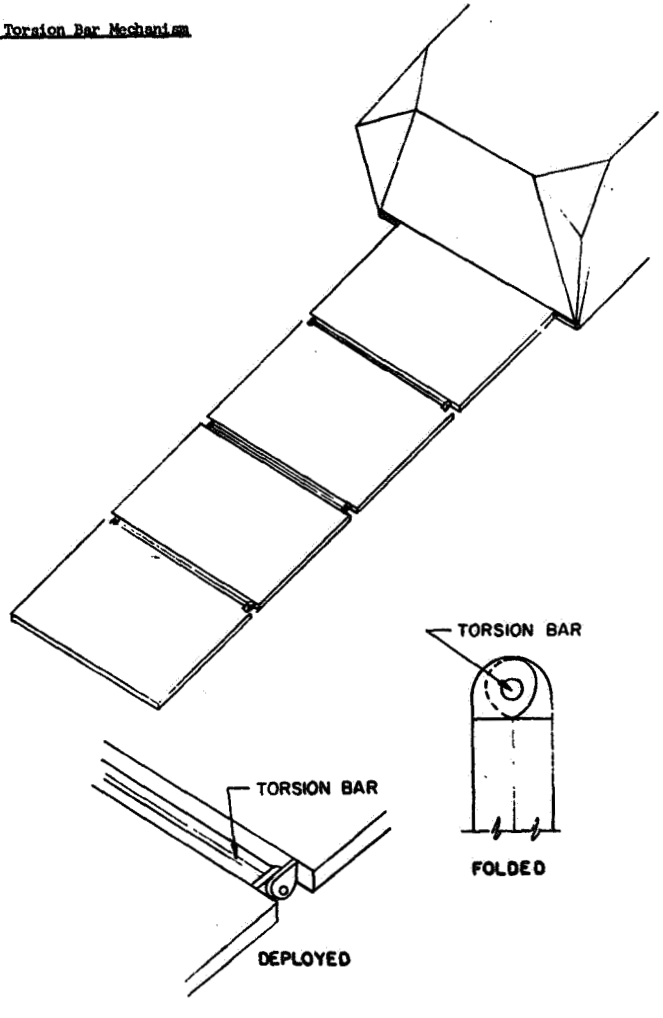

EVALUATION TABLE

DESIGN FACTORS	A.	B.	C.
1. Simplicity	G	F	E
2. Reliability	F	E	G
3. Power-Reqd.-External	E	F	E
4. Deployment Control	G	E	P
5. Lubrication Reqd.	G	F	E
6. Equipment Space Reqd.	P	G	E
7. Retraction	F	E	P
8. Hand Operative	G	F	G
9. Side-Fold Possible	F	P	F
10. Rigidity	F	E	P
11. Damping	F	G	G
12. Dynamic Stability	G	G	F

E - Excellent (most desirable) (1) F - Fair (3)

G - Good (2) P - Poor (4)

Based on a point system of one for excellent down to four for poor, the system A scored 30, system B scored 26, and system C scored 28. On this basis, the scissor mechanism appears to be the best and is studied further in the section below.

3. DESIGN CONSIDERATIONS FOR THE SCISSOR MECHANISM

The following items were considered as problem areas or solutions to problem areas and are summarized for future reference.

3.1 Analysis of slack in mechanism

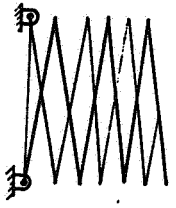

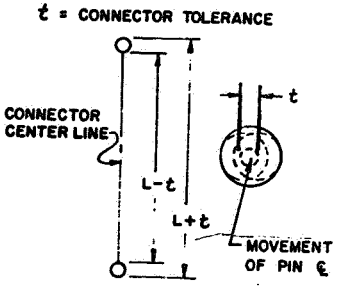

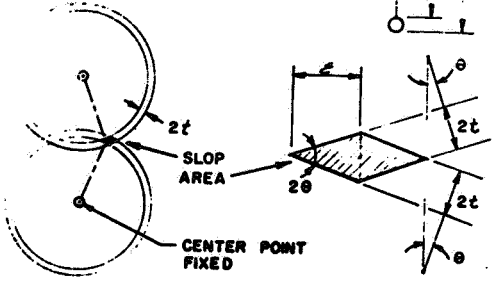

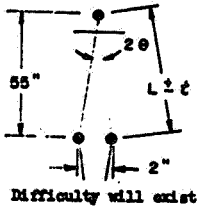

$\frac{t}{\epsilon} = \sin\theta$

$\epsilon = \frac{t}{\sin\theta}$

$\sin\theta \doteq \frac{1}{55}$

$\epsilon = 55t$

SOME ERROR DUE TO CURVE SIDES
SLOP AREA PARALLELOGRAM

Difficulty will exist in completely folding up the panel array.

3.2 Belt drive for Link A:

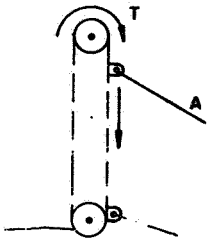

This mechanism is less likely to bind but has a flexability in the horizontal direction. Belt may be a chain device.

3.3 Elimination of Sliding Contact:

All joints should have a loose fit or large tolerances. Torsion bars can eliminate joints

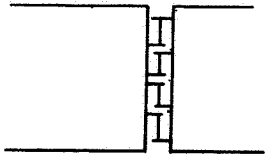

(see Analysis of Torcion Bar)

3.4 Central scissor:

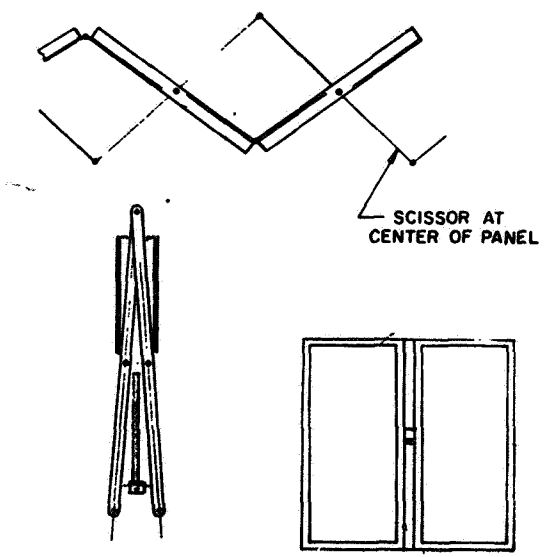

For Link A

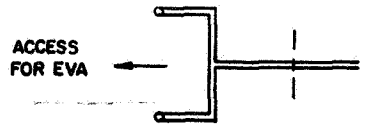

4. IDEAS FOR OTHER MECHANISMS

4.1 Joint balloon

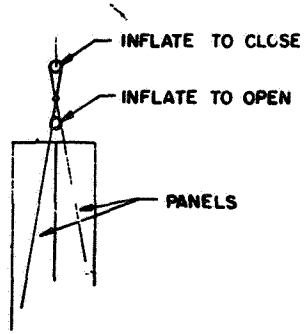

4.2 Magnetic devices

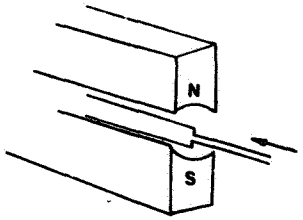

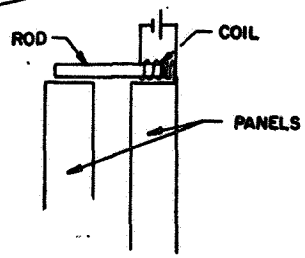

4.3 Torsion bar analysis

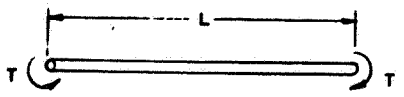

$\theta = \frac{TL}{GJ}$ · G = Shear Modulus
J = Cross-section Constant

Consider Steel Tube

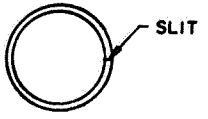

For a $3\frac{3}{4}$" tube .095" thick

The twist per inch is:

1.) For unslit tube = .0031 rad./in.

2.) For slit tube = .062 rad./in.

20 times as much for the slit tube. Torque 1.) 41,000 in. lb.

2.) 700 in. lb. (1.7%)

4.4 Panel Data (4-12-67)

Weight	158	lbs.
Width	101.13	in.
Length	102.75	
Kinematic Radius	52.13	in.
Thickness	2.00	in.

Solar Panel Array

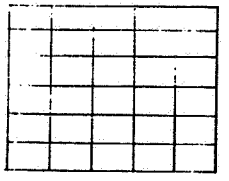

Frame made of
Alum. tube

1" x 2" x .06"

$I = .179 \text{ in.}^4$

$= 1.076 \text{ in.}^4$

$E = 10^7 \#/\text{in.}^2$

$EI = 1.076 \times 10^7 \#/\text{in.}^2$

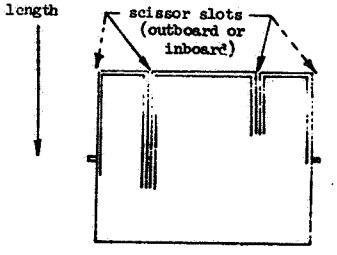

½ honeycomb panel

5# per module

20" x 24.625"

One Solar Panel

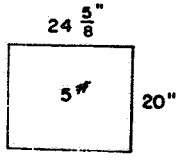

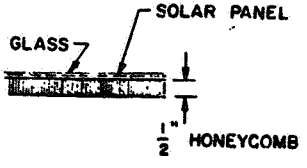

2. SOLAR PANEL DEPLOYMENT - GRAPHICAL STUDY

Four-Bar Mechanism

Drawing # 1

Required deployment of the panels cannot be achieved because arms A and B are not of proper length. Link A and the scissor section C form a straight line at the joint in the center of the panel.

Drawing # 2

Link A and scissors section C form a straight line. Link B has been lengthened from previous drawing; therefore, link A must be lengthened. To have specified deployment of panel under these conditions an angle of 131.5° will exist between links A & B. Link C will not reach correct position.

Drawing # 3

σ = angle between the scissors section and link A when panels are stored. Specified conditions:

$\alpha = 10.5°$ = angle between panels and structure-stored position.

$\lambda = 5°30'$ = angle between panels and horizontal-deployed position.

Arm B rotates 102°. Scissor link C will still not reach its correct deployed position.

Drawing # 4

Link A and scissors section form straight line. Required deployment and storage is achieved for the panel and approximately achieved for the link C.

Drawing # 5

This shows the required deployment with the arms A & B of minimum length. Link B and the scissors section form a straight line. Link C will still be in error but opposite to the other two cases.

GENERAL COMMENTS

Consider the links A & B to form a straight line when fully deployed. An extension of link C when deployed bisects the L-shaped area available for location of the driving link support, as shown below as line a-a.

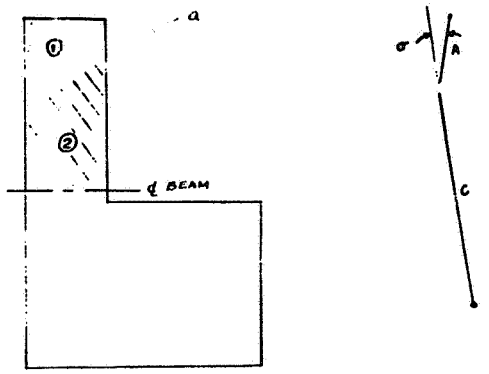

With the pin in area (1) the scissor link A + C must be bent so that σ is negative. This interferes with the panels when retracted. With the pin in area (2), the scissor link A + C must be bent so that σ is positive. This is desirable. With the pin along a - a the scissor link A + C will be straight which may be the most desirable.

Note that a dip action occurs in the mechanism center line as it is folded out. This is shown in more detail with numerical results in Fig. 6.

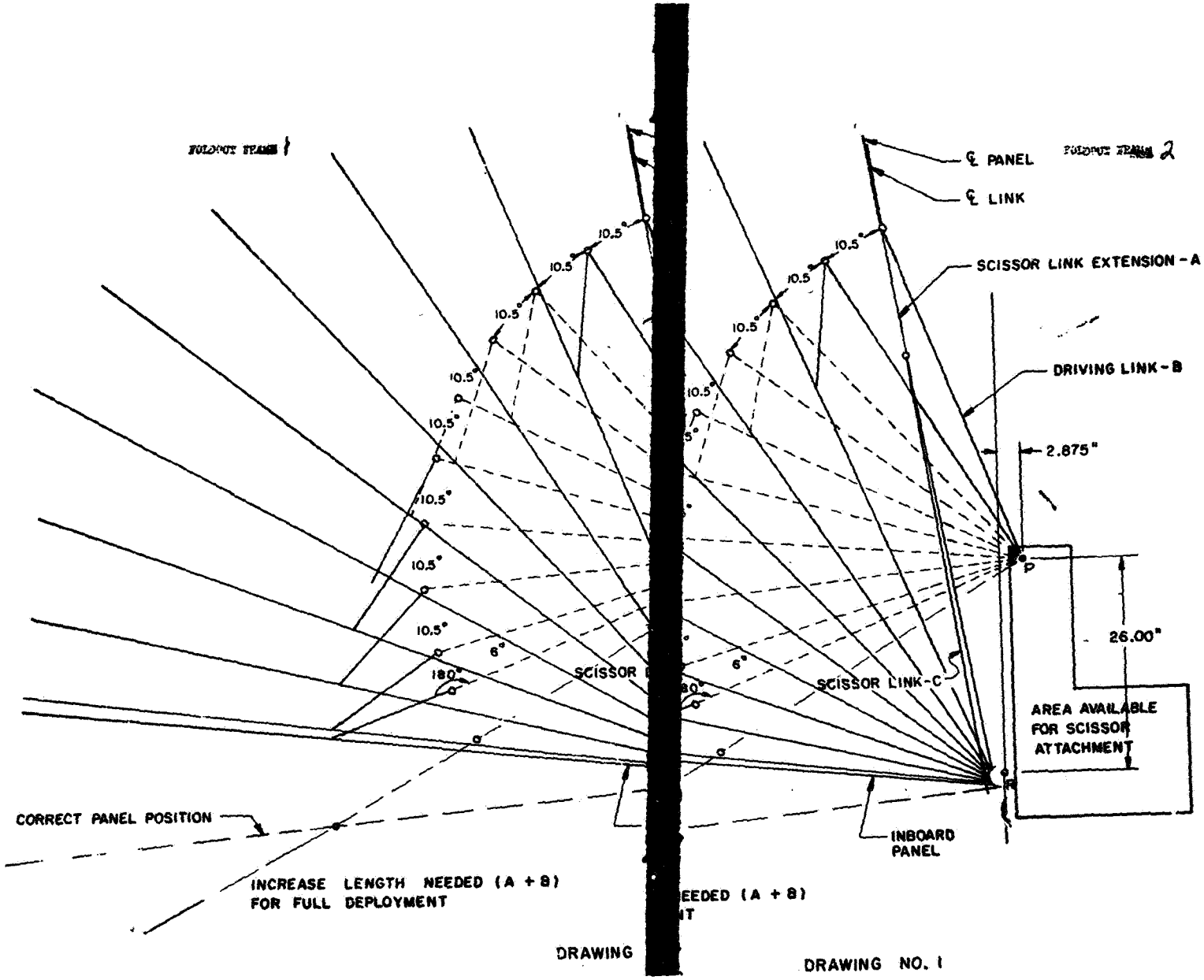

DRAWING

DRAWING NO. 1

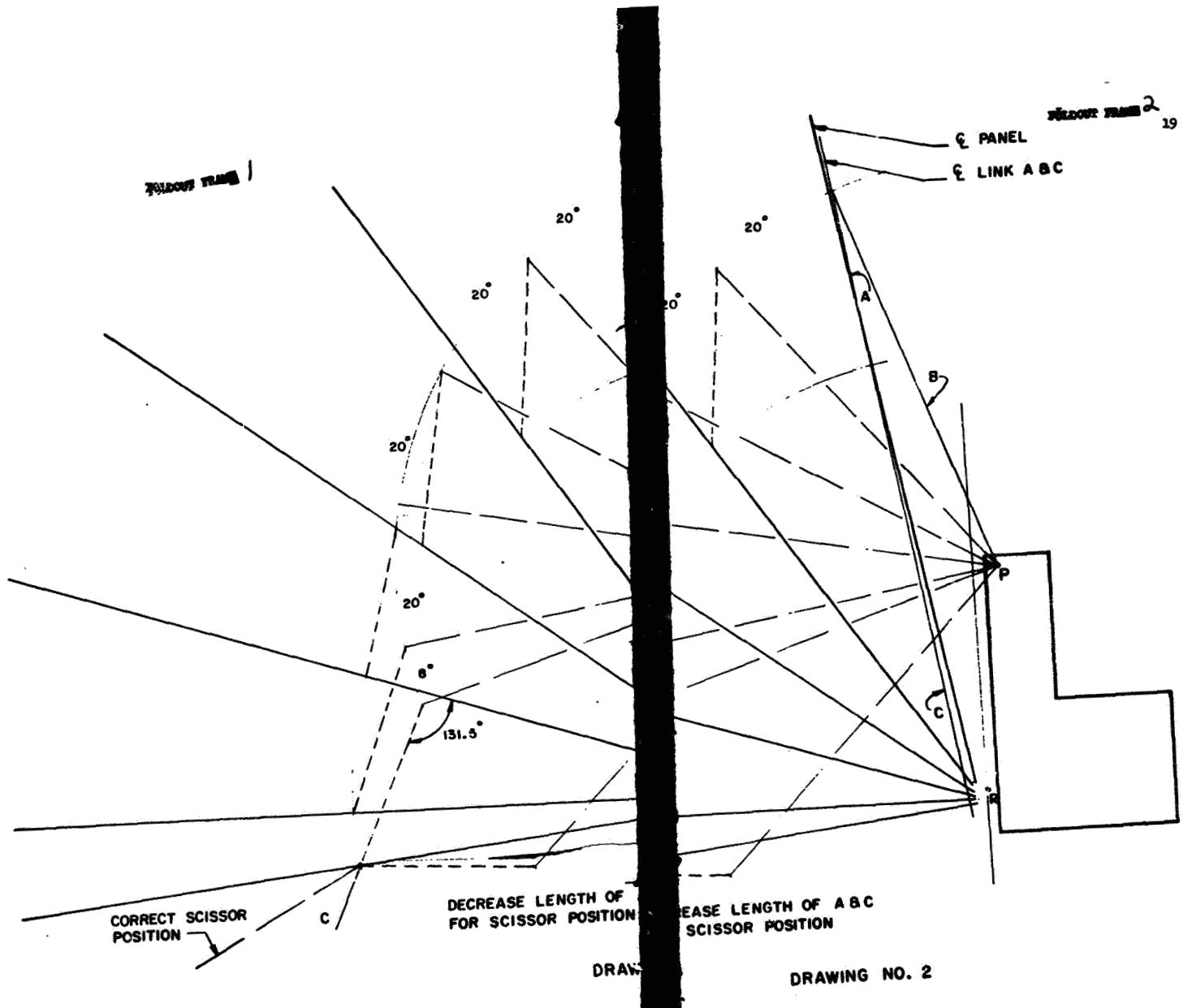
FOLDOUT FRAME 1
FOLDOUT FRAME 2
19
℄ PANEL
℄ LINK A B C
20°
20°
20°
20°
20°
20°
A
B
C
P
R
8°
131.5°
CORRECT SCISSOR POSITION
C
DECREASE LENGTH OF
FOR SCISSOR POSITION
EASE LENGTH OF A B C
SCISSOR POSITION
DRAW
DRAWING NO. 2

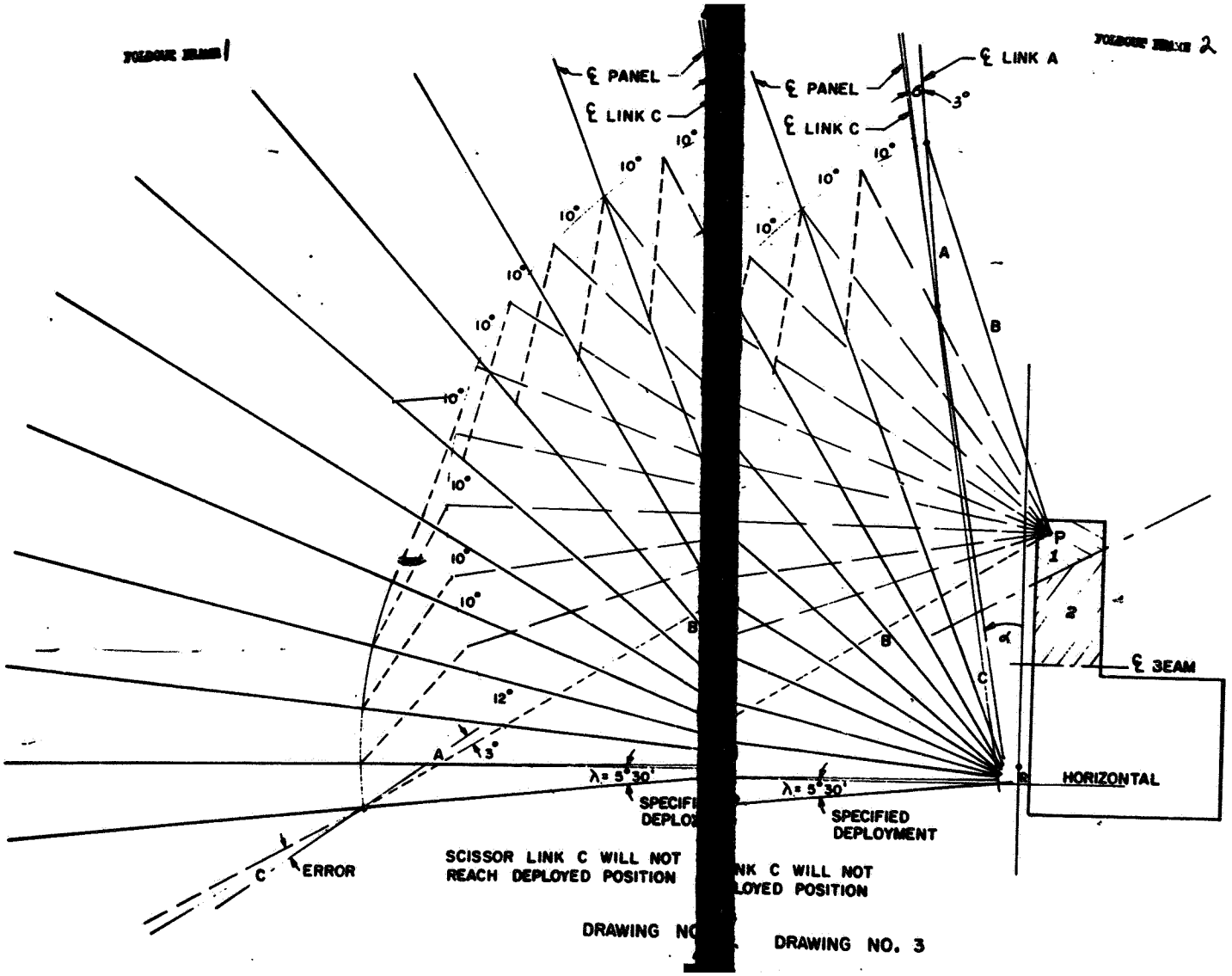
℄ PANEL
℄ LINK C
℄ PANEL
℄ LINK C
℄ LINK A
3°
10°
A
B
P
1
2
α
C
℄ BEAM
HORIZONTAL
12°
A
3°
λ = 5°30'
λ = 5°30'
SPECIFIED DEPLOYMENT
C
ERROR
SCISSOR LINK C WILL NOT REACH DEPLOYED POSITION
DRAWING NO. 3

FOLDOUT FRAME 1

FOLDOUT FRAME 2

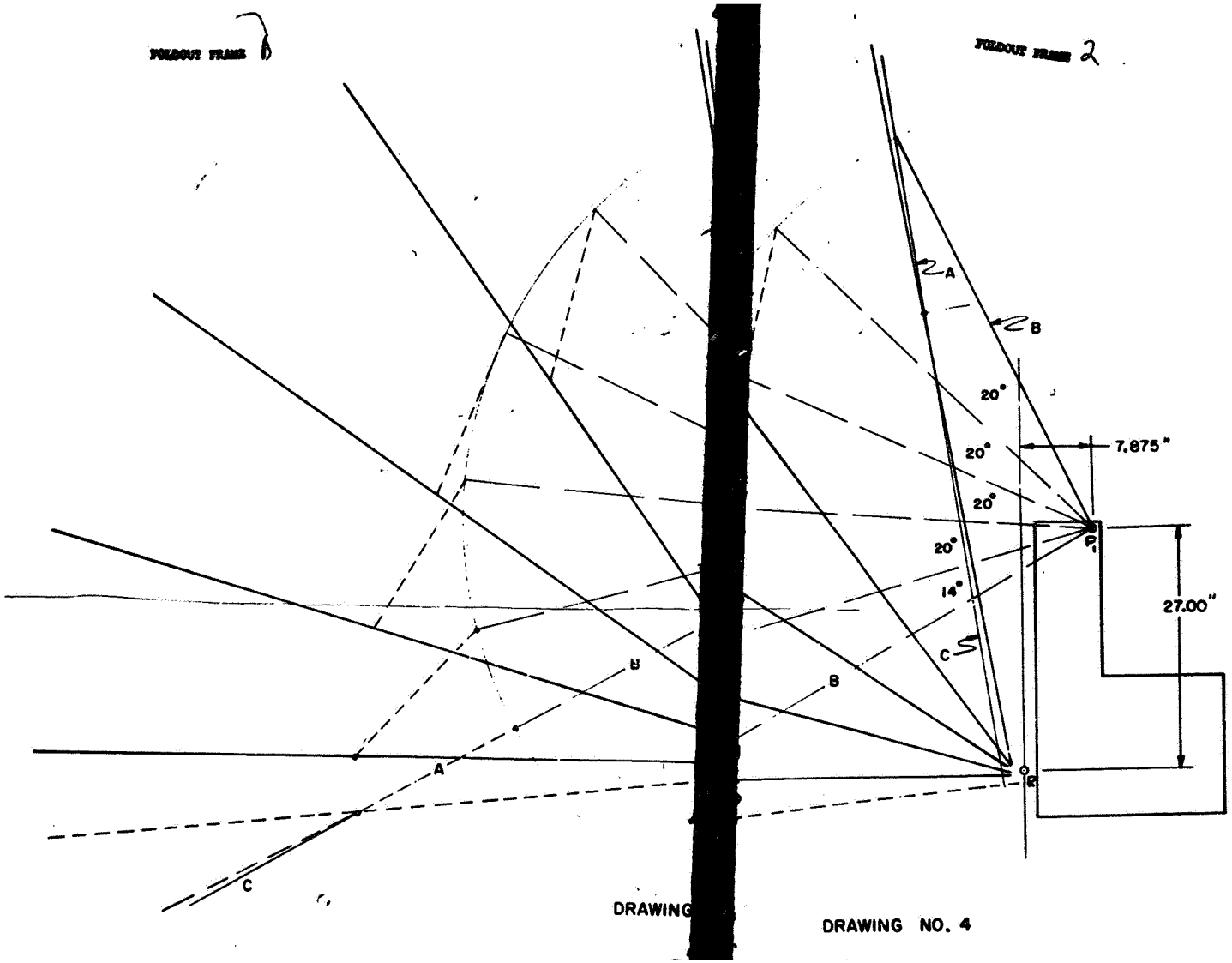

DRAWING

DRAWING NO. 4

FOLDOUT FRAME 1

FOLDOUT FRAME 2

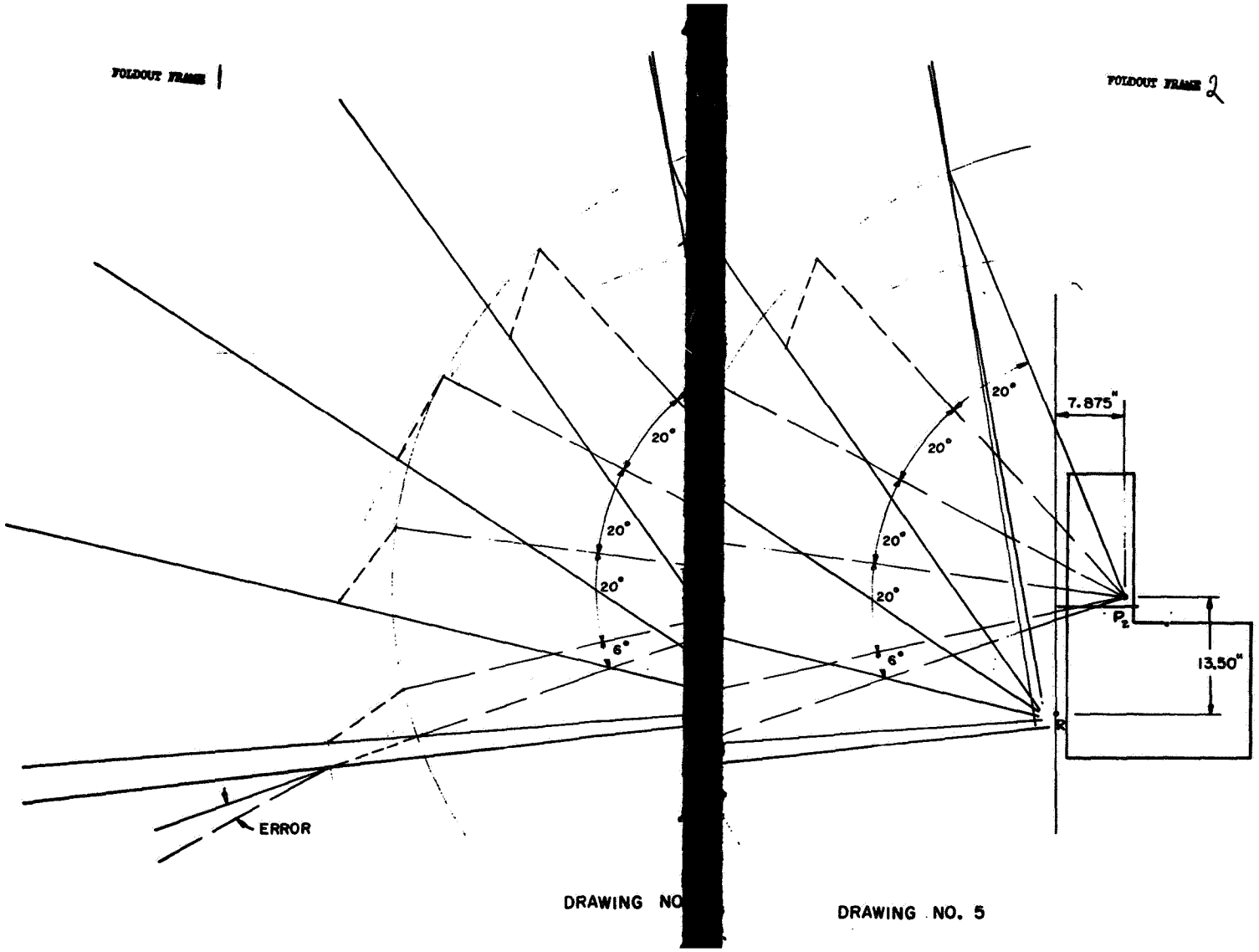

DRAWING NO

DRAWING NO. 5

6. KINEMATICS OF SCISSOR MECHANISM

In the following pages, the displacements velocities and accelerations of the panels and scissor links are obtained. First, the nomenclature and sign convention for the inboard 4-bar linkage and slider are shown along with that for the outboard sections. Secondly, the dynamic variables are solved for and shown in Tables 6.1 and 6.2. Then, idealized curves and data for the angular motion of the 4-bar driving link are shown. The idealized curves and data for the slider are shown next. Furthermore, curves showing a comparison for certain important variables and different deployment times (60 sec. and 120 sec.) and methods (4-bar verses slider) are provided.

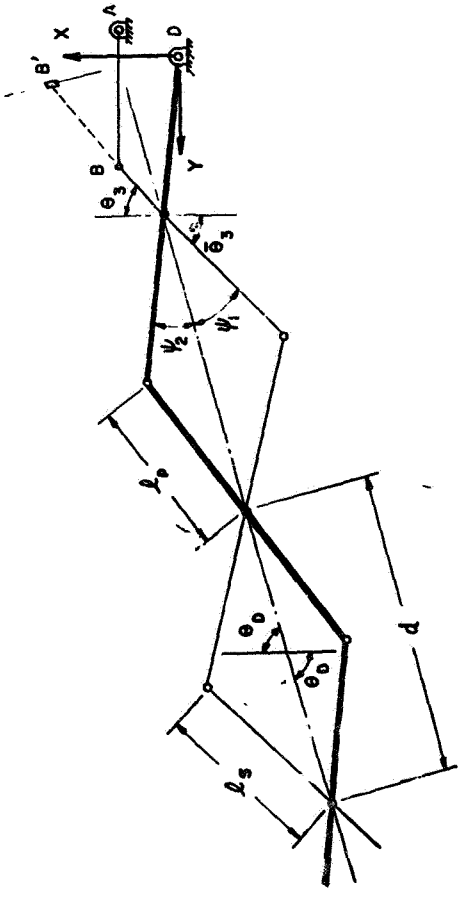

SIGN CONVENTION
OUTBOARD

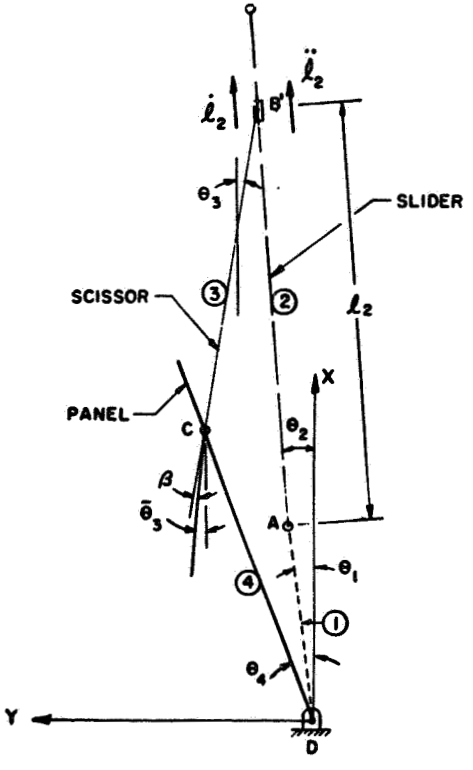

SIGN CONVENTION

SLIDER

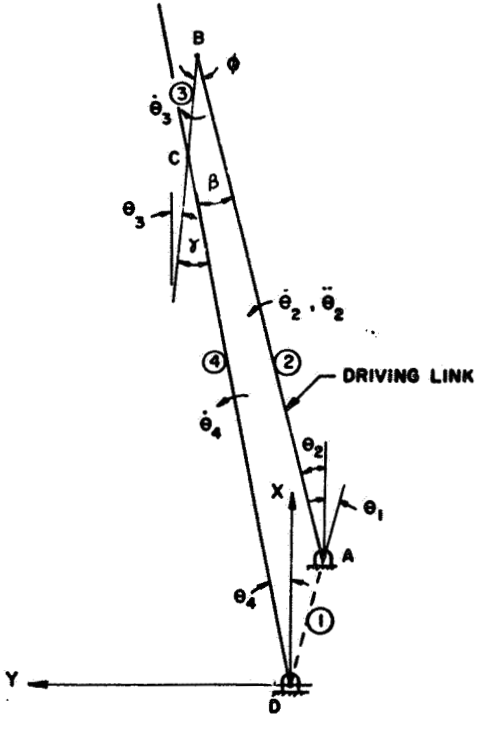

SIGN CONVENTION

4 – BAR

TABLE 6.1

ANGULAR MOTION OF INBOARD DRIVING MECHANISM

	4-Bar Linkage	Slider Drive
	ℓ_2 = Constant $\theta_2, \dot{\theta}_2, \ddot{\theta}_2$ all set	$\ell_2, \ell_2, \ddot{\ell}_2$ all set θ_2 = Constant
$\dot{\theta}_3$	$\dot{\theta}_3 = -\frac{\ell_2}{\ell_3}\dot{\theta}_2\frac{\sin(\theta_4-\theta_2)}{\sin(\theta_3+\theta_4)}$	$\dot{\theta}_3 = \frac{-\dot{\ell}_2}{\ell_3}\frac{\cos(\theta_4-\theta_2)}{\sin(\theta_3+\theta_4)}$
$\dot{\theta}_4$	$\dot{\theta}_4 = \frac{\ell_2}{\ell_4}\dot{\theta}_2\frac{\sin(\theta_3+\theta_2)}{\sin(\theta_4+\theta_3)}$	$\dot{\theta}_4 = \frac{-\dot{\ell}_2}{\ell_4}\frac{\cos(\theta_2+\theta_3)}{\sin(\theta_3+\theta_4)}$
$\ddot{\theta}_3$	$\ddot{\theta}_3 = \frac{-1}{\ell_3\sin(\theta_3+\theta_4)}[\ell_4(\dot{\theta}_4)^2$ $+\ell_2\ddot{\theta}_2\sin(\theta_4-\theta_2)$ $-\ell_2(\dot{\theta}_2)^2\cos(\theta_4-\theta_2)$ $+\ell_3(\dot{\theta}_3)^2\cos(\theta_3+\theta_4)]$	$\ddot{\theta}_3 = \frac{-1}{\ell_3\sin(\theta_3+\theta_4)}[\ell_4(\dot{\theta}_4)^2$ $+\ddot{\ell}_2\cos(\theta_2-\theta_4)$ $+\ell_3(\dot{\theta}_3)^2\cos(\theta_3+\theta_4)]$
$\ddot{\theta}_4$	$\ddot{\theta}_4 = \frac{-1}{\ell_4\sin(\theta_3+\theta_4)}[\ell_3(\dot{\theta}_3)^2$ $-\ell_2\ddot{\theta}_2\sin(\theta_2+\theta_3)$ $-\ell_2(\dot{\theta}_2)^2\cos(\theta_2+\theta_3)$ $+\ell_4(\dot{\theta}_4)^2\cos(\theta_3+\theta_4)]$	$\ddot{\theta}_4 = \frac{-1}{\ell_4\sin(\theta_3+\theta_4)}[\ell_3(\dot{\theta}_3)^2$ $+\ddot{\ell}_2\cos(\theta_2+\theta_3)$ $+\ell_4(\dot{\theta}_4)^2\cos(\theta_3+\theta_4)]$

TABLE 6.2

OUTBOARD CENTERLINE, JOINT, AND PANEL-SCISSOR MOTION

For 4-Bar and Slider Mechanisms

$$\psi_1 + \psi_2 = \pi - \bar{\theta}_3 - \theta_4, \quad \cos\psi_1 = \frac{\ell_p}{\ell_s}\cos\psi_2$$

$$d = 2\ell_p\cos\psi_2, \quad \theta_D = \psi_1 + \bar{\theta}_3, \quad \bar{\theta}_3 = \theta_3 \mp \beta$$

$$\dot{\psi}_1 = \frac{-(\dot{\bar{\theta}}_3 + \dot{\theta}_4)}{1 + \frac{\ell_p\sin\psi_1}{\ell_s\sin\psi_2}}$$

$$\dot{\psi}_2 = \frac{\ell_p\sin\psi_1}{\ell_s\sin\psi_2}\dot{\psi}_1$$

$$\dot{d} = \frac{-d\sin\psi_1}{\cos\psi_1}\dot{\psi}_1$$

$$\dot{\theta}_D = \dot{\psi}_1 + \dot{\bar{\theta}}_3$$

$$\ddot{\psi}_1 = \frac{-(\ddot{\bar{\theta}}_3 + \ddot{\theta}_4) - \frac{\ell_p\cos\psi_1}{\ell_s\sin\psi_2}(\dot{\psi}_1)^2 + \frac{\cos\psi_2}{\sin\psi_2}(\dot{\psi}_2)^2}{1 + \frac{\ell_p\sin\psi_1}{\ell_s\sin\psi_2}}$$

$$\ddot{d} = \frac{-d\sin\psi_1\ddot{\psi}_1 - d\cos\psi_1(\dot{\psi}_1)^2 - 2\dot{d}\sin\psi_1\dot{\psi}_1}{\cos\psi_1}$$

$$\ddot{\theta}_D = \ddot{\psi}_1 + \ddot{\bar{\theta}}_3$$

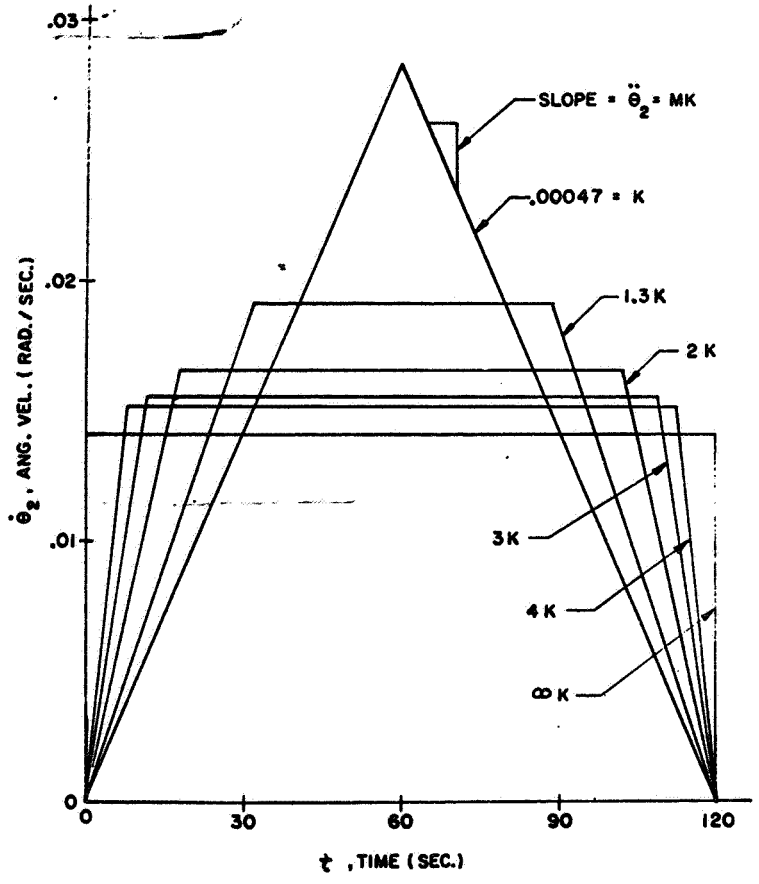

FIGURE 6.1. $\dot{\theta}_2$ VS. t – DRIVING LINK 120 SEC.

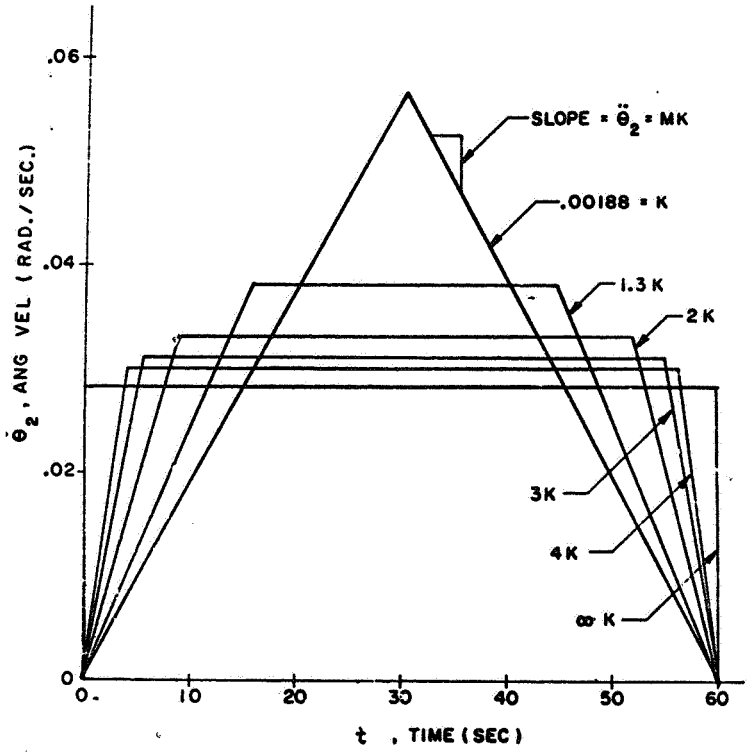

FIGURE 6.2. $\dot{\theta}_2$ VS t – DRIVING LINK 60 SEC.

$\dot{\theta}_2$ & t for equal θ_2	ANGULAR ACCELERATION MK = $\ddot{\theta}_2$ (rad./sec.^{2})					
	± .00047	± .00061	± .00094	± .00141	± .00188	± ∞
$\dot{\theta}_2(1)$	0	0	0	0	0	.0141
t(1)	0	0	0	0	0	0+
$\dot{\theta}_2(2)$	.01263	.01442	.01656	.01556	.01515	.0141
t(2)	26.87006	23.57965	19.05498	16.37809	15.32603	12.0
$\dot{\theta}_2(3)$	.0178	.01910	.01656	.01556	.01515	.0141
t(3)	37.95	33.4277	29.28523	27.18825	26.67853	24.0
$\dot{\theta}_2(4)$	.02186	.01910	.01656	.01556	.01515	.0141
t(4)	46.50416	42.31356	39.51598	37.99844	38.03103	36.0
$\dot{\theta}_2(5)$	.02526	.01910	.01656	.01556	.01515	.0141
t(5)	53.74165	51.19942	49.79573	48.80863	44.38553	48.0
$\dot{\theta}_2(6)$	.0282	.01910	.01656	.01556	.01515	.0141
t(6)	60.0	60.0	60.0	60.0	60.0	60.0
$\dot{\theta}_2(7)$	.02526	.01910	.01656	.01556	.01515	.0141
t(7)	66.25835	68.80058	70.20427	71.19137	70.61647	72.0
$\dot{\theta}_2(8)$	.02186	.01910	.01656	.01556	.01515	.0141
t(8)	73.49584	77.63644	80.48402	82.00156	81.96897	84.0
$\dot{\theta}_2(9)$	.0178	.01910	.01656	.01556	.01515	.0141
t(9)	82.05	86.5723	90.71477	92.81175	93.32147	96.0
$\dot{\theta}_2(10)$	.01263	.01442	.01656	.01556	.01515	.0141
t(10)	93.12994	96.42035	100.94502	103.62191	104.67397	108.0
$\dot{\theta}_2(11)$	0	0	0	0	0	.0141
t(11)	120	120	120	120	120	120
t_m	60	31.31147	17.65957	11.13475	7.95212	0

TABLE 6.3-Angular Accelerations and Velocities with Equal Angular Displacements for 2 Minute Deployment.

$\dot{\theta}_2$ & t for equal θ_2	ANGULAR ACCELERATION MK= $\ddot{\theta}_2$(rad./sec.^{2})					
	± .00188	± .00244	± .00376	± .00564	± .00752	± ∞
$\dot{\theta}_2(1)$	0	0	0	0	0	.02828
t(1)	0	0	0	0	0	0+
$\dot{\theta}_2(2)$	.02525	.02883	.03312	.03113	.03030	.02828
t(2)	13.43	11.779	9.52892	8.21246	7.64106	6.0
$\dot{\theta}_2(3)$	.035772	.03819	.03312	.03113	.03030	.02828
t(3)	19.0	16.70964	14.55331	13.66618	13.28147	12.0
$\dot{\theta}_2(4)$	.04373	.03819	.03312	.03113	.03030	.02828
t(4)	23.259	21.13519	19.7777	19.1199	18.92188	18.0
$\dot{\theta}_2(5)$	.05052	.03819	.03312	.3113	.03030	.02828
t(5)	26.87006	25.56074	24.90209	24.57362	24.56229	24.0
$\dot{\theta}_2(6)$	.0564	.03819	.07312	.03113	.03030	.02828
t(6)	30.0	30.0	30.0	30.0	30.0	30.0
$\dot{\theta}_2(7)$	.05052	.03819	.03312	.03113	.03030	.02828
t(7)	33.12994	34.43426	35.09791	35.42638	35.43771	36.0
$\dot{\theta}_2(8)$	.04373	.03819	.03312	.03113	.03030	.02828
t(8)	36.741	38.86481	40.2223	40.8801	41.07812	42.0
$\dot{\theta}_2(9)$	.03572	.03819	.03319	.03113	.03030	.02828
t(9)	41.0	43.29036	45.3467	46.33382	46.71853	48.0
$\dot{\theta}_2(10)$	.02525	.02883	.03312	.03113	.03030	.02828
t(10)	46.57	48.221	50.4711	51.78754	52.35894	54.0
$\dot{\theta}_2(11)$	0	0	0	0	0	.02828
t(11)	60	60	60	60	60	60
t_m	30	15.71721	8.80851	5.51773	4.00265	0

TABLE 6.4-Angular Accelerations & Velocities with Equal Angular Displ. for 1 Minute Deployment.

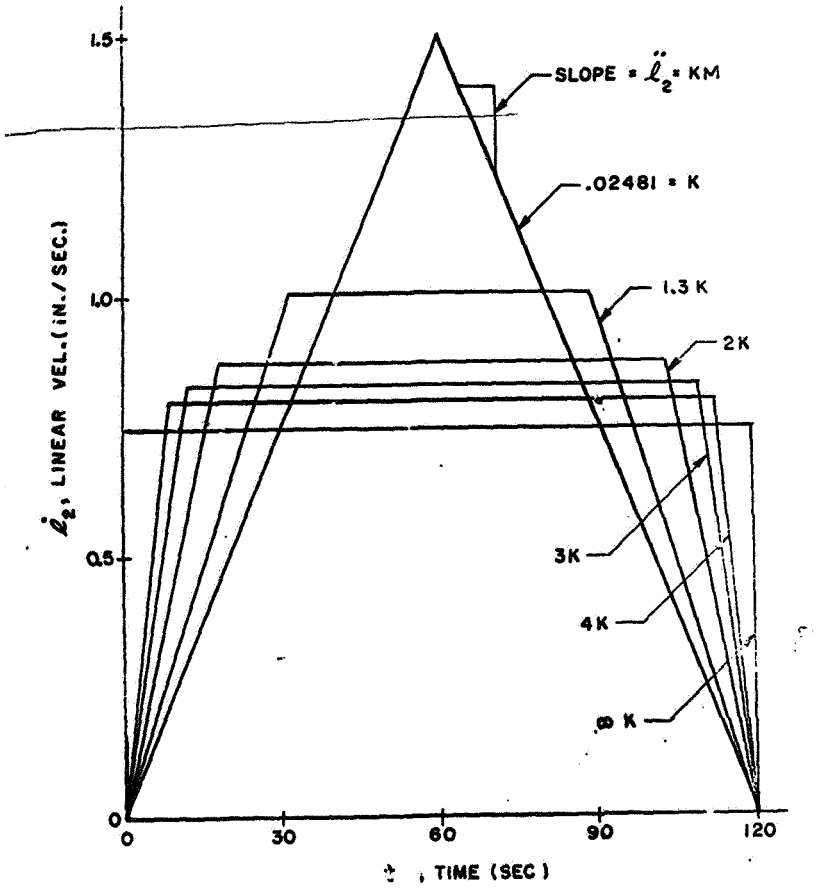

FIGURE 6.3. $\dot{\ell}_2$ VS. t - SLIDER 120 SEC.

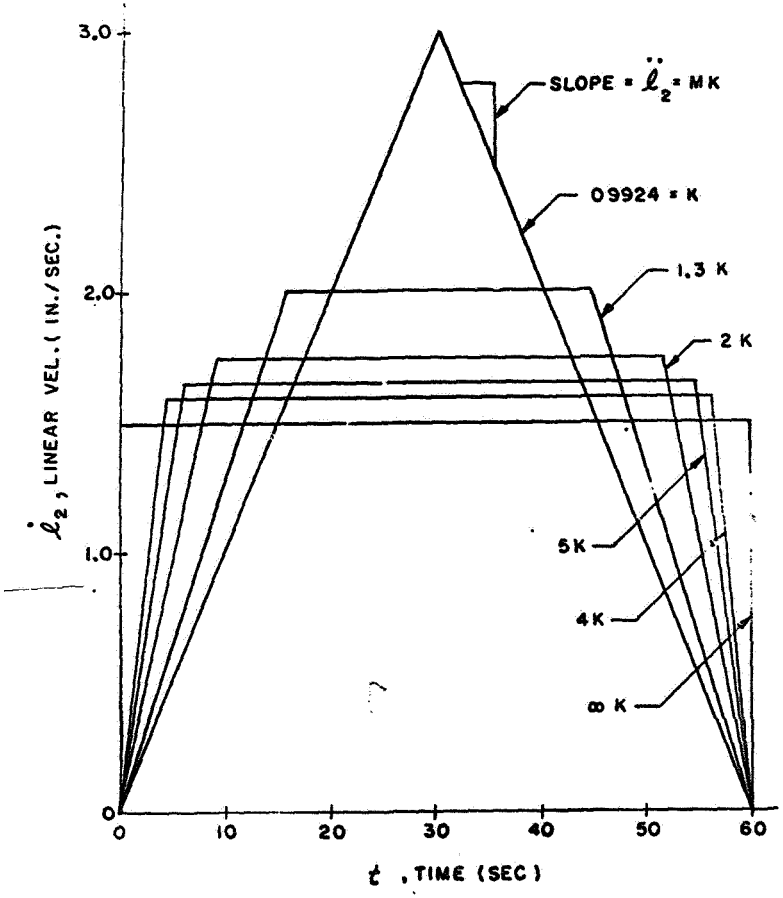

FIGURE 6.4. $\dot{\ell}_2$ VS. t - SLIDER 60 SEC.

ℓ_2 & t for equal ℓ_2	LINEAR ACCELERATION MK = $\ddot{\ell}_2$ (in./sec.^{2})					
	.02481	.03225	.04962	.07443	.09924	∞
$\ell_2(1)$	.00000	.00000	.00000	.00000	.00000	.74430
t(1)	.00000	.00000	.00000	.00000	.00000	.00000
$\ell_2(2)$	.66572	.75904	.87200	.81949	.79774	.744
t(2)	26.83	23.53	19.03	16.04	1[illegible]	12.0
$\ell_2(3)$	.94147	1.00555	.87200	.819449	.79774	.74430
t(3)	37.95	33.34	29.27	27.30	26.41	24.0
$\ell_2(4)$	.94147	1.00555	.87200	81949	.79774	.74430
t(4)	46.48	42.23	39.51	[illegible].20	37.61	36.0
$\ell_2(5)$	1.33144	1.00555	.87200	.81949	.79774	.7443[illegible]
t(5)	53.67	51.12	49.67	49.76	48.80	48.0
$\ell_2(6)$	1.48860	1.00555	.87200	.81949	.79774	.74430
t(6)	60.0	60.0	60.0	60.0	60.0	60.0
$\ell_2(7)$	1.33144	1.00555	.87200	.81949	.79774	.74430
t(7)	66.33	68.88	70.24	70.90	71.20	72.0
$\ell_2(8)$	1.15306	1.00555	.87200	.81949	.79774	.74430
t(8)	73.72	77.77	80.49	81.80	82.39	84.0
$\ell_2(9)$	.94147	1.00555	.87200	.81949	.79774	.74430
t(9)	82.05	86.65	90.73	92.70	93.59	96.0
$\ell_2(10)$	.66572	.75904	.87200	.81949	.79774	.74430
t(10)	93.17	96.47	100.97	103.60	104.78	108.0
$\ell_2(11)$	.00000	.00000	.00000	.00000	.00001	.74430
t(11)	120	120	120	120	120	120
t_m	60.0	31.18	17.57	11.01	8.04	0.00
Maximum Height	1.48860	1.00555	.87200	.81949	.79774	.74430

TABLE 6.5- Linear Accelerations and Velocities with Equal Angular Displacements for Two-Minute Deployment.

ℓ_2 & t for equal ℓ_2	LINEAR ACCELERATION MK = $\ddot{\ell}_2$ (in./sec.^{2})					
	.09924	.12901	.19848	.29772	.39696	∞
$\ell_2(1)$	.00000	.00000	.00000	.00000	.00000	1.48860
t(1)	.00000	.00000	.00000	.00000	.00000	.00000
ℓ_2[illegible]	1.33144	1.51808	1.74400	1.63898	1.59548	1.48860
t[illegible]2)	13.42	11.77	4.51	8.20	7.61	6.0
$\ell_2(3)$	1.88295	2.01110	1.74400	1.63898	1.59548	1.48860
t(3)	18.97	16.68	14.64	13.65	13.21	12.0
$\ell_2(4)$	2.30613	2.01110	1.74400	1.63898	1.59548	1.48860
t(4)	23.24	21.12	19.76	19.10	18.80	18.0
$\ell_2(5)$	2.66289	2.01110	1.74400	1.63898	1.59548	1.48860
t(5)	26.83	25.56	24.88	24.55	24.40	24.0
$\ell_2(6)$	2.97720	2.01110	1.74400	1.63898	1.59548	1.48860
t(6)	30.0	30.0	30.0	30.0	30.0	30.0
$\ell_2(7)$	2.66289	2.01110	1.74400	1.63898	1.59548	1.48860
t(7)	33.17	34.44	35.12	35.45	35.60	36.0
$\ell_2(8)$	2.30613	2.01110	1.74400	1.63898	1.59548	1.48860
t(8)	36.76	38.88	40.24	40.90	41.20	42.0
$\ell_2(9)$	1.88295	2.01110	1.74400	1.63898	1.59548	1.48860
t(9)	41.03	43.32	45.36	46.35	46.79	48.0
$\ell_2(10)$	1.33141	1.51808	1.74400	1.63898	1.59548	1.48860
t(10)	46.58	48.23	50.49	51.80	52.39	54.0
$\ell_2(11)$	.00000	.00000	.00000	.00000	.00000	1.48860
t(11)	60.0	60.0	60.0	60.0	60.0	60.0
t_m	30.0	15.59	8.79	5.51	4.02	0.00
Maximum Height	2.97729	2.01110	1.74400	1.63898	1.59548	1.48860

TABLE 6.6-Linear Accelerations and Velocities with Equal Angular Displacements for One-Minute Deployment.

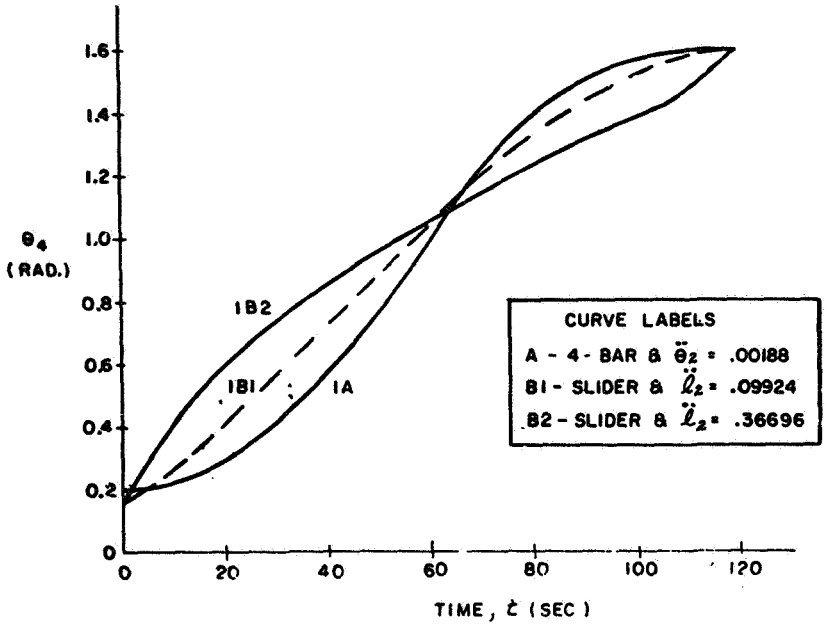

FIGURE 6.5. θ_4 VS. TIME

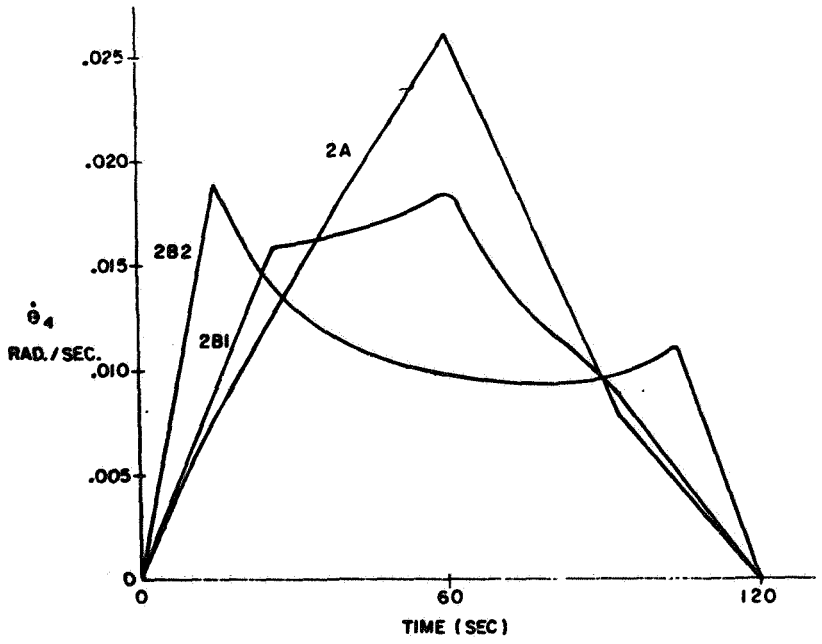

FIGURE 6.6. $\dot{\theta}_4$ VS. TIME

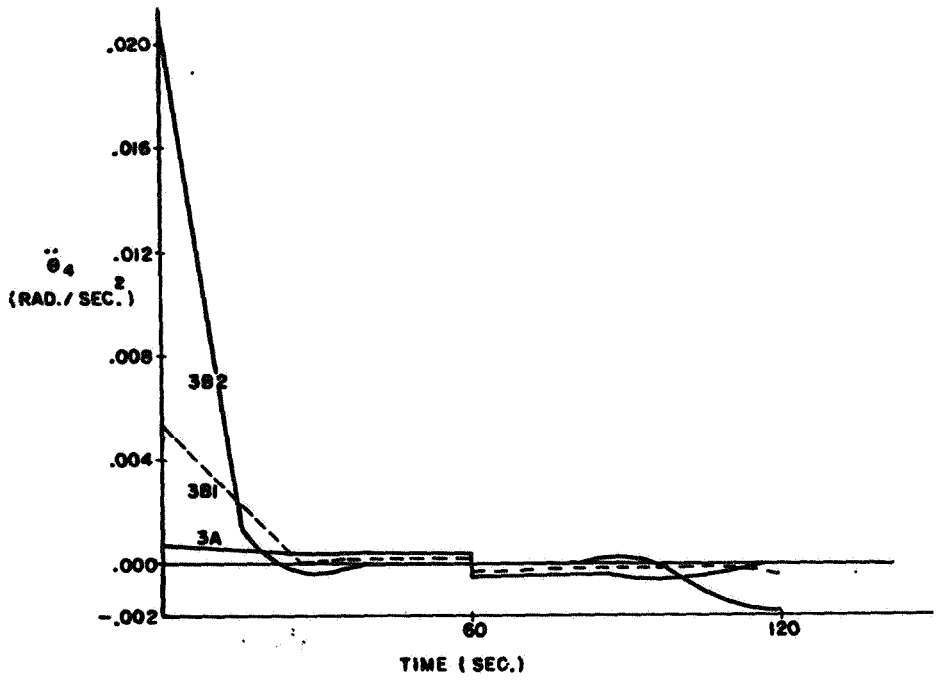

FIGURE 6.7. $\ddot{\theta}_4$ VS. TIME

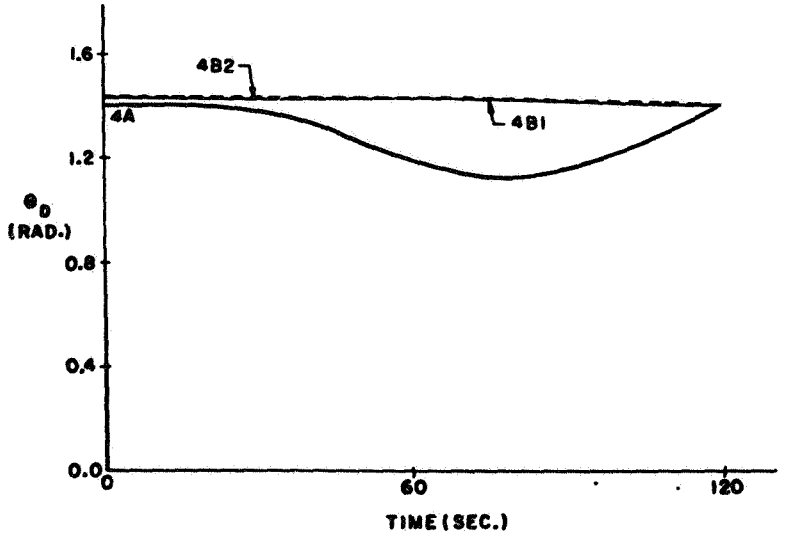

FIGURE 6.6 a θ_D VS. TIME

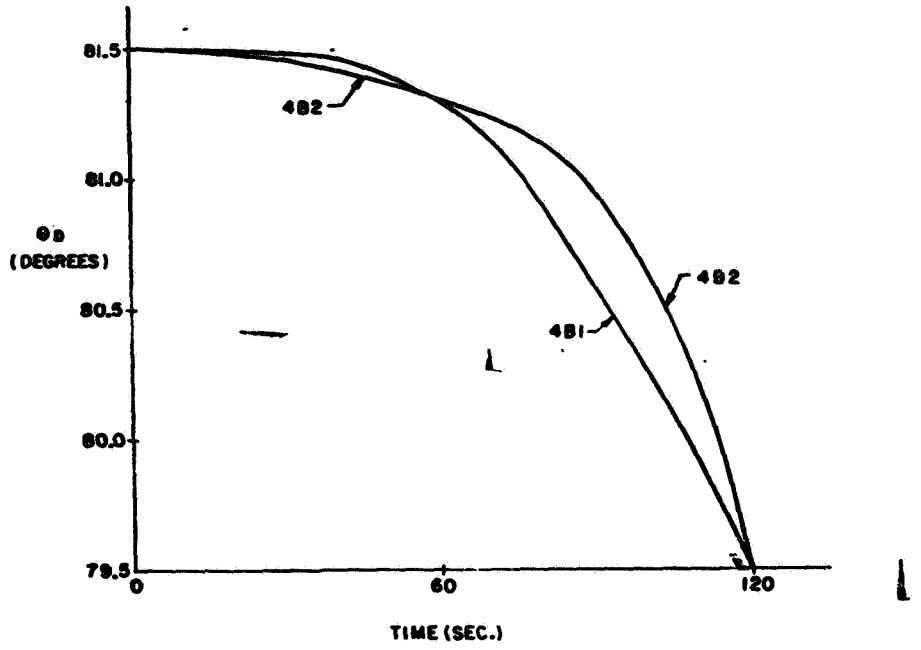

FIGURE 6.8 b. θ_D VS. TIME

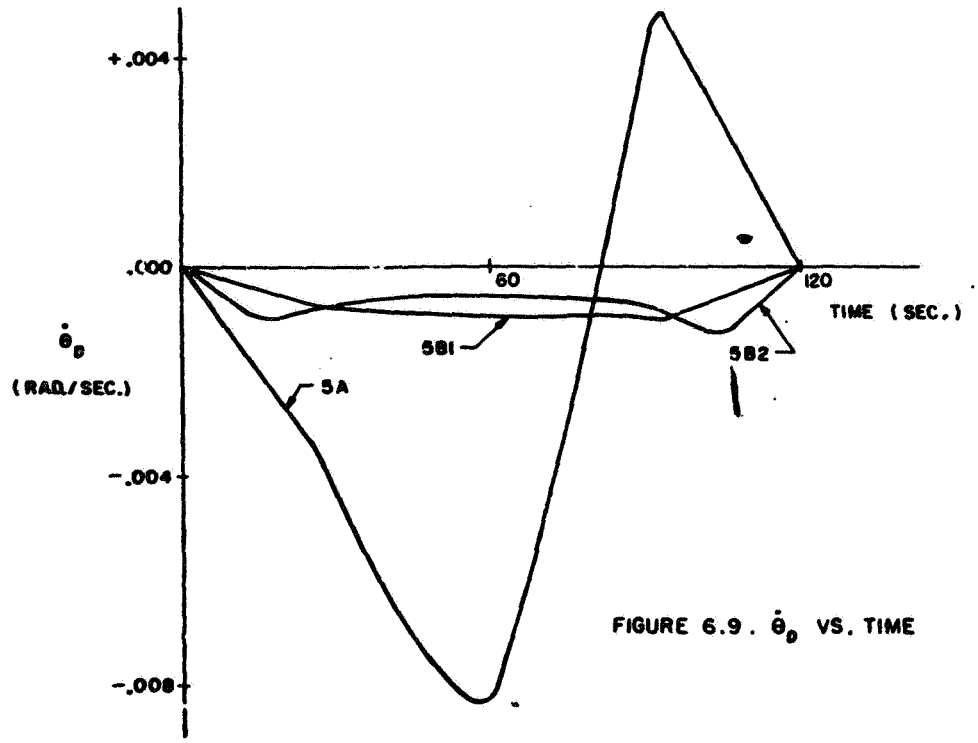

FIGURE 6.9 . $\dot{\theta}_D$ VS. TIME

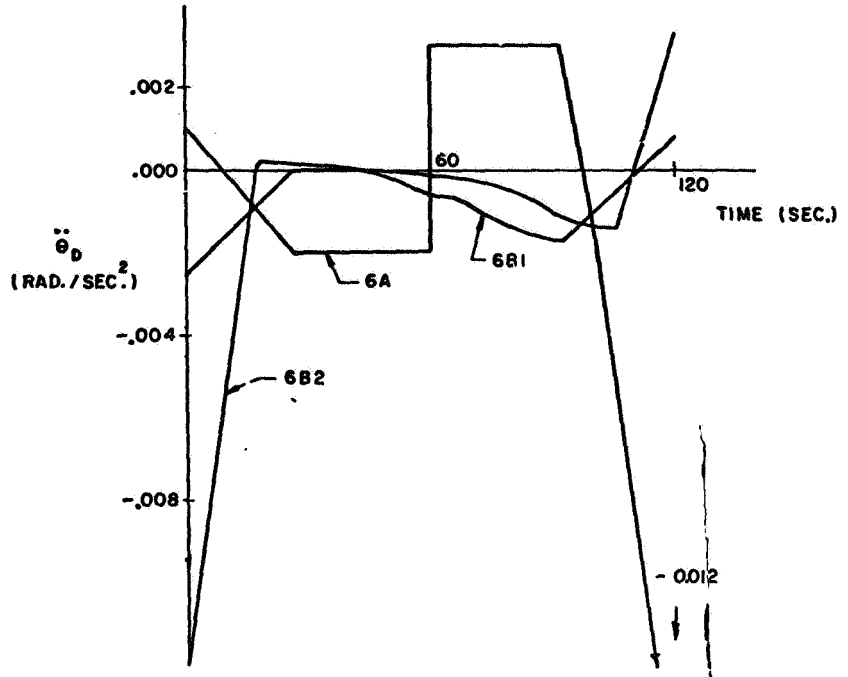

FIGURE 6.10. $\ddot{\theta}_D$ VS. TIME

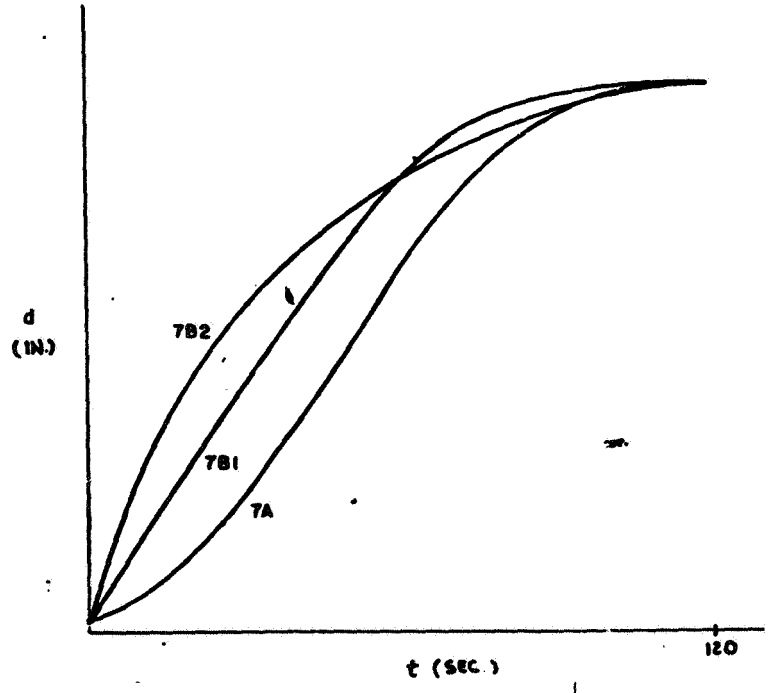

FIGURE 6.11. d VS. TIME

7. KINETICS OF SCISSOR MECHANISM

A summary of the procedure to find forces at the jcints (rigid bars) and driving forces is shown below.

Kinematics: (see section 6)

a. Given: $\theta_1, \theta_2, \theta_3, \theta_4, \ell_1, \ell_2, \ell_3, \ell_4, \ell_p, \ell_s, x_A, y_A, \dot{\theta}_2$

b. Calculate: $\dot{\theta}_3, \dot{\theta}_4, \ddot{\theta}_3, \ddot{\theta}_4, \phi, \alpha$, and β.

c. Calculate: $\psi_1, \psi_2, d, \dot{\theta}_d, \dot{\theta}_d$, and $\ddot{\theta}_d$

d. Calculate: $\theta_3, \theta_4, \dot{\psi}_1, \dot{\psi}_2, \ddot{\psi}_1, \ddot{\psi}_2, \dot{d}, \ddot{d}, \dot{\theta}_3, \dot{\theta}_4, \ddot{\theta}_3, \ddot{\theta}_4$

e. Calculate: a_{Hi} and a_{vi} (The panel center accelerations)

Kinetics:

f. Given: $\theta_3, \theta_4, \ddot{\theta}_3, \ddot{\theta}_4, a_{Hi}$, and a_{Vi}

g. Given: $H_{s6}, V_{s6}, H_{p6}, V_{p6}$

h. Calculate: $H_{si}, V_{si}, H_{pi}, V_{pi}, H_i, V_i$

i. The inboard calculations: H_B, V_B or H_A, V_A, T

7.1 Link Forces-Nomenclature

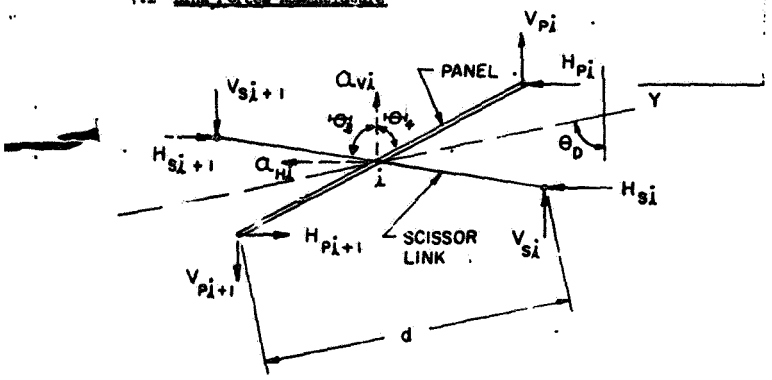

X

Panel:

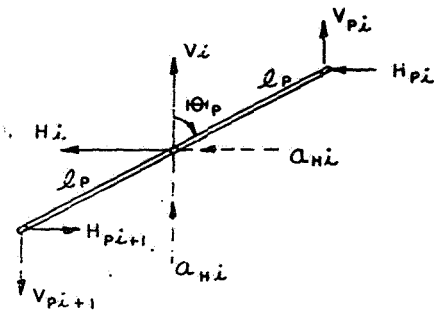

Dynamic Equations (rigid bar)

$$\Sigma F_x = m\bar{a}_x$$
$$\Sigma F_y = m\bar{a}_y$$
$$\Sigma M_G = I_p\alpha$$

Horizontal Forces

$$H_{pi} + H_i - H_{pi+1} = m_p a_{Hi}$$

Vertical Forces

$$V_{pi} + V_i - V_{pi+1} = m_p a_{vi}$$

Moments

$$(V_{pi} + V_{pi+1})\,\ell_p \sin\theta_p + (H_{pi} + H_{pi+1})\ell_p \cos\theta_p = -I_p\ddot{\theta}_p$$

Scissor:

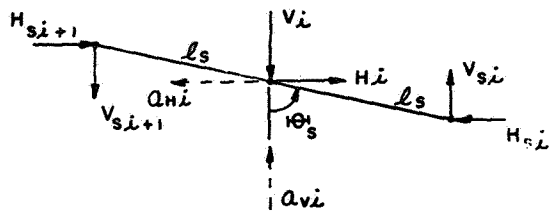

Dynamic Equations (rigid bars)

$$\Sigma F_x = m\bar{a}_x$$
$$\Sigma F_y = m\bar{a}_y$$
$$\Sigma M_G = I_G\alpha$$

Horizontal Forces

$$H_{si} - H_i - H_{si+1} = m_s a_{Hi}$$

Vertical Forces

$$V_{si} - V_i - V_{si+1} = m_s a_{Vi}$$

Moments

$$(V_{si} + V_{si+1})\ell_s \sin\theta_s - (H_{si} + H_{si+1})\ell_s \cos\theta_s = +I_s\ddot{\theta}_s$$

7.2 Acceleration of Link Centers (Joints)

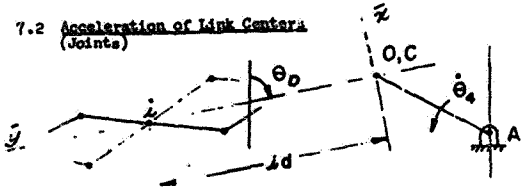

Pivot point A having no acceleration, the acceleration of the center, i, of each panel and acissor is found from the relative acceleration eq. $\bar{a}_i = \bar{a}_o + \bar{a}_{i/o}$

where

$$a_{i/o} = (a_{i/o})\text{ radial} + (a_{i/o})\text{ transverce} = (a_{i/o})_{\bar{y}} + (a_{i/o})_{\bar{x}}$$

and

$$a_o = (a_o)_{\bar{y}} + (a_o)_{\bar{x}}$$

A simple rotation to the original x and y axis will then yield the desired horizontal and vertical accelerations used in the above equations. That is,

$$(a_i)_y = a_{Hi} = [i\ddot{d} - id(\dot{\theta}_D)^2]\sin\theta_D + [id\ddot{\theta}_D + 2\dot{i}\dot{d}\dot{\theta}_D]\cos\theta_D + \ell_4\ddot{\theta}_4\cos\theta_4 - \ell_4(\dot{\theta}_4)^2\sin\theta_4,\ i = 0,1,2,3,4,5$$

$$(a_i)_x = a_{Vi} = -[i\ddot{d} - id(\dot{\theta}_D)^2]\cos\theta_D + [id\ddot{\theta}_D + 2\dot{i}\dot{d}\dot{\theta}_D]\sin\theta_D - \ell_4\ddot{\theta}_4\sin\theta_4 - \ell_4(\dot{\theta}_4)^2\cos\theta_4,\ i = 0,1,2,3,4,5$$

Driving Link (4 bar linkage):

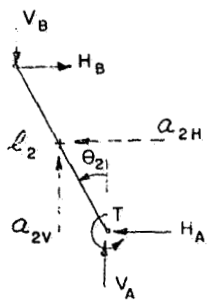

$$a_{2H} = \frac{\ell_2}{2}\ddot{\theta}_2 \cos\theta_2 - \frac{\ell_2}{2}(\dot{\theta}_2)^2 \sin\theta_2$$

$$a_{2V} = -\frac{\ell_2}{2}\ddot{\theta}_2 \sin\theta_2 - \frac{\ell_2}{2}(\dot{\theta}_2)^2 \cos\theta_2$$

$$\Sigma F_H = -H_B + H_A = m_2 a_{2H}$$

$$\Sigma F_V = -V_B + V_A = m_2 a_{2V}$$

$$\Sigma M_2 = (V_B + V_A)\frac{\ell_2}{2}\sin\theta_2 - (H_A + H_B)\frac{\ell_2}{2}\cos\theta_2 + T = I_2\ddot{\theta}_2$$

The driving forces for the slider mechanism are H_B and V_B. The driving force for the 4-bar linkage is the torque T; with reactions H_A and V_A.

7.3 Joint Accelerations - Deployed Position

General Conditions:

A. The individual members are considered as rigid.
B. The supports are considered to be stationary.
C. All members have zero angular velocities.
D. The x and y axis are parallel and perpendicular respectively to the vehicle axis.
E. Geometry is as defined by NASA in Table 1 obtained 7/10/67.
F. Angular acceleration of the driving link is specified.

Nomenclature:

a = acceleration, in./sec.^{2}

i = the i + 1 intersection of panel and scissor moving outboard

θ_2 = position of driving link from vertical, rad.

t = time, sec.

t_m = time to reach maximum velocity, sec.

k = minimum angular acceleration of driving link, rad./sec.^{2}

m = factor multiplying the minimum ang. acc.

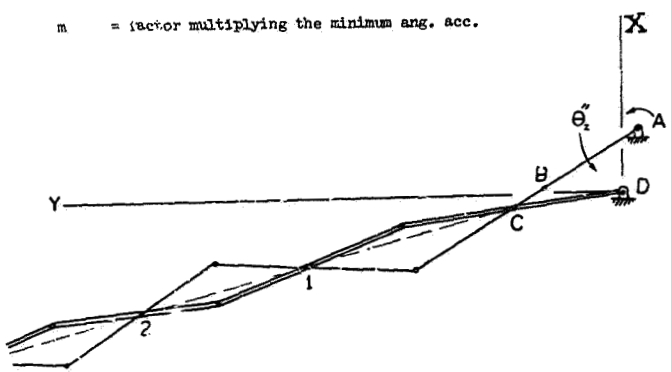

Accelerations:

$a_{Bx} = -43.1\ \ddot{\theta}_2$

$a_{By} = -21.2\ \ddot{\theta}_2$

$a_c = 0$

$a_{nx} = 86.3\ \dot{\theta}^2\ddot{\theta}_2$

$a_{ny} = 23.57\ \dot{\theta}^2\ddot{\theta}_2$

The angular acceleration of the driving link, $\ddot{\theta}_2$, are produced by the torque at A. Specifying one will determine the other. In this case consider the angular acceleration to be specified. A minumum angular acceleration, $(\ddot{\theta}_2)_{min.} = K$ is shown in Section 6 for deployment to a final angle θ_2. Furthermore, the above accelerations were used to calculate joint forces which were used in an existing (NASA) program for static deformations and forces. This program assumes elastic members, and the results show that deformations and forces were small in comparison with some maneuving conditions.

7.4 Typical Outboard Joint Reactions

A recurrence matrix is obtained from the equations given above for calculating joint reactions as follows:

$$\begin{bmatrix} 1 & 1 & 0 & 0 & 0 & 0 \\ 0 & 0 & 1 & 1 & 0 & 0 \\ \ell_p \cos\theta_p & 0 & \ell_p \sin\theta_p & 0 & 0 & 0 \\ 0 & -1 & 0 & 0 & 1 & 0 \\ 0 & 0 & 0 & -1 & 0 & +1 \\ 0 & 0 & 0 & 0 & -\ell_s \cos\theta_s & +\ell_s \sin\theta_s \end{bmatrix} \begin{bmatrix} H_{pi} \\ H_i \\ V_{pi} \\ V_i \\ H_{si} \\ V_{si} \end{bmatrix} = \begin{bmatrix} m_p a_{Hi} + H_{pi+1} \\ m_p a_{Vi} + V_{pi+1} \\ -I_p\ddot{\theta}_p - V_{pi+1}\ell_p \sin\theta_s + H_{pi+1}\ell_p \cos\theta_p \\ m_s a_{Hi} + H_{si+1} \\ m_s a_{Vi} + V_{si+1} \\ I_s\ddot{\theta}_s - V_{si+1}\ell_s \sin\theta_s + H_{si+1}\ell_s \cos\theta_s \end{bmatrix}$$

$$[C] \qquad [R] = [F]$$

Thus, in matrix notation the recurrence formula is

$$[C]^{-1}[C][R] = [C]^{-1}[F]$$

or

$$[R] = [C]^{-1}[F]$$

The matrix [C] is constant and reactions [R] are used in [F] for the next inboard scissor-panel pair.

7.5 Forces in Inboard Linkage:

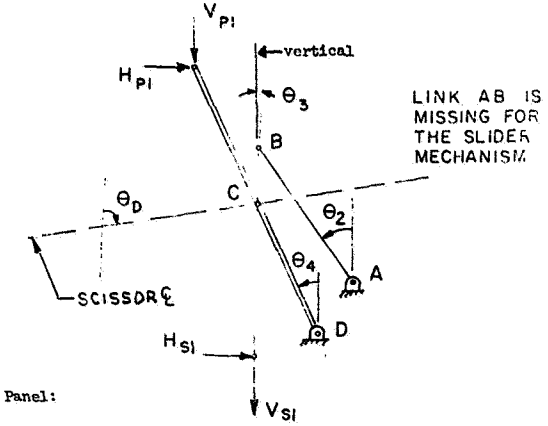

Inboard Panel:

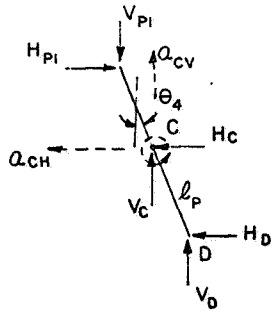

$$\Sigma F_H = -H_{pl} + H_C + H_D = m_p a_{cH}$$

$$\Sigma F_V = -V_{pl} + V_C + V_p = m_p a_{cV}$$

$$\Sigma M_{CG} = (H_{pl} + H_D)\ell_p \cos\theta_4 - (V_{pl} + V_D)\ell_p \sin\theta_4 = -I_P \ddot{\theta}_4$$

Inboard Scissor:

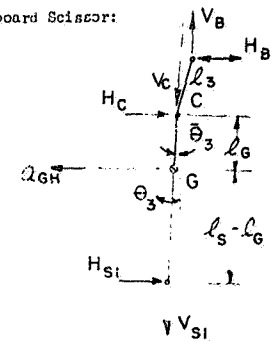

$\bar{\theta}_3 = \theta_3 - \delta$

δ = dog leg angle

$\bar{a}_G = \bar{a}_C + \bar{a}_{G/C}$

$\bar{a}_{G/C} = r\ddot{\theta}_3$ $\ddot{\theta}_3, r = \ell_G$

$+ r(\dot{\theta}_3)^2$ $\dot{\theta}_3$

$$\left.\begin{aligned} \overset{+}{\leftarrow} a_{GH} &= a_{CH} + \ell_G \ddot{\theta}_3 \cos\bar{\theta}_3 - \ell_G(\dot{\theta}_3)^2 \sin\bar{\theta}_3 \\ \overset{+}{\uparrow} a_{GV} &= a_{CV} + \ell_G \ddot{\theta}_3 \sin\bar{\theta}_3 + \ell_G(\dot{\theta}_3)^2 \cos\bar{\theta}_3 \end{aligned}\right\} \quad r = \ell_G$$

$$\Sigma F_H = H_B - H_C - H_{SI} = M_{SO} a_{GH}$$

$$\Sigma F_V = V_B - V_C - V_{SI} = M_{SO} a_{GV}$$

$$\Sigma M_G = -V_B[\ell_G \sin\bar{\theta}_3 + \ell_3 \sin\theta_3] - H_B[\ell_G \cos\bar{\theta}_3 + \ell_3 \cos\theta_3] + V_C \ell_G \sin\bar{\theta}_3 + H_C \ell_G \cos\bar{\theta}_3 - V_{SI}(\ell_S - \ell_G)\sin\bar{\theta}_3 - H_{SI}(\ell_S - \ell_G)\cos\bar{\theta}_3 = I_{SO}\ddot{\theta}_3$$

8. SCISSOR MECHANISM VIBRATION

Joint Reactions and Damping

Considering the scissor and panel mechanism as shown to be a cantilever beam of variable inertia,

$$E\frac{\partial^2}{\partial y^2}\left[I(y)\frac{\partial^2 x}{\partial y^2}\right] = W(y,t) - Y\frac{\partial^2 x}{\partial t^2}$$

is the equation of motion, where W is the external load

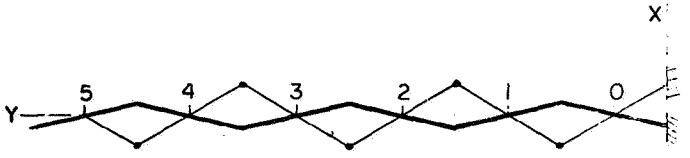

Rather than considering the mechanism as a distributed system, it is easier and sufficiently accurate to reduce it to a lumped system. Approximating this beam by a single equivalent lumped mass, $\bar{m}$, supported by a cantilever beam of zero mass and length ℓ as shown below, the dynamic loading and deformation are easily obtained. That is,

$$\bar{P} = \bar{m}\left.\frac{d^2x}{dt^2}\right|_{y=\ell}$$

$$\bar{\Delta} = \frac{P\ell^3}{3EI}$$

where EI is the equivalent stiffness.

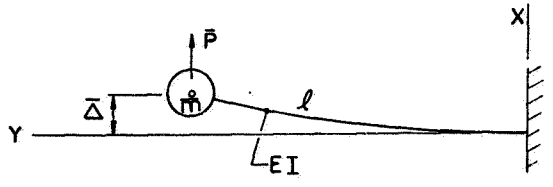

This approximation is accurate for certain dynamic studies.

A better approximation is to consider a multiple-mass system, as shown below. In this case each panel and scissor combination is replaced by a lumped mass at the intersection of panel and scissor. The loads P_n, n = 0, 1,2, ..., are due to the accelerations of each mass in the first vibration mode.

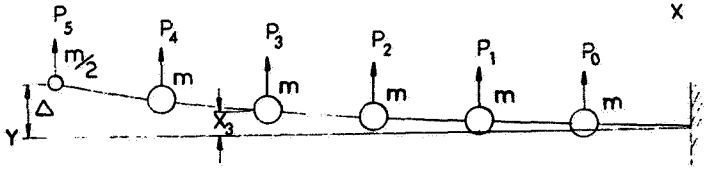

A static analysis of the scissor mechanism, with the loading due to the dynamic vibration, will yield the desirable reactions, R_i, at each joint as well as the maximum deflection of each mass. In the following paragraphs, reactions are calculated for three different loading conditions to form a comparison.

8.1 Loads and Joint Reactions

First, consider the reactions, R_i, at panel and scissor joints are due to the near sinusoidal vibration of the cantilever scissor-panel framework. Thus,

$$X_n = X(y_n,t) = X(y_n)T(t)$$

$$= \Delta\left[1 - \sin\frac{\pi(\ell - y_n)}{2}\right]T(t)$$

For sinusoidal time variation

$$T(t) = \sin \omega t$$

$$\omega = .6283 \text{ (estimated) rad./sec.}$$

Thus

$$\ddot{X}_n = -\omega^2\Delta[1 - \sin\frac{\pi(\ell - y_n)}{2}]\sin\omega t$$

The forces at the mass points are

$$P_n = m_n\ddot{X}_n = m_n\omega^2\Delta[1 - \sin\frac{\pi(\ell - y_n)}{2}]\sin\omega t$$

The maximum load occurs when $\omega t = \pi/2$ and

$$P_0 = m\omega^2\Delta[1 - \sin\frac{\pi \times 574.6}{2 \times 574.6}]$$

$$= m\omega^2\Delta[1 - .9901] = .0099\ m\omega^2\Delta$$

$$P_1 = m\omega^2\Delta[1 - \sin\frac{\pi}{2} \times \frac{443.1}{574.6}]$$

$$= m\omega^2\Delta[1 - .919] = .080\ m\omega^2\Delta$$

$$P_2 = m\omega^2\Delta[1 - \sin\frac{\pi}{2} \times \frac{311.6}{574.6}]$$

$$= m\omega^2\Delta[1 - .760] = .240\ m\omega^2\Delta$$

$$P_3 = m\omega^2\Delta[1 - \sin\frac{\pi}{2} \times \frac{220.1}{574.6}]$$

$$= m\omega^2\Delta[1 - .541] = .459\ m\omega^2\Delta$$

$$P_4 = m\omega^2\Delta[1 - \sin\frac{\pi}{2} \times \frac{104.6}{574.6}]$$

$$= m\omega^2\Delta[1 - .282] = .718\ m\omega^2\Delta$$

$$P_5 = \frac{\pi}{2}\omega^2\Delta = 1.000\ m\omega^2\Delta$$

System constants are

$$m = m_p + m_s = \frac{148}{386} + \frac{22}{386} = .409 + .058 = .467 \quad \frac{\text{lb. sec.}^2}{\text{in.}}$$

$$\omega^2 = .3945\ (\text{rad./sec.})^2$$

$$m\omega^2 = .1840 \quad \frac{\text{lb.}}{\text{in.}}$$

Secondly, from the information obtained from the sponsor on mode shapes, the normalized deflections are as follows for the first mode

$$x_0 = .0016$$

$$x_1 = .0627$$

$$x_2 = .202$$

$$x_3 = .443$$

$$x_4 = .693$$

$$x_5 = 1.000$$

Thus, the maximum inertia loads are

$$P_n = m_n\omega^2 x_n = .1840\ x_n,\ n = 1,2,3,4$$

which becomes, for the above x_n

$$P_0 = .000295$$

$$P_1 = .0115$$

$$P_2 = .0372$$

$$P_3 = .0761$$

$$P_4 = .1275$$

$$P_5 = .1840 \quad (m_n = \frac{m}{2},\ x_5 = 1.0)$$

Furthermore, based on a sinusoidal space variation, those loads which should produce a unit deflection at the outboard node (n = 5) are

$$P_0 = .091820$$

$$P_1 = .01596$$

$$P_2 = .0442$$

$$P_3 = .0845$$

$$P_4 = .1322$$

$$P_5 = .3920$$

From the Univac 1107 computer, the deflections were obtained using a program written by the sponsor. These results are shown in the table below with the given loading conditions above. From the equation for the inertia load

$$P_n = m_n\ddot{X}_n = m_n\omega^2 X_n$$

one can calculate the frequency to compare with the extimated value given previously as .6283 rad./sec. (0.10 cps.). That is, with the load, mass,

and displacement known at each joint

$$\omega^2 = \frac{P_n}{m_n x_n}$$

If the true mode shape has been used to calculate the loads P_n, the frequency will be independent of n (the joint used to calculate ω). These variations are obvious from the table. Furthermore, the maximum kinetic energy of each lumped mass is

$$E_n = \tfrac{1}{2} m_n \dot{x}_n^2 = \tfrac{1}{2} m_n \omega^2 x_n^2 = \tfrac{1}{2} P_n x_n$$

These values and their sum are also shown in the table.

From the table it is shown that the second set of loads, obtained from the normalized first mode shape, are more accurate when a comparison is made using the variation of ω^2. However, the sinusoidal deflection curve yields fairly accurate results also. Comparing results due to the first and last set of loads, which are both with a sinusoidal deflection curve, one can see that the system is fairly linear. Thus, multiplying each load by a factor proportionately increases the deflection.

The joint reactions for the second set of loads are shown below. These results were also obtained from the computer program furnished by the sponsor. Joint reactions, R_1, will be used in the following section to determine joint damping.

8.2 Joint Friction Damping

The following sketch represents a typical joint which undergoes an angle change.

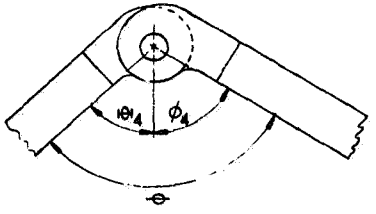

LUMPED MASS LOAD AND RESPONCE DATA

Mass Point (n)	P_n, lb.	x_n, in.	ω^2	E_n
0	.0099	.0000		0
1	.090	.1295	1.488	.00582
2	.240	.430	1.194	.05160
3	.459	.875	1.123	.2008
4	.718	1.446	1.063	.5191.
5	.500	2.054	1.043	.51350
Total E_n				1.29085
0	.00029	.0000	-	0
1	.01154	.0224	1.103	.0001293
2	.03720	.0751	1.060	.001398
3	.07610	.1537	1.060	.00584
4	.1275	.255	1.069	.01625
5	.0920	.363	1.085	.01671
Total E_n				.04033
0	.00182	.0000	-	0
1	.01656	.0235	1.507	.0001945
2	.0442	.0786	1.202	.001737
3	.0845	.1602	1.129	.00678
4	.1322	.265	1.068	.01753
5	.0920	.377	1.044	.01733
Total E_n				.04357

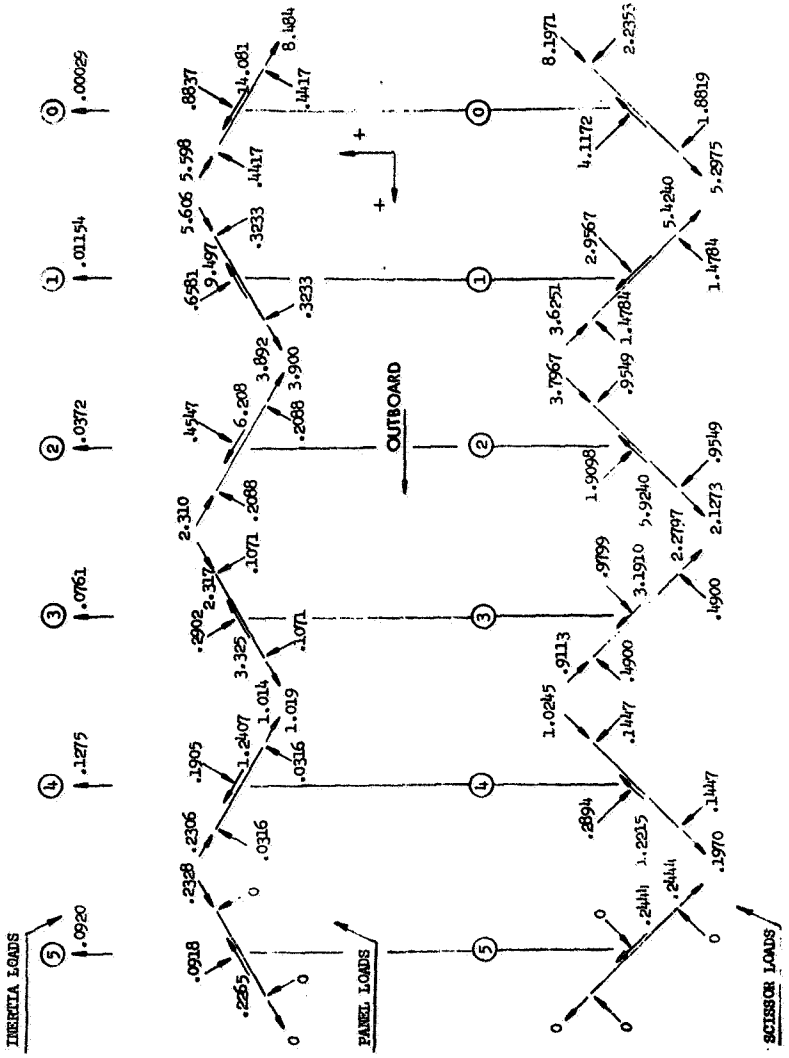

Work Done = Force x Distance = Moment x Angle Change

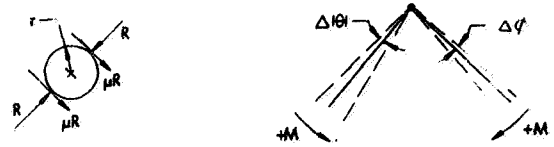

When relative motion occurs between parts

$$\text{Moment} = \mu\, r\, R$$

A typical moment versus rate of angle change curve is shown below.

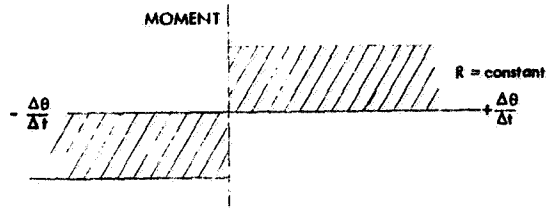

The direction of the moment depends on whether the angle is increasing or decreasing.

The amplitude of the angle change in one cycle is

$$\Delta\theta_i = \Delta\phi_i + \Delta\theta_i = \Delta(\phi + \theta)_i$$

Thus, for a constant joint force

$$\text{Work Done/Cycle} = +\mu r R \Delta\theta$$

for each joint in the mechanism. In general, the joint force will change with time or angular position of members. Thus,

$$\text{Work Done/Cycle} = +\mu r \int_{-\Delta\theta}^{\Delta\theta} R\, d\theta$$

The total energy of vibration is

$$E = \sum_{n=1}^{r} \tfrac{1}{2} m_n v_n^2 = \tfrac{1}{2} \int_0^{\ell} (\dot{x}^2 + \dot{y}^2)\gamma \, dy$$

with r masses. Also, with a sinusoidal driving force, $F = A \sin \omega t$,

$$\text{Work Done/Cycle} = \int F \, dx$$

With joint forces varying sinusoidally redefine joint reactions as

$$R_i = R_i \left|\sin \omega t\right|$$

Thus, with k joints

$$\Delta W = \text{Work Done/Cycle} = -\sum_{i=1}^{k} \mu r_i \int_{\text{cycle}} R_i \left|\sin \omega t\right| \theta_i$$

$$= -\sum \mu r_i R_i \int_{\text{period}} \left|\sin \omega t\right| \left(\frac{d\theta}{dt}\right) (\operatorname{sgn} \dot{\theta}) dt$$

When periodic motion occurs as shown below

$$\theta = \theta_o + \Delta\theta_i \sin \omega t$$

$$\frac{d\theta}{dt} = + \Delta\theta_i \, \omega \cos \omega t$$

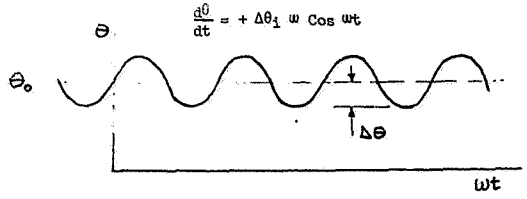

Also, as shown above

$$\Delta\theta_i = \Delta(\phi + \Theta)_i$$

the angular change between connected members.

Starting from a relaxed position (t = 0)

$$\theta = \theta_o + \Delta\theta \sin \omega t = \theta_o$$

$$M = \mu_R R_i \left|\sin \omega t\right| (\operatorname{sgn} \dot{\theta}) = 0$$

The moment then varies sinusoidally but is discontinuous depending on whether the joint angle is decreasing or increasing. Thus, the moment varies as shown below.

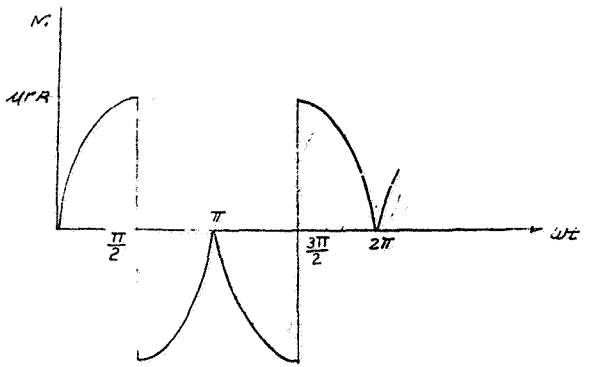

With the normalized time

$$\tau = \omega t$$

$$d\tau = \omega dt$$

$$\frac{d\theta}{d\tau} = \frac{1}{\omega} \frac{d\theta}{dt}$$

$$\operatorname{sgn} \frac{d\theta}{dt} = \operatorname{sgn} \frac{d\theta}{d\tau}$$

and the work done per cycle becomes

$$\Delta W = -\sum \mu r_i \, R_i \int_{\text{period}} \left|\sin \tau\right| \left(\operatorname{sgn} \frac{d\theta}{d\tau}\right) \frac{d\theta}{d\tau} \, d\tau$$

From above

$$\frac{d\theta}{d\tau} = \Delta\theta_i \cos \tau$$

which is positive $0 < \tau < \pi/2$ and $3\pi/2 < \tau < 2\pi$ and negative $\pi/2 < \tau < 3\pi/2$.

Therefore

$$\Delta W = -\sum \mu r_i \, R_i \, \Delta\theta_i \left[\int_0^{\pi/2} \left|\sin \tau\right| \cos \tau \, d\tau \right.$$

$$\left. - \int_{\pi/2}^{\pi} \left|\sin \tau\right| \cos \tau \, d\tau - \int_{\pi}^{3\pi/2} \left|\sin \tau\right| \cos \tau \, d\tau + \int_{3\pi/2}^{2\pi} \left|\sin \tau\right| \cos \tau \, d\tau \right]$$

Now

$$\text{Cos } \tau |\text{Sin } \tau| = \tfrac{1}{2} |\text{Sin } 2\tau| \text{ sgn } (\cos \tau)$$

$$\tfrac{1}{2} \int_a^b |\text{Sin } 2\tau \, d\tau = \tfrac{1}{4} \text{ sgn } (\cos \tau) |\cos 2\tau \Big]_a^b \Big|$$

Evaluating each integral

$$\Delta W = -\sum 2\mu r_i \, R_i \Delta\theta_i \qquad (1)$$

Components of the joint reactions, R_i, are given in the previous section. The joint angle changes, $\Delta\theta_i$, are obtained from the analysis of each panel and scissor linkage with their assumed loading condition. The angle changes of each component where they join another component is of interest. These are obtained as a superposition of angle changes due to (1) the uniform inertia load, (2) the joint reaction at the center of each panel, and (3) the eccentric compression load. These three cases are shown below.

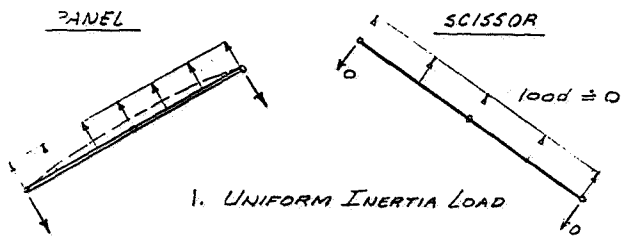

1. Uniform Inertia Load

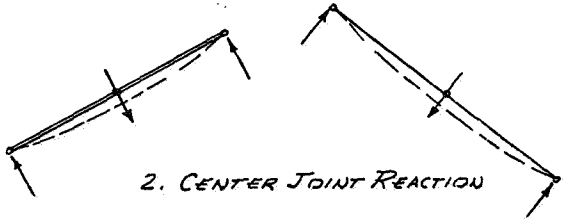

2. Center Joint Reaction

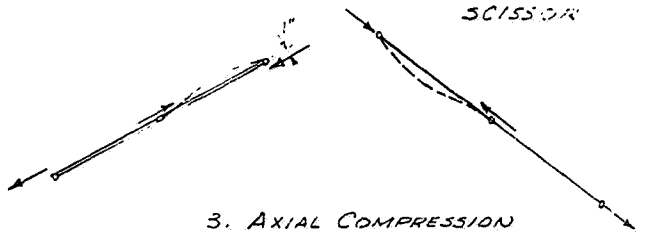

3. Axial Compression

Some of the assumptions made in obtaining the angle changes are obvious from the sketches. The uniform inertia load on the scissor link produces a small angle change in relation to the center joint reaction and has been neglected. The axial load causes angle changes in only the compression half of each component. Furthermore, the total angle change is the algebraic sum of each of the three conditions shown. Note that the small moments at each joint have been neglected when computing the angle changes and joint reactions.

The table shown below indicates the angle changes at the end of each member for the three loading cases shown above. The angle changes at the intersection of each panel and scissor is zero due to the assumed symmetry of the loading. Angle changes due to the entire mechanism being in a deformed state (all members considered to be straight) were found to be insignificant in comparison to those due to flexability of the members.

The desired angle changes are the algebraic sum of those due to each loading case for each member that is connected at a particular joint. This sum or resultant is shown for each joint on the figure below.

NOTES: (1) Members above the neutral axis have axial compression for upward loading

(2) Angle changes are for inertial loads shown previously (upward)

(3) The angles decrease for joints above the neutral axis and increase for others

ANGLE CHANGE AMPLITUDES $\Delta\theta_i$ IN RADIANS X10^{-4}

END JOINT ANGLE CHANGES FOR 3 LOADING CASES (Radians x 10^{-4})

Center Point P	PANEL Case I*	PANEL Case II	PANEL Case III*	SCISSOR Case II	SCISSOR Case II & III
0	-.00014	.61424	-.16792	1.8674	3.7347
1	-.01337	1.14655	-.40177	2.3820	4.7640
2	-.04310	.79228	-.16552	2.0747	4.1494
3	-.06816	.20623	-.16552	1.8820	3.7641
4	-.14777	.33190	-.01670	.55	1.1115
5	-.10059	.15993	-.02389	0.0	0.0

* minus sign indicates an angle change opposite to the resultant angle change.

Note that the angle changes are for the maximum upward inertia loading. As indicated above, the angles decrease from the angles shown through zero to some angle for the maximum downward loading. Thus, the angles shown are taken as the amplitude $\Delta\theta_i$ of the periodic angle change.

As shown by the energy loss Eq. (1), it is also necessary to know the radius r_i of the joint connectors. The different types of connectors are shown below.

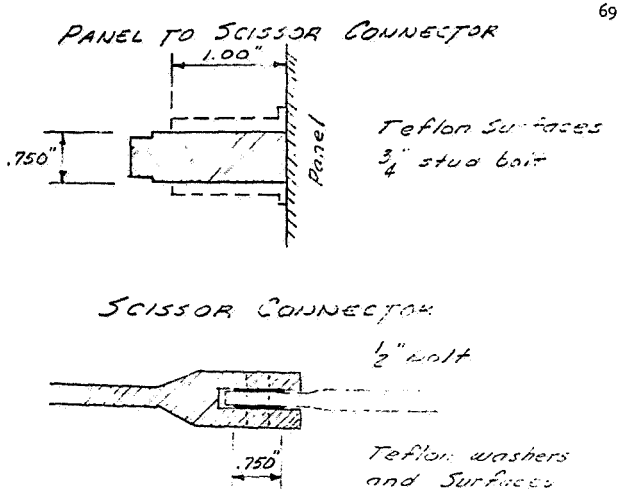

The joint connector radii, r_i, used for the inboard panel is .344 in., for the outboard panels is .265 in., and for all scissors is .313 in. The panel to scissor joint connector radius of .750 in., is not used because no angle change occurs at these joints.

The coefficient of friction, μ, depends on the material in contact at the sliding surfaces. For most surfaces in contact a Teflon coating is provided. The coefficient of friction for these surfaces is approximately 0.10. For some contact surfaces a combination of woven glass and Teflon, called Fibroid, has been proposed. For Fibroid surfaces in contact at 20°c the coefficient of friction is 0.05. For the purposes of this study μ = 0.10 will be used for all joints; realizing that the energy loss per cycle is directly proportional to μ.

All information is now available for calculating the energy loss per

cycle for each joint, which can be summed to give total energy loss per cycle. The following table summarizes this procedure.

ENERGY LOSS PER CYCLE, IN LB./CYCLE X 10^{-4} (μ = 0.10)

Joint	r_i, in.	R_i, lb.	Moment $\mu r_i R_i$, in. lb.	$\Delta\theta_i$, rad. X 10^{-4}	ΔW_i
S0	.313	8.480	.265424	3.735	[illegible]
S1	.313	[illegible]	.176563	4.249	[illegible]
S2	.313	[illegible]	.12[illegible]6	8.91[illegible]	[illegible]
S3	.313	2.359	.073812	3.957	[illegible]
S4	.313	1.037	.032[illegible]	4.876	.[illegible]
S5	.313	0.244	.0076[illegible]	0.[illegible]6	.[illegible]
P0	.344	9.360	.322[illegible]	0.[illegible]6	.[illegible]
P1	.344	6.475	.222740	1.209	.[illegible]
P2	.265	4.425	.117263	1.882	.[illegible]
P3	.265	2.550	.067575	0.836	.[illegible]
P4	.265	1.069	.028329	0.692	.[illegible]
P5	.265	0.233	.006175	0.197	.002433
0	.750	14.110	1.058250	0.0	0.0
1	.750	9.525	.714375	0.0	0.0
2	.750	6.225	.466875	0.0	0.0
3	.750	3.340	.250500	0.0	0.0
4	.750	1.237	.094275	0.0	0.0
5	.750	0.244	.018300	0.0	0.0
all			SUM = ΔW = .00081233		

Finally, the energy loss per cycle is .000812β in. lb. per cycle compared to the total energy per cycle of .04033 in lb. per cycle obtained previously. The ratio of energy loss to total energy as a percentage is

$$\Delta W/W = \frac{.000812\beta}{.04033} \times 100 = 2.02\% \qquad (3)$$

For practical considerations this percentage is proportional to the amount of the initial amplitude that is lost each cycle. The following concerns itself with the loss in amplitude as related to energy loss per cycle.

From Eq. (1) page 65 the energy loss is a function of joint reaction and angle change. Joint reactions are directly proportional to the amplitude of each mode. That is, a proportionate increase in the amplitude of each mass results in a proportionate increase in the inertia forces and corresponding reactions for the linear system. Furthermore, angle changes are also increased proportionately. The result is that energy loss is proportional to modal amplitude squared. Thus

$$\Delta W \propto A^2$$

where A is the modal amplitude. Previous investigations by this author have shown that the modal damping term in the modal differential equation of motion which yields energy loss proportional to amplitude squared has the form

$$\text{Damping Force} = C_o|Q|[\operatorname{sgn} \frac{dQ}{dt}]$$

where $Q = A \sin \omega t$ is the modal displacement. That is, the energy loss per cycle becomes

$$\int_{\text{cycle}} C_o|Q|[\operatorname{sgn} \dot{Q}]dQ = 2C_o A^2$$

It has been previously shown by this author (NASA TN D-3861) that the ratio of energy loss to total energy for a damping force as shown is

$$\Delta W/W = \frac{4C_o}{M\omega^2}.$$

Also, it has been shown that critical damping (no oscillation) would occur when

$$C_o = C_{oc} = M\omega^2$$

A damping factor ζ is the ratio of actual damping to critical damping, or

$$\zeta = \frac{C_o}{C_{oc}} = \frac{C_o}{M\omega^2} = \frac{\Delta W}{4W}$$

Thus from Eq. 2, page 71.

$$\zeta = \frac{\Delta W}{4W} = .505\% \qquad (3)$$

or about one half of one percent.

It may be desirable to have the modal equation of motion for the first mode. This can be expressed in terms of the modal displacement, Q, as

$$M\ddot{Q} + C_o|Q|[\operatorname{sgn} \dot{Q}] + KQ = 0$$

for the free vibration case. Simplifying and using parameters previously defined.

$$\ddot{Q} + \frac{\zeta M\omega^2}{M}|Q|[\operatorname{sgn} \dot{Q}] + \frac{K}{M}Q = 0$$

or

$$\ddot{Q} + \zeta\omega^2|Q|[\operatorname{sgn} \dot{Q}] + \omega^2 Q = 0 \qquad (4)$$

From the above results, the first mode system parameters are

$$\zeta = .00505$$
$$\omega^2 = 1.075 \qquad (5)$$

Starting with some initial displacement $Q(t = 0) = Q_o$ and initial velocity $\dot{Q}(t = 0) = \dot{Q}_o$ the modal displacement Q may be obtained.

8.3 Summary and Conclusions

The deployed scissor and panel mechanism was analyzed as a lumped parameter system. The first mode shape of the free vibration was assumed and justified by analysis. A sinusoidal mode shape was also investigated. An accurate first mode frequency was obtained. The inertia forces from the first mode vibration were used to calculate joint forces for the mechanism.

Of primary interest was the system or modal damping from the friction in the joints. This was obtained from an energy approach by considering energy losses due to joint moments times angle changes. A ratio of energy losses to total energy is used to calculate the damping factor as a percentage of critical damping. Finally, a modal equation of motion for the first mode was obtained with known coefficients.

It is shown that the sinusoidal approximation of the first mode shape is reasonably accurate. The total energy of the sinusoidal mode is only 8% higher than that of the true mode and the frequencies differ by only 12%. Using the true model shape the first mode frequency is 1.037 rad/sec. or 0.165 cps.

The energy loss per cycle is that due to friction in the joints and the material damping. The material damping was considered to be small due to the low stress condition in most of the members. The joint friction and slippage cause work to be done in the joints each cycle of vibration. This was found to be directly proportional to the coefficient of friction, radius of the joint connector, amplitude of the joint reaction, and the amplitude of the joint angle change. For a vibration mode (first mode) with a total energy of .04033 inch pound the energy loss was .000813 inch pound, or 2.02 percent of the total.

The joint moments due to friction were found to be small in comparison to the moments in the members due to joint reactions. For the panels, joint moments were approximately 10% of the maximum moment due to joint reactions, and for the scissors it was approximately 5%. This shows that neglecting joint moments when computing joint forces and deflections is a reasonable simplification.

The energy loss is shown to be a function of the vibration amplitude squared. This type of energy loss is known to be that which occurs when

the damping force is a function of amplitude, with the sign of the velocity. That is, damping force is proportional to $|Q|$ times $[\operatorname{sgn} \dot{Q}]$, where Q is the modal displacement. Furthermore the percent of critical damping for this damping term was found to be $\zeta = .505\%$, or about one half of one percent of critical. With the frequency given above, this indicates about 7 minutes and 70 cycles before the amplitude of the first mode reduces to 10% of its initial value.

From the above information the equation of motion for the first mode of vibration becomes $\ddot{Q} + \zeta_w^2 |Q| [\operatorname{sgn} \dot{Q}] + w^2 Q = 0$. This is for the free vibration and, with appropriate initial conditions, can be solved for the response.

To extend this study to provide a more complete analysis and to suggest methods for increasing damping, the following items are important. First, this general analysis can be used for higher modes of vibration and to the scissor-panel mechanism in a semi-deployed configuration. Secondly, the analysis can be extended to include material damping as the member stresses can be found from given forces and moments. Thirdly, one can add a clamping pressure at the scissor joints which would cause additional friction in those joints and increase the energy loss per cycle. Finally, by extending the inboard panel or scissor at the support points a dash-pot or friction clutch could easily be added to increase energy losses.

Chapter III

RESPONSE OF SINGLE-DEGREE OF FREEDOM SCISSOR STRUCTURE

1. INTRODUCTION

The scissor structure shown in Fig. 1 may be treated as a single degree of model as shown in Fig. 2. This model consists of a massless beam with a single mass attached at the end. The usefulness of this approximation appears, particularly when motion of the right end, (which is attached to the spacecraft), is considered.

2. VALIDITY OF APPROXIMATION

An idea of the accuracy of the single degree of freedom model may be obtained by comparing with the exact solution for the first mode of a cantilever beam. (The cantilever beam being absolutely fixed at its base.)

Following Tong. (Ref. 1), the equation for the vibration of a cantilever beam is:

$$\frac{EI}{\rho A}\frac{\partial^4 w}{\partial x^4} + \frac{\partial^2 w}{\partial t^2} = 0 \qquad (1)$$

E - Young's modulus
I - moment of inertia of cross-sectional area
ρ - mass density
A - cross-sectional area
t - time
w - deflection from an absolutely fixed reference line

Equation (1) may be solved, using $w = \sin \omega t\, r(x)$. For a cantilever beam, this leads to [1]:

$$r = \sinh \beta x - \sin \beta x + \gamma(\cosh \beta x - \cos \beta x) \qquad (2)$$

$$r\big|_{x=L} = \gamma(\cosh \beta L - \cos \beta L) + \sinh \beta L - \sin \beta L \qquad (2\text{-b})$$

$$\left.\frac{d^2 r}{dx^2}\right|_{x=0} = 2\gamma\beta^2 \qquad (2\text{-c})$$

$$\left.\frac{d^3 r}{dx^3}\right|_{x=0} = 2\beta^3 \qquad (2\text{-d})$$

where:

$$\beta^4 = \frac{\rho A \omega^2}{EI} \qquad (3)$$

$$-\gamma = \frac{\sinh \beta L + \sin \beta L}{\cosh \beta L + \cos \beta L} \qquad (4)$$

The frequency equation is:

$$\cos \beta L \cosh \beta L = -1 \qquad (5)$$

For the first mode, the root is:

$$\beta L = 1.875$$

Hence, the frequency:

$$\omega = \sqrt{\frac{EI}{\rho A}}\,\beta^2 = \sqrt{\frac{EI}{\rho A}}\,\frac{(1.875)^2}{L^2} \qquad (6)$$

The equation of motion of the approximate model is

$$m^1 \ddot{\delta} + k\delta = 0 \qquad (7)$$

This is true if the reference line (from which the deflection δ of the left end is measured), is fixed. This is the case here, since we are considering the right end fixed.

In Eq. (7), m^1 is the mass of the particle at the left, k is the stiffness of the massless beam.

But, for a massless cantilevered beam

$$\frac{1}{k} = \frac{L^3}{3EI} \qquad (8)$$

The natural frequency of the model is then

$$\omega = \sqrt{\frac{3EI}{m^1 L^3}} \qquad (9)$$

This frequency is set equal to first mode frequency (Eq. 6).

$$\sqrt{\frac{EI}{\rho A}}\,\frac{(1.875)^2}{L^2} = \sqrt{\frac{3EI}{m^1 L^3}} = \sqrt{\frac{EI}{mL^3}}\,(1.875)^2$$

Solving

$$m^1 = \frac{3m}{(1.875)^4} = 0.243m = m^1 \qquad (10)$$

Here m is the total mass of the continuous beam. Equation (10) tells us what value to use for m^1 in order to make the frequencies the same. To

compare the beam and the approximate model, we compare the two ratios M_a/M_e and V_a/V_e at the support for some deflection at the free end.

M_a - moment for the approximation

M_e - moment for the exact case

V_a - vertical shear force for the approximatic

V_e - vertical shear force for exact cas

Now:

$$M = EI\, w'', \quad V = EI\, w \quad \text{(exact)}$$

$$\delta_e = Y(\cosh \beta L - \cos \beta L) + \sinh \beta L - \sin \beta L \tag{11}$$

Then from equations (2-c) and (11)

$$\frac{\delta_e}{M_e} = \frac{1}{EI\beta^2} \frac{(\cosh \beta L \sin \beta L - \cos \beta L \sinh \beta L)}{(\sinh \beta L + \sin \beta L)}$$

Also, using Eq. (8):

$$\frac{\delta_a}{M_a} = \frac{L^2}{3EI} \tag{12}$$

Then

$$\frac{M_a}{M_e} = \frac{3}{\beta^2 L^2} \frac{\cosh \beta L \sin \beta L - \cos \beta L \sinh \beta L}{\text{Sinh } \beta L + \sin \beta L}$$

$$= \frac{3}{(1.875)^2} \frac{(3.34)(.956) + (.292)(3.19)}{3.19 + 0.956}$$

$$\frac{M_a}{M_e} = 0.85 \tag{13}$$

Similarly: (since $V_a = \delta_a\, 3EI/L^3$)

$$\frac{V_a}{V_e} = \frac{1}{\beta^3 L^3} \frac{\cosh \beta L \sin \beta L - \cos \beta L \sinh \beta L}{\text{Sinh } \beta L + \sin \beta L}$$

$$= \frac{3}{(1.875)^3}\ 0.993 = 0.45 \tag{14}$$

So fairly good information is obtained for moments, but not for shear forces.

We will consider these results to indicate that a fairly accurate

representation for transient analyses and deflections resulting from motions of the base of the beam.

CALCULATION OF THE STIFFNESS

The stiffness of the scissor structure, k, may be computed by applying a unit load T, as shown in Fig. 1 and calculating the deflection at the point of load application. All the members in the structure are pin-connected and deform due to both bending (beam action) and stretching (tensile action). It is shown later, that deflections due to stretching are small compared to those due to bending. Hence, interaction between the two effects may be neglected at the outset. Figure 3 displays the forces acting on the individual members. The scissor arms are longer than the panel arms.

θ - angle the scissor makes with the horizontal (measured from a straight line joining pin connections)

ψ - angle the panel makes with the horizontal (measured from a straight line joining pins)

h - height of panel (or scissor)

ℓ - length of the panel (or scissor)
We assume here that these are almost the same and the difference may be neglected in many equations

$p - \frac{h}{\ell}$ (called panel angle)

The forces shown in Fig. 3 assume that the structure is undeflected. This, then, yields the stiffness k, for small deflections only. As long as the end deflection does not become too large, it is probably a satisfactory value. Further, it is assumed that $\cos(\theta + \psi) = 1$; $\sin(\theta + \psi) = \theta + \psi$.

DEFLECTION OF BEAM

Since the individual beam which makes up a structure has simple support at three points (its two ends, and the centre) the deflection characteristic may be obtained from a single number Δ_B in Fig. 4-c.

This number is due to the sum of three forces. P in the middle, M_1, at the left end, and M_2 at the right end.

Due to the couple M at the end, the deflection at the center is:

$$\Delta = \frac{M\ell^2}{16EI} \tag{15}$$

Due to the concentrated load P at the center, the deflection is:

$$\Delta = \frac{P\ell^3}{48EI} \tag{16}$$

Hence, the total deflection at the center, due to the combined action of M_1, M_2, and P is:

$$\Delta_T = \frac{\ell^2}{48EI}[P\ell - 3(M_1 + M_2)] \tag{17}$$

Then the deflection Δ_B, with reference to a straight line passing through the right end and the center of the beam is:

$$\Delta_B = \frac{\ell^2}{24EI}[P\ell - 3(M_1 + M_2)] \tag{18}$$

$$= \frac{\ell^3}{EI}\frac{1}{\theta+\psi}Q$$

where

$$Q = \frac{1}{24}[P - \frac{3}{\ell}(M_1 + M_2)](\theta + \psi) \tag{19}$$

Then, values of Q are:

No.	Panels	Scissors	
4 :	$\frac{1}{6}(\psi - \frac{p}{2})$	$\frac{1}{6}(\theta - \frac{p}{2})$	(20-a)
3 :	$\frac{1}{3}(\psi - \frac{p}{2})$	$\frac{1}{3}(\theta - \frac{p}{2})$	(20-b)
2 :	$\frac{1}{2}(\psi - \frac{p}{2})$	$\frac{1}{2}(\theta - \frac{p}{2})$	(20-c)
1 :	$\frac{2}{3}(\psi - \frac{p}{2})$	$\frac{2}{3}(\theta - \frac{p}{2})$	(20-d)

4.1 Numerical Values of Beam Deflections

The moment of inertia of the cross section is:

$$I = 2[\frac{1}{12}h^3 + w(\frac{h}{2})^2]t \tag{21-a}$$

$$I = \frac{h^2t}{6}(h + 3w) \tag{21-b}$$

e.g. - take h = 2"; w = 1"; t = $\frac{1}{16}$"; I = 0.208 in^4. The cross sectional area of the cross section is:

$$A = 2(h + w)t = 0.375\ in^2$$

Using the numerical values:

$$\psi = 4^\circ = 0.070 \text{ radians}; \quad \theta = 26^\circ = 0.453 \text{ radians}, \quad \ell = 100"$$

$$p = \frac{h}{\ell} = \frac{2}{100} = 0.02 \text{ radians}; \quad E = 10 \times 10^6\ \#/in^2$$

Then using equations (18) and (20), we obtain the following beam deflections Δ_B:

No.	Panel	Scissor	
4	0.00914	0.0672	(22-a)
3	0.0182	0.134	(22-b)
2	0.0273	0.201	(22-c)
1	0.0365	0.268	(22-d)

4.2 Numerical Values of Tensile Deflections

From Fig. 3, we see that the members are all in tension above the centerline of the panel and all in compression below the centerline.

We will asume that both scissors and panel have the same sectional properties. Then the stretch (or compression) in any half member is:

$$s = \frac{\ell}{2AE}F$$

where F denotes the tension (or compression) in the half member.

$$\frac{\ell}{2AE} = \frac{100}{2 \times .375 \times 10^7} = 1.33 \times 10^{-5}\ \text{in./\#}.$$

In a later section, we will show that the downward deflection due to the tensile stretch is negligible, compared to the beam deflection.

Stretch - inches

No.	Panel	Scissor	
1	17.8×10^{-5} (s3)	22.9×10^{-5} (s1)	(23-a)
2	17.8×10^{-5} (s1)	13 $\times 10^{-5}$ (s3)	(23-b)
3	7.6×10^{-5} (s3)	13 $\times 10^{-5}$ (s1)	(23-c)
4	7.6×10^{-5} (s1)	2.6×10^{-5} (s3)	(23-d)
5		1.3×10^{-5} (s1)	

The compression may be obtained by interchanging the panel and scissor columns, above. The meaning of s1 and s3 is explained in the next section.

Deformation of a Structural "Element"

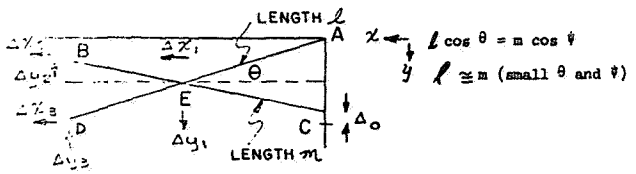

The structural "element" consists of 2 flexible members, one of length "ℓ", and one of length "m". Pinned together at the center and pinned to other structural elements at the ends (pts. A,C,B, and D). For beam action in a plane, the total deformation may be characterized by three quantities.

(1) The drop, Δy_2 of point B (due to both elastic deformation and due to an initial lowering Δ_o of point C on the right side).

(2) The relative extension $\Delta y_3 - \Delta y_2 = \Delta_1$ of the left side. (This will be an input into the next structural "element" - equivalent to Δ_o for the present element.

(3) The rotation of the left side relative to the right side

$$\varphi = \frac{\Delta x_2 - \Delta x_3}{\frac{\ell}{2} \sin\theta + \frac{m}{2} \sin\psi}$$

Assumptions will be stated as we go along

Consider triangle AEC.

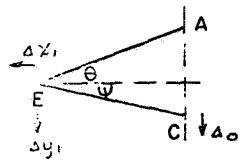

s1 - Stretch in AE (tensile force)
s2 - stretch in EC

$\delta\theta$, $\delta\psi$, changes in θ and ψ due to both initial drop Δ_o and the elastic stretches s1 and s2.

Assumption - Assume that s2 = -s1 (true if tension in EA is negative of compression in EC) and if EA and EC have the same elastic properties in tension.

Geometric Compatibility - x direction: $(s_1 + \frac{\ell}{2})\cos(\theta + \delta\theta) =$

$$(s_2 + \frac{m}{2})\cos(\psi + \delta\psi) \qquad (24)$$

Assumption - $\delta\theta \ll \theta \qquad \delta\psi \ll \psi$

$$-s_1 \ll \frac{\ell}{2} \qquad \ll \frac{m}{2}$$

Then (24) becomes: (with $s_1 = -s_2$)

$$s_1(\cos\theta + \cos\psi) = \delta\theta\frac{\ell}{2}\sin\theta - \delta\psi\frac{m}{2}\sin\psi \qquad (24)'$$

y direction:

$$(s_1 + \frac{\ell}{2})\sin(\theta + \delta\theta) + (s_2 + \frac{m}{2})\sin(\psi + \delta\psi) = \frac{\ell}{2}\sin\theta + \frac{m}{2}\sin\psi + \Delta_o \qquad (25)$$

Then:

$$s_1(\sin\theta - \sin\psi) - \Delta_o = -\delta\theta\frac{\ell}{2}\cos\theta - \delta\psi\frac{m}{2}\cos\psi \qquad (25)'$$

Equations (24)' and (25)' may be solved for $\delta\theta$, $\delta\psi$:

$$\delta\theta = \frac{2s_1}{\ell}\,\frac{1 + \cos(\theta + \psi)}{\sin(\theta + \psi)} + \frac{2\Delta_o \sin\psi}{\ell\sin(\theta + \psi)} \qquad (26)$$

$$\delta\psi = \frac{-2s_1}{m}\,\frac{1 + \cos(\theta + \psi)}{\sin(\theta + \psi)} + \frac{2\Delta_o \sin\theta}{m\sin(\theta + \psi)} \qquad (27)$$

For θ and ψ small:

$$\delta\theta = \frac{4s_1}{\ell(\theta + \psi)} + \frac{2\psi\Delta_o}{\ell(\theta + \psi)} \qquad (26)'$$

$$\delta\psi = \frac{4s_1}{m(\theta + \psi)} + \frac{2\theta\Delta_o}{m(\theta + \psi)} \qquad (27)'$$

Also:

$$\Delta x_1 = (\frac{\ell}{2} + s_1)\cos(\theta + \delta\theta) - \frac{\ell}{2}\cos\theta \qquad (28)$$

$$\Delta y_1 = (\frac{\ell}{2} + s_1)\sin(\theta + \delta\theta) - \frac{\ell}{2}\sin\theta \qquad (29)$$

For θ and ψ small:

$$\Delta x_1 = \frac{2s_1(\psi - \theta)}{\theta + \psi} - \frac{\Delta_o\,\psi\theta}{\theta + \psi} \qquad (28)'$$

$$\Delta y_1 = \frac{2s_1}{\theta + \psi} + \frac{\Delta_o\psi}{\theta + \psi} \qquad (29)'$$

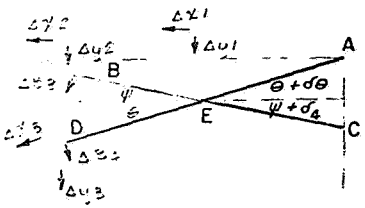

Entire element -

Δ_{b3} and Δ_{b4} are beam deflections relative to the straight lines AE' and C'E', where C' and E' are the new positions of E and C.

s_3 - stretch of BE

s_4 - stretch of DE

We have:

$$\Delta x_2 = (\frac{m}{2} + s_3)\cos(\psi + \delta\psi) - \frac{m}{2}\cos\psi + \Delta x_1 + \Delta_{b3}\sin\psi \qquad (30)$$

$$\Delta x_3 = (\frac{\ell}{2} + s_4)\cos(\theta + \delta\theta) - \frac{\ell}{2}\cos\theta - \Delta_{b4}\sin\theta + \Delta x_1 \qquad (30)'$$

Making the same assumptions as before plus $s_4 = -s_3$

$$\Delta x_2 - \Delta x_3 = 2s_1 + 2s_3 + \Delta_{b3}\psi + \Delta_{b4}\theta \qquad (31)$$

Then rotation of left end

$$\mathcal{R} = \frac{2s_1 + 2s_3 + \Delta_{b3}\psi + \Delta_{b4}\theta}{\frac{\ell}{2}(\theta + \psi)} \qquad (32)$$

Now, $\Delta y_2 = \Delta y_1 + \frac{m}{2}\sin\psi - (\frac{m}{2} + s_3)\sin(\psi + \delta\psi) + \Delta_{b3}\cos\psi$ (33)

$$\Delta y_2 = \frac{4s_1}{\theta + \psi} - s_3\psi + \frac{\Delta_o(\psi - \theta)}{\theta + \psi} + \Delta_{b3} \qquad (33)'$$

Also: $\Delta y_3 = \Delta y_1 + (\frac{\ell}{2} + s_4)\sin(\theta + \delta\theta) - \frac{\ell}{2}\sin\theta + \Delta_{b4}\cos\theta$

$$\Delta y_2 = \frac{4s_1}{\theta+\psi} + s_4\theta + \frac{2\psi\Delta_o}{\theta+\psi} + \Delta_{b4} \qquad (34)$$

Relative extension $\Delta_1 = \Delta y_1 - \Delta y_2$

$$\boxed{\Delta_1 = s_3(\psi - \theta) + \Delta_o + \Delta_{b4} - \Delta_{b3}} \qquad (34)'$$

Reviewing CASE A:

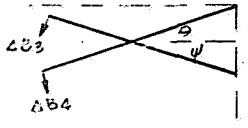

$$\mathcal{R} = \frac{2s_1 + 2s_3 + \Delta_{b3}\psi + \Delta_{b4}\theta}{\frac{\ell}{2}(\theta + \psi)} \qquad (32)$$

$$\Delta y_2 = \frac{4s_1}{\theta+\psi} + \frac{\Delta_o(\psi - \theta)}{\theta+\psi} + \Delta_{b3} - s_3\psi \qquad (33)$$

$$\Delta_1 = s_3(\psi - \theta) + \Delta_o + \Delta_{b4} - \Delta_{b3} \qquad (34)$$

If we interchange θ and ψ : CASE B:

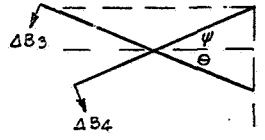

$$\mathcal{R} = \frac{2s_1 + 2s_3 + \Delta_{b3}\theta + \Delta_{b4}\psi}{\frac{\ell}{2}(\theta + \psi)} \qquad (32)$$

$$\Delta y_2 = \frac{4s_1}{\theta+\psi} - s_3\theta + \frac{\Delta_o(\theta - \psi)}{\theta + \psi} + \Delta_{b3} \qquad (33)$$

$$\Delta_1 = s_3(\theta - \psi) + \Delta_o + \Delta_{b4} - \Delta_{b3} \qquad (34)$$

We see from equations (32), (33), and (34) that the dependent quantities depend (in addition to geometry) on the beam bending deflections Δ_{b3} and Δ_{b4}; the tensile displacements s_1 and s_3 and the initial downward deflection Δ_o. Therefore, we must start calculating deflections at the right end of structure as shown in Fig. 1, where Δ_o for the first element is zero. The rotations $\mathcal{R}$ of an element results in a downward deflection at the end of $\mathcal{R}\bar{\ell}$ where $\bar{\ell}$ is the distance from the left end of the element to the left end of the entire structure. The total deflection of the left end is the sum

of the deflections $\mathcal{R}\bar{\ell}$ for each element plus Δy_2, the downward deflection of each element. Then, for panel and scissor 1:

$$\mathcal{R} = \frac{2s_1 + 2s_3 + \Delta_{b3}\psi + \Delta_{b4}\theta}{\frac{\ell}{2}(\theta+\psi)}$$

$$= \frac{[46 + 36 + 260 + 12{,}000] \times 10^{-5}}{50(0.523)} = 0.00475 \qquad (35)$$

We see that the rotation due to s_1 and s_3 is negligible compared to $\Delta_{b4}\theta$; $\Delta_{b4}\psi$ is relatively small.

$$\Delta y_2 = \frac{4s_1}{\theta+\psi} - s_3\psi + \frac{\Delta_o(\psi-\theta)}{(\theta+\psi)} + \Delta_{b3}$$

All contributions to the above expression are neglible except Δ_{b3}. Hence $\Delta y_2 \simeq \Delta_{b3}$. Then the contribution to deflection of the left end of structure is

$$\Delta_{end_1} = \mathcal{R}_1\bar{\ell}_1 + (\Delta y_2)_1 = (0.00475)(350) + .0365 = 1.70" \qquad (36)$$

Also, we need $\Delta_1 = s_3(\psi-\theta) + \Delta_o + \Delta_{b4} - \Delta_{b3}$

$$\Delta_1 \simeq \Delta_{b4} - \Delta_{b3} = 0.268 - 0.037 = 0.231 \qquad (37)$$

Δ_1 is used as the deflection Δ_o in the calculation for the next panel.

Proceeding in the same way, we have

$$\Delta_{end\ 2} = \mathcal{R}_2\bar{\ell}_2 + (\Delta y_2) = (0.00349(250) + 0.370 = 1.24" \qquad (38)$$

$$(\Delta_1)_2 \simeq \Delta_{b4} - \Delta_{b3} + \Delta_o = 0.057" \qquad (39)$$

$$(\Delta_{end})_3 = \mathcal{R}_3\bar{\ell}_3 + (\Delta y_2)_3 + (0.00232)(150) - 0.023 = 0.325 \qquad (40)$$

$$(\Delta_1)_3 = 0.173 \qquad (41)$$

$$(\Delta_{end})_4 = \mathcal{R}_4\bar{\ell}_4 + (\Delta y_2)_4 = (0.0016)(50) + 0.17 = 0.25 \qquad (42)$$

$$(\Delta_1)_4 = 0.02 \qquad (43)$$

For the fifth section, from equation (29)'

$$\Delta y \simeq \frac{\Delta_{o5}\psi}{\theta+\psi} = .003 \qquad (44)$$

Adding equations (36), (38), (40), (42), and (44): the total deflection at the left end is 3.50". This means that for a single scissor arm the stiffness

$$k = 0.3\#/in. \tag{45}$$

5. CALCULATION OF NATURAL FREQUENCY

Using equation (10) for the equivalent mass, and solving equation (7), we obtain

$$f = \frac{1}{2\pi}\sqrt{\frac{2 \times 386k}{0.242\ m}} \tag{46}$$

here:

k - is the stiffness of a single scissor arm in #/in..

m - is the mass of structure in #.

Then $f = \frac{1}{2\pi}(1.26) = 0.20$ (47)

if m = 600# and k = 0.3 #/in. Or one cycle occurs in 5 secs.

6. TRANSIENT ANALYSIS

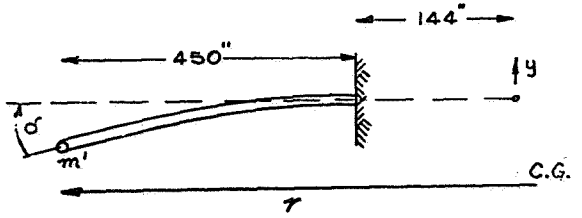

If the vehicle moves, the equation of motion , (7), becomes:

$$m'a + k\delta = 0 \tag{48}$$

Here a is the acceleration of m' in the y direction and δ is the deflection.

If the vehicle is subjected to an acceleration $\bar{a}$ in the y direction:

$$\text{then } a = \bar{a} + \ddot{\delta} \tag{49}$$

Equation (48) becomes:

$$m'\ddot{\delta} + k\delta = -m'\bar{a} \tag{50}$$

If $\bar{a}$ is constant for an interval of time t_o:

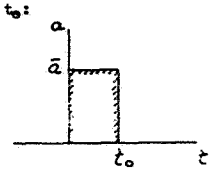

and if the initial conditions are

$$\dot{\delta}_o = \delta_o = 0$$

then:

$$\delta = -\frac{\bar{a}}{\omega^2}(\cos \omega t - 1) \qquad t < t_o \tag{51}$$

$$\delta = \frac{\bar{a}}{\omega^2}[\sin \omega t_o \sin \omega t + (\cos \omega t_o - 1)\cos \omega t] \qquad t > t_o \tag{52}$$

here $\omega^2 = \frac{k}{m'}$.

We notice, that for expression (51), the maximum deflection occurs in one half of a cycle.

$$|\delta_{max}| = \left(\frac{2\bar{a}}{\omega^2}\right) \tag{53}$$

6.1 Step Angular Acceleration - (6 Gyros)

If the vehicle is subjected to a step angular acceleration, then $\bar{a} = r\alpha$, where r is the distance from the centre of gravity; and α is the angular acceleration in radians/sec.^{2}. Here r = 450" + 144". If $\alpha = 1^\circ \sim 1/57.3$ radian/sec^2, then equation (53) yields; for $\omega = 1.26$ rad/sec

$$\delta_{max} = \frac{2(600)}{(57.3)(1.6)} = \underline{13.1}\ \text{in.} \tag{54}$$

This assumes that the load stays on for 2.5 secs.

6.2 Docking Load

If the vehicle is subjected to a docking load $\bar{a} = 0.1g = 38.4$ in/sec^2,

Then equation (53) yields:

$$\delta_{max} = \frac{2(38.4)}{1.6} = 48 \text{ in.} \tag{55}$$

This assumes that the load stays on for a half-cycle or 2.5 secs.

6.3 Step Angular Velocity - (Thrusters)

A step angular velocity may be taken into account by solving equation (43) with the initial conditions:

$$\dot{\delta}_o = r\Omega; \ \delta_o = 0$$

Here Ω is the step angular velocity. The solution becomes:

$$\delta = \sqrt{\frac{m}{k}}\ \dot{\delta}_o \sin\sqrt{\frac{k}{m}}t \tag{56}$$

The maximum deflection is

$$\delta_{max} = \sqrt{\frac{m}{k}}\ \dot{\delta}_o = \sqrt{\frac{m}{k}}\ r\Omega$$

if $\sqrt{\frac{m}{k}} = \frac{1}{\omega} = \frac{1}{1.26}$

$$\delta_{max} = r\frac{\Omega}{\omega} = (600)\frac{(7.5)}{(57)(1.26)} = 62.5" \tag{57}$$

here $\Omega = 7.5/57$ radians/sec. The maximum deflection occurs after 1/4 of a cycle or in this case after 1.25 secs.

7. TORSION OF PANELS

We will follow a procedure similar to that used for beam bending.

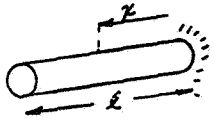

Consider a rod of uniform circular cross-section. Let $\phi(x,t)$ define the rotation of a cross-section. Then the torque T, at any cross-section is given by:

$$T = I_p G \frac{\partial \phi}{\partial x} \tag{58}$$

Here I_p is the polar moment of inertia and G is the torsional rigidity. For a statically applied torque T_e at the free end, we have

$$T_e = \frac{I_p G}{\ell}\ \phi_e = k_T \phi_e \tag{59}$$

Here k_T is the "total" stiffness and ϕ_e is the "total" twist. The equation of motion for the continuous rod is:

$$\phi_{xx} = \frac{1}{c^2}\phi_{tt} \tag{60}$$

Here $c^2 = \frac{k_T \ell}{\rho I_p}$

ρ [mass/ volume]

A solution of equation (60) is:

$$\phi = \phi_o \sin \omega t \sin \frac{\omega x}{c} \tag{61}$$

where $\omega = \frac{\pi}{2}\frac{c}{\ell}$

Equation (61) corresponds to the first mode vibration. If we consider an equivalent system to consist of a single disk at the end, having mass moment of inertia I_{eg} then the equation becomes:

$$I_{eg}\ddot{\phi} + k_T \phi = 0 \tag{62}$$

as before we make the requirement that the natural frequency is the same as that for the continuous system

$$\frac{\pi}{2}\frac{c}{\ell} = \sqrt{\frac{k_T}{I_{eq}}} \tag{63}$$

Solving

$$I_{eq} = \frac{4}{\pi^2} I \tag{64}$$

here I is the total mass moment of inertia of the rod.

To get an idea of the accuracy of this model, we compare the torque at the base.

Torque $= I_p G \phi_x$

$T_{exact} = [\phi_o \frac{\pi}{2}\frac{1}{\ell}\cos\frac{\pi}{2}\frac{x}{\ell} \sin \omega t]\, k_T \ell$

$$T_{exact} = \left[\phi_o \frac{\pi}{2} k_T \cos\frac{\pi}{2}\ x \sin \omega t\ \right]_{x=0}$$

$$T_{approx} = \phi_o k_T \sin \omega t$$

Then:

$$\frac{T_{approx}}{T_{exact}} = \frac{2}{\pi} = 0.636 \qquad (65)$$

This approach will at least give us an idea of the approximate response in torsion. We will consider the panels themselves to have no torsional rigidity. All torsional loads are carried in the scissor arms. From Fig. 5, for a rotation of the end given by ϕ_o;

$$\text{torque} = 2 \times \frac{K}{2} k \delta = k \frac{K^2}{2} \phi_o$$

Then the equation of motion becomes:

$$\ddot{\phi}_o I_{eq} + \frac{kK^2}{2}\phi_o = 0 \qquad (66)$$

But $I_{eq} = \frac{4}{\pi^2} I = \frac{4}{\pi^2}\frac{1}{12} MK^2 = \frac{M}{3\pi^2} K^2$

$$\frac{MK^2}{3\pi^2}\ddot{\phi}_o + \frac{kK^2}{2}\phi_o = 0$$

$$\ddot{\phi}_o + \frac{k}{M}\frac{3\pi^2}{2}\phi_o = 0 \qquad (67)$$

The application of a step angular velocity Ω, yields the solution

$$\phi_o = \frac{\Omega}{\sqrt{\frac{k}{M}\frac{3\pi^2}{2}}} \sin \sqrt{\frac{k}{M}\frac{3\pi^2}{2}}\ t \qquad (68)$$

the deflection: $\delta = \frac{K}{2}\phi$

Its maximum value occurs in 1/4 cycle. If $\Omega = 7\frac{1}{2}/57$ rad/sec, k = 0.3#/in; $M = 600/386\ \frac{\#\text{-sec}^2}{\text{in}}$

$$\phi_o = \frac{7.5}{(57)(1.69)} = 0.078 \text{ rad.} \quad \delta_{max} = (50)(.078) = \underline{3.9"} \qquad (69)$$

The above analysis for transient response should give a good approximate idea of the maximum values of deflection encountered.

REFERENCES

1. Tong: Theory of Mechanical Vibration, Wiley

2. W. T. Thomson, "Mechanical Vibrations," Prentice-Hall

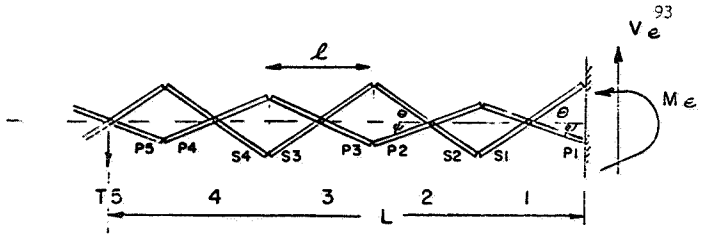

FIGURE 1.

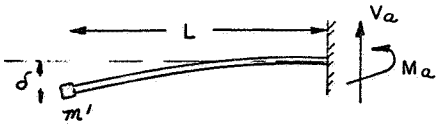

FIGURE 2.

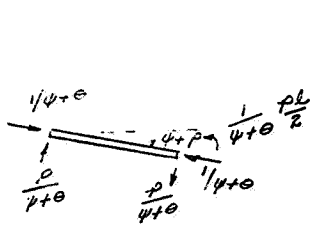

PANEL 5

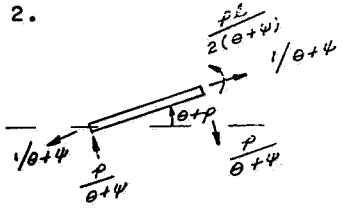

SCISSOR 5

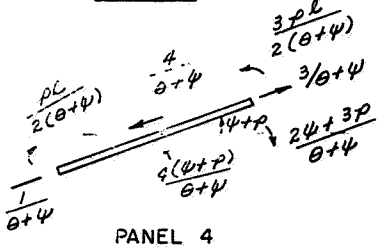

PANEL 4

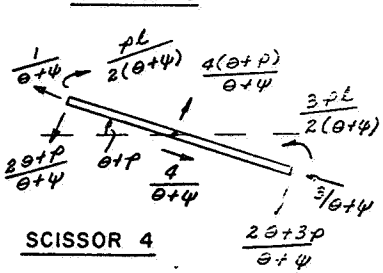

SCISSOR 4

FIGURE 3.

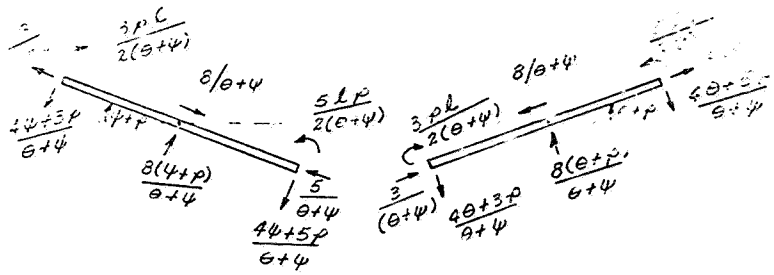

PANEL 3

SCISSOR 3

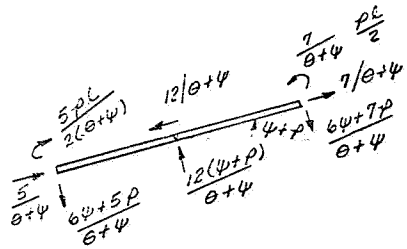

PANEL 2

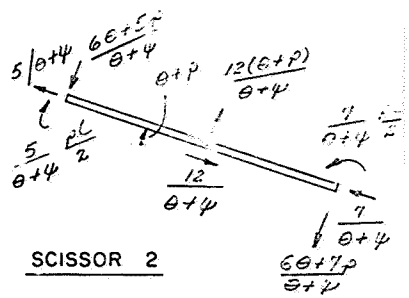

SCISSOR 2

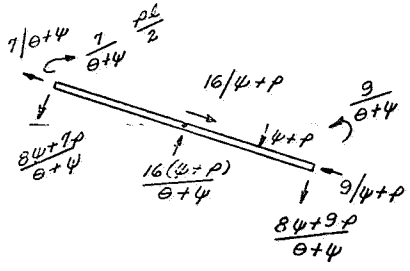

PANEL 1

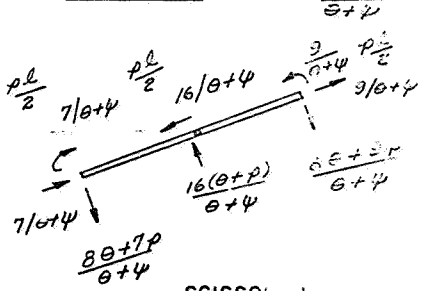

SCISSOR 1

FIGURE 3. (CONTINUED)

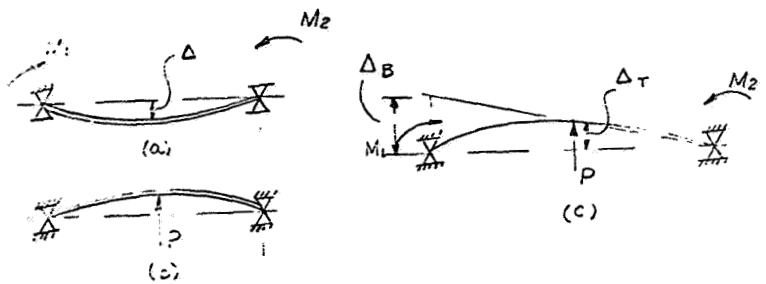

FIGURE 4.

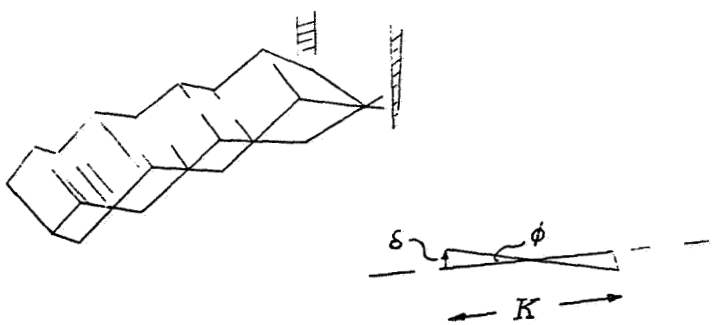

FIGURE 5.

Chapter IV

TEMPERATURE CONTROL OF EXPERIMENTS

1. Examination of Models of Operation for the G.S.F.C. X-Ray Telescope

During the early stages of this contract an attempt was made to determine possible modes of operation for the x-ray telescope consistent with the optical constraints. Due to the extremely short wave length of the x-rays, and the fact that the telescope has a fixed focal length, the optical requirements were for a straight axis and a stable length. The requirement of a straight axis was related thermally to the circumferential temperature gradient which produces changes in the curvature of the axis of the telescope. Similarly, the axial temperature gradient was related to changes in the length of the telescope.

A preliminary thermal analysis performed by Sperry Space Support Division indicates that the circumferential temperature gradients are negligible as a result of the telescope's thick walls and high thermal conductivity. In the absence of a circumferential temperature gradient, the axial temperature gradient became the significant thermal design factor. Thus, a one-dimensional thermal model was introduced for a gross analysis of the behavior of the telescope.

The one-dimensional model consisted of a rod as shown below,

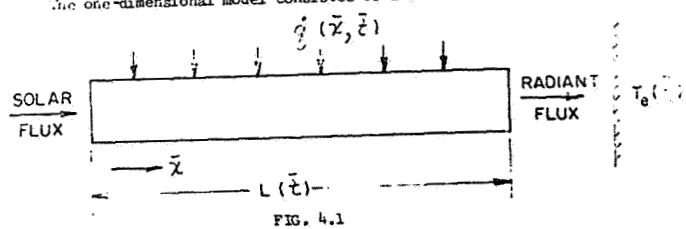

FIG. 4.1

where the energy input, $\dot{q}(\bar{x},\bar{t})$, which might be associated with a heater blanket was treated as internal generation. In this case, the heat conduction equation reduced to

$$\frac{\partial T}{\partial \bar{t}} = \alpha \frac{\partial^2 T}{\partial \bar{x}^2} + \frac{\dot{q}(\bar{x},\bar{t})}{\rho c} \tag{4-1}$$

with the appropriate boundary conditions

$$\frac{\partial T(o,\bar{t})}{\partial \bar{x}} = -\frac{q(o,\bar{t})}{kA}$$

$$\frac{\partial T(L,\bar{t})}{\partial \bar{x}} = \frac{B}{kA}\left(T^4(L,\bar{t}) - T^4(\bar{t})\right) \tag{4-2}$$

$$T(\bar{x},o) = T_o$$

Before an analysis of the thermal model was made, the overall operating criteria was examined by considering the thermal strains induced in a one-dimensional, unrestrained rod.

The thermal strain, ϵ_x is given by

$$\epsilon_x = \alpha_T[T(\bar{x},\bar{t}) - T_o] \tag{4-3}$$

Since the strain is the gradient of the displacement, u, then

$$\epsilon_x = \frac{\partial u}{\partial \bar{x}} = \alpha_T[T(\bar{x},\bar{t}) - T_o] \tag{4-4}$$

Thus, the displacement of a point from its position when $T = T_o$, is given by integrating (assuming the $\bar{x}$ coordinate to move with the end of the rod corresponding to $\bar{x} = 0$).

$$\int_o^{u(\bar{x},\bar{t})} \frac{\partial u(\bar{\xi},\bar{t})}{\partial \bar{\xi}}\, d\bar{\xi} = \int_o^{\bar{x}} \alpha_T[T(\bar{\xi},\bar{t}) - T_o]d\bar{\xi}$$

or

$$u(\bar{x},\bar{t}) = \int_o^{\bar{x}} \alpha_T[T(\bar{\xi},\bar{t}) - T_o]d\bar{\xi} \,. \tag{4-5}$$

If the integration is extended to the end of the rod

$$u(L,\bar{t}) = \int_o^{L} \alpha_T[T(\bar{\xi},\bar{t}) - T_o]d\bar{\xi} \,.$$

Now the displacement of the end of the rod may be given by its length, ie.

$$u(L,\bar{t}) = L(\bar{t}) - L(o)$$

thus

$$L(\bar{t}) = L(o) + \int_o^{L(\bar{t})} \alpha_T\, T(\bar{\xi},\bar{t})d\bar{\xi} - \int_o^{L(\bar{t})} \alpha_T\, T_o d\bar{\xi}$$

or

$$L(\bar{t}) = \frac{1}{1 + \bar{\alpha}_T T_o}\left\{L(o) + \int_o^{L(\bar{t})} \alpha_T\, T(\bar{\xi},\bar{t})d\bar{\xi}\right\} \tag{4-6}$$

where $\bar{\alpha}_T$ is the average coefficient of thermal expansion.

For the case under consideration, the change in $L(\bar{t})$ must be very small, thus

$$L(\bar{t}) \simeq L(o)$$

hence

$$\int_o^{L(o)} \alpha_T\, T(\bar{\xi},\bar{t})d\bar{\xi} = \alpha_T L(o) T_o \tag{4-7}$$

Although an infinite number of distributions might satisfy this relationship for variable properties, in its simplest form these results state that small displacements of the end require the average temperature of the rod to be constant.

With the above results in mind, several possible modes of operation were considered. Three of these were:

1. Insulate housing and radiate from the camera end.
2. Insulate housing and radiate from support.
3. Insulate housing and radiate from support and camera end simultaneously.

Here as before, a gross analysis was performed, which began by evaluating the overall conductance of the cylinder from one end to the other

$$K_1 = \frac{kA}{L} = 1.17 \quad \frac{Btu}{hr^\circ F} \qquad (4\text{-}8)$$

and the conductance for the support ring considering heat supplied to the ring on one side and removed from the other side,

$$K_2 = 2 \frac{Btu}{hr^\circ F} \qquad (4\text{-}9)$$

The area of the telescope which must be left uninsulated in order to dissipate the expected solar flux of four watts was computed as a function of the environment temperature based upon a telescope temperature of 70°F, and as shown below:

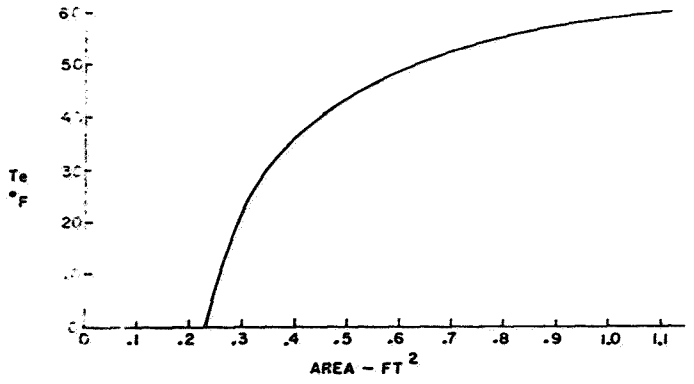

FIG. 4-2

Based upon the above facts, the following conclusions were reached for the possible heater configurations:

1. Insulate the telescope except for a small section at the camera end.
   a. This would produce an axially symmetric temperature field

and thus minimize circumferential temperature gradients. This would result only in an elongation. The circumferential gradients, which produce bending, would occur at the end and thus would be minimized.

   b. This would permit operation with or without heating.
      i. If no heat were rejected during operation, the average temperature would increase by approximately 1/4° per orbit due to the 4 watt influx. This mode of operation would require shutters.
      ii. If a steady state throughput of 4 watts were maintained during operation, the telescope would experience an approximate axial temperature gradient of 6 to 10°F. In addition the orbital variation of the solar flux and the canister temperature would require a variation in the heating rate.
   c. The number of heaters, control, and distribution of heat would necessitate the knowledge of permissible variations which may be tolerated from an optical standpoint.

2. Insulate the telescope except for a small section at the support.
   a. The operation would be similar to case 1.
   b. In this case, care must be exercised to insure the circumferential gradients occur in the support and not in the telescope. The support could be designed to carry a moment produced by thermal stresses within the permissible range of deflections. If the gradients occurred in the telescope at this point, they would produce the maximum deflection due to the cantilevering of the telescope.

c. This mode of operation would reduce the thermal gradient, from one end of the telescope to the other end, to approximately one-half of the value produced in case one. This resulted from the distribution of the 4 watts as absorbed at various points.

3. Insulate the telescope except for small sections at the camera end and at the support.

a. The operation would be similar to case 1.

b. In this mode, since the heat rejected at each section would be reduced, the circumferential gradients would also be reduced, compared with the two previous cases.

Even though each mode has some merit, it seems that mode one would be the most practical, since the only requirements to be placed upon the thermal control system are that it produce minimal circumferential gradients and that it maintain a constant average temperature during operation. In the event a steady state operation is decided upon, the long time lag between a change in the boundary condition at one end and its effect at the other end of the telescope, which is the order of 1.75 hours, must be considered.

2. Comparison of Circumferential Temperature Gradients in Experiment Packages

An analysis which compared experimental packages of square and circular cross-sections for circumferential temperature gradients was performed. The basic geometries which were considered are as shown below:

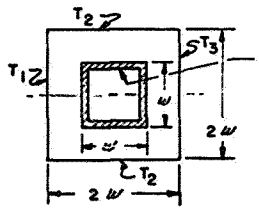

FIG. 4-3

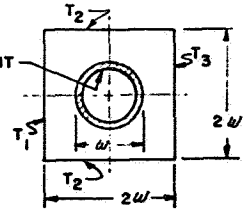

FIG. 4-4

In both cases each surface was assumed black and the surfaces 1, 2, and 3 were assumed to be isothermal. Thus, as a result of symmetry, the experiment package wall temperature distribution became a one-dimensional heat transfer problem. Since only a comparison showing the effect of geometry was desired, these simplifications were not deemed serious.

For the development of the appropriate equation, consider an element of the experiment package wall as shown below:

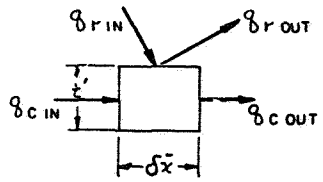

FIG. 4-5

For a unit depth into the page,

$$q_{c_{in}} = -k\,t' \left(\frac{\partial T}{\partial \bar{x}}\right)_{\bar{x}=\bar{x}}$$

and considering T to be expanded in a Taylor series, then

$$q_{c_{out}} = -k\,t' \left[\left(\frac{\partial T}{\partial \bar{x}}\right)_{\bar{x}=\bar{x}} + \left(\frac{\partial^2 T}{\partial \bar{x}^2}\right)_{\bar{x}=\bar{x}} \delta\bar{x}\right]$$

thus

$$\left(q_{c_{net}}\right)_{in} = q_{c_{in}} - q_{c_{out}} = k\,t'\,\delta\bar{x}\,\frac{\partial^2 T}{\partial \bar{x}^2}. \qquad (4\text{-}10)$$

For the thermal radiation,

$$q_{r_{in}} = \alpha_r G\,\delta\bar{x} = (1-\rho)G\,\delta\bar{x}$$

where G is the irradiation, and

$$q_{r_{out}} = \epsilon \sigma \delta \bar{x} \, T^4$$

thus
$$\left(q_{r_{net}}\right)_{in} = q_{r_{in}} - q_{r_{out}} = [(1-\rho)G - \epsilon\sigma T^4]\delta\bar{x} \qquad (4\text{-}11)$$

For steady state operation,

$$\left(q_{c_{net}}\right)_{in} + \left(q_{r_{net}}\right)_{in} = 0$$

thus
$$\frac{d^2T}{d\bar{x}^2} = \frac{\sigma}{kt'}\left[\epsilon T^4 - \frac{(1-\rho)}{\sigma} G\right] \qquad (4\text{-}12)$$

If only black surfaces are considered, then

$$\rho = 0$$

$$\epsilon = 1$$

and
$$G = \sum_{j=1}^{3} \sigma T_j^4 F_{\delta\bar{x}-A_j} = \sigma(T_1^4 F_{\delta\bar{x}-1} + T_2^4 F_{\delta\bar{x}-2} + T_3^4 F_{\delta\bar{x}-3}) \qquad (4\text{-}13)$$

Then after taking a limit as $\delta x \to 0$

$$\frac{d^2T}{d\bar{x}^2} = \frac{\sigma}{kt'}\left[T^4 - T_1^4 F_{d\bar{x}-1} - T_2^4 F_{d\bar{x}-2} - T_3^4 F_{d\bar{x}-3}\right] \qquad (4\text{-}14)$$

where $\bar{x}$ is the distance measured along the conduction path from the point of symmetry facing surface one. The resulting boundary conditions become

$$\text{at } \bar{x} = 0, \ \frac{dT}{d\bar{x}} = 0 \quad \text{and} \quad \text{at } \bar{x} = L, \ \frac{dT}{d\bar{x}} = 0 \qquad (4\text{-}15)$$

where L is the total length of the conduction path.

The solution may be simplified if the non-dimensional variables

$$V = \frac{T}{T_1}$$
$$x = \frac{\bar{x}}{L} \qquad (4\text{-}16)$$

and

$$N_c = \frac{\sigma T_1^3 L}{kt'}$$

are introduced. The resulting equation is

$$\frac{d^2V}{dx^2} = N_c[V^4 - F_{dx-1} - V_2^4 F_{dx-2} - V_3^4 F_{dx-3}] \qquad (4\text{-}17)$$

with the boundary conditions

$$\text{at } x = 0, \ \frac{dV}{dx} = 0 \quad \text{and} \quad \text{at } x = 1, \ \frac{dV}{dx} = 0. \qquad (4\text{-}18)$$

The solution may then be found in a number of ways once the configuration factors are known.

The configuration factors were determined by utilizing the well-known configuration factor between two infinite strips on elongated surfaces

$$dF_{dA_i - dA_j} = \tfrac{1}{2} \, d(\sin \beta) \qquad (4\text{-}19)$$

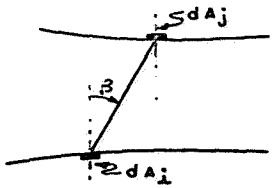

FIG. 4-6

which may be integrated to cover a finite surface A_j. This resulted in

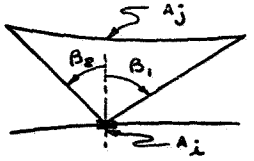

FIG. 4.7

$$F_{dA_i - A_j} = \int_{-\beta_1}^{\beta_2} \tfrac{1}{2}\, d(\text{Sin } \beta) = \tfrac{1}{2}[\text{Sin } \beta_2 - \text{Sin } (-\beta_1)]$$

but

$$\text{Sin } (-\beta_1) = -\text{Sin } (\beta_1)$$

therefore

$$F_{dA_i - A_j} = \tfrac{1}{2}[\text{Sin } \beta_2 + \text{Sin } \beta_1] \qquad (4\text{-}20)$$

The above results were used, with the following coordinates, to obtain the configurations needed in this problem.

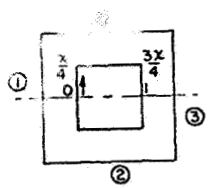

FIG.4-8

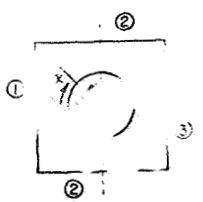

FIG. 4-9

The following results were obtained for the configuration factors:

1. SQUARE CROSS-SECTION

Let $\phi_1 = \dfrac{2a}{\sqrt{16a^2+1}}$ and $\phi_2 = \dfrac{2b}{\sqrt{16b^2+1}}$ (4-21)

then for $0 \leq x \leq \frac{1}{4}$

$$F_{dx-1} = \phi_1 + \phi_2, \quad F_{dx-2} = 1 - \phi_1 - \phi_2, \quad F_{dx-3} = 0, \qquad (4\text{-}22)$$

$a = \dfrac{x - \frac{1}{4}}{2}$, and $b = \dfrac{\frac{1}{4} - x}{2}$

For $\frac{1}{4} \leq x \leq \frac{3}{4}$

$$F_{dx-1} = \tfrac{1}{2} - \phi_1, \quad F_{dx-2} = \phi_1 + \phi_2, \quad F_{dx-3} = \tfrac{1}{2} - \phi_2, \qquad (4\text{-}23)$$

$a = x$, and $b = 1 - x$

For $\frac{3}{4} \leq x \leq 1$

$$F_{dx-1} = 0, \quad F_{dx-2} = 1 - \phi_1 - \phi_2, \quad F_{dx-3} = \phi_1 + \phi_2, \qquad (4\text{-}24)$$

$a = \dfrac{2x-1}{2}$, and $b = \dfrac{2-2x}{2}$

2. CIRCULAR CROSS-SECTION

Let $\phi_1 = \dfrac{2\sqrt{2}\,\text{Sin}(Y - \frac{\pi}{4})}{\sqrt{9-4\sqrt{2}\,\text{Cos}(Y - \frac{\pi}{4})}}$ $\phi_2 = \dfrac{2\sqrt{2}\,\text{Cos}(Y - \frac{\pi}{4})}{\sqrt{9-4\sqrt{2}\,\text{Sin}(Y - \frac{\pi}{4})}}$ (4-25)

where $Y = \pi x$ is in radians, then

for $0 \leq Y < 0.423$

$$F_{dx-1} = \tfrac{1}{2}(\phi_2 - \phi_1), \quad F_{dx-2} = 1 - \tfrac{1}{2}(\phi_2 + \phi_1), \text{ and } F_{dx-3} = 0 \qquad (4\text{-}26)$$

For $0.423 \leq Y < 1.145$

$$F_{dx-1} = \tfrac{1}{2}(1 - \phi_1), \quad F_{dx-2} = \tfrac{1}{2}(1 + \phi_1), \text{ and } F_{dx-3} = 0. \qquad (4\text{-}27)$$

For $1.145 \leq Y < 1.995$

$$F_{dx-1} = \tfrac{1}{2}(1 - \phi_1), \quad F_{dx-2} = \tfrac{1}{2}(1 - \phi_2), \text{ and } F_{dx-3} = \tfrac{1}{2}(\phi_1 + \phi_2). \qquad (4\text{-}28)$$

For $1.995 \leq Y < 2.715$

$$F_{dx-1} = 0, \quad F_{dx-2} = \tfrac{1}{2}(1 + \phi_2), \text{ and } F_{dx-3} = \tfrac{1}{2}(1 - \phi_2). \qquad (4\text{-}29)$$

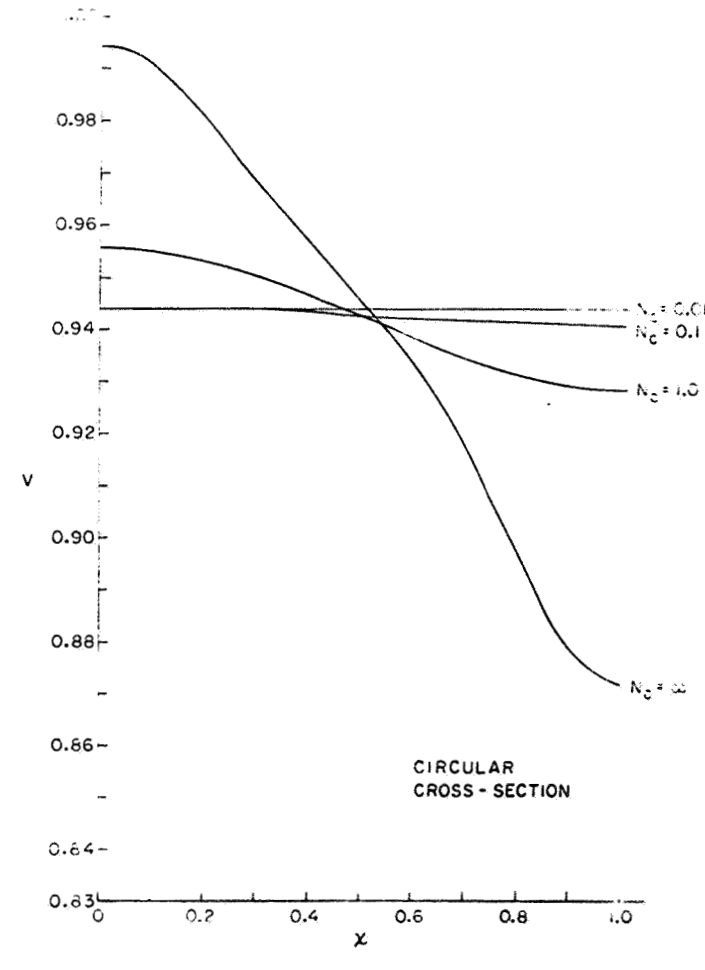
0.98
0.96
0.94
0.92
0.90
0.88
0.86
0.64
0.83
V
0
0.2
0.4
0.6
0.8
1.0
X
N_c = 0.01
N_c = 0.1
N_c = 1.0
N_c = ∞
CIRCULAR
CROSS - SECTION

FIGURE 4.10

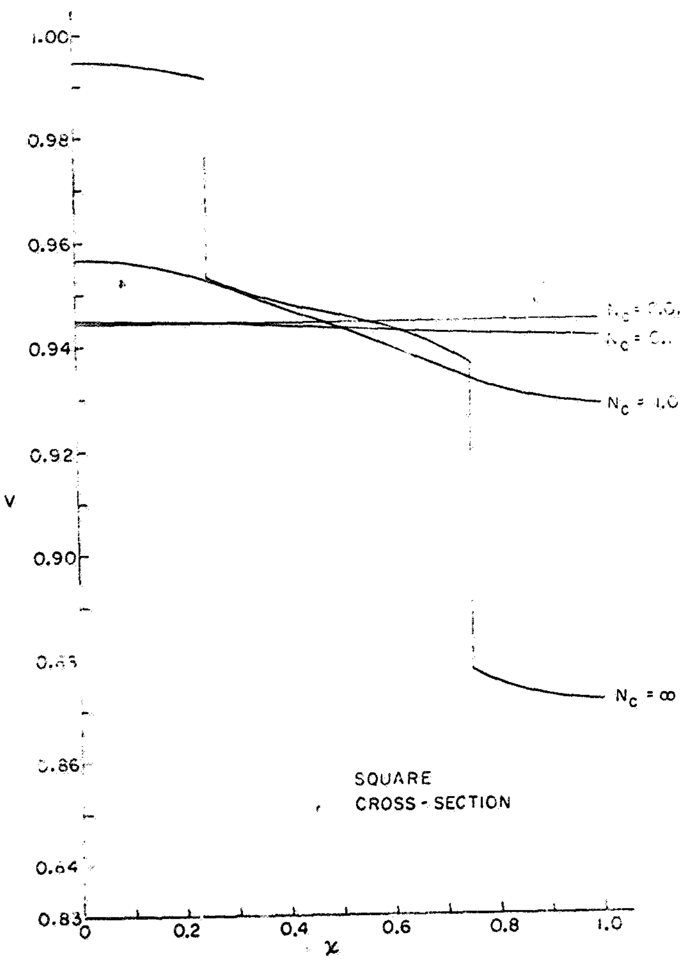

FIGURE 4.11

[illegible] given by

$$\frac{\partial T}{\partial \bar{x}} = \frac{1}{L}\frac{\partial T}{\partial x} \qquad (4-[illegible])$$

[illegible] for a square $\qquad L = 2w \qquad (4-[illegible])$

and for a circle $\qquad L = [illegible]$

thus for the same dimensionless [illegible] $\frac{\partial T}{\partial \bar{x}}$, then

$$\left.\frac{\partial T}{\partial x}\right)_{square} = [illegible] \left.\frac{\partial T}{\partial x}\right)_{circle} \qquad (4-[illegible])$$

[illegible]

The [illegible]dimensional thermal model was chosen to be the same as that shown in Fig. [illegible] with the following [illegible]:

1. [illegible]

2. The $\bar{x}$ coordinate system was taken to be measured from [illegible] (this was a mathematical simplification).

The appropriate heat conduction equation and boundary conditions were:

$$\frac{\partial T}{\partial \bar{t}} = \alpha \frac{\partial^2 T}{\partial \bar{x}^2} + \frac{\overset{o}{q}(\bar{x},\bar{t})}{\rho c} \qquad (4-[illegible])$$

B.C.

$$\frac{\partial T(o,\bar{t})}{\partial \bar{x}} = \frac{\sigma \mathscr{P}}{kA}[T^4(o,\bar{t}) - T_e^4(\bar{t})]$$

$$\frac{\partial T(L,\bar{t})}{\partial \bar{x}} = \frac{q(L,\bar{t})}{kA} \qquad (4-[illegible])$$

$$T(\bar{x},o) = T_o$$

The mathematical solution to the thermal model was simplified by introducing the following dimensionless variables:

$$V = \frac{T}{T_o} \quad x = \frac{\bar{x}}{L} \quad t = \frac{\alpha \bar{t}}{L^2} \qquad (4-[illegible])$$

$$\frac{q(\bar{x},\bar{t})L^2}{kT_o} \quad Q = \frac{q(L,\bar{t})L}{kA\,T_o} \quad N = \frac{\sigma T_o^3 L \mathscr{P}}{k}$$

Then the differential equation becomes

$$\frac{\partial V}{\partial t} = \frac{\partial^2 V}{\partial x^2} + F(x,t) \tag{4-37}$$

with the boundary conditions

$$\begin{aligned} V(x,0) &= 1 \\ V_x(0,t) &= R(V^1(0,t) - V_c^h(t)) = J(t) \\ V_x(1,t) &= G(t) \end{aligned} \tag{4-38}$$

where $J(t)$ was introduced for convenience.

When a Laplace transformation on t was applied to equation (4-37), it became

$$sv(x,s) - V(x,0) = V_{xx}(x,s) + F(x,s)$$

where the lower case symbols represent the Laplace transform with respect to t of the upper case variable.

Introducing $V(x,0) = 1$, the transformed equation became

$$V_{xx}(x,s) - sv(x,s) = -1 - F(x,s) \tag{4-39}$$

and the transformed boundary conditions were

$$\begin{aligned} V_x(0,s) &= J(s) \\ V_x(1,s) &= G(s) \end{aligned} \tag{4-40}$$

Next a Finite Fourier Cosine transform was applied where

$$\mathcal{F}_c\{V_{xx}\} = -n^2\pi^2\bar{V}(n,s) - \{V_x(0,s) - V_x(1,s)\cos n\pi\}$$

or

$$\mathcal{F}_c\{V_{xx}\} = -n^2\pi^2\bar{V}(n,s) - J(s) + G(s)\cos n\pi$$

where

$$\bar{V}(n,s) = \mathcal{F}_c\{v\}$$

also

$$\mathcal{F}_c\{1\} = \left\{ \int_0^1 (1)\cos n\pi\xi\, d\xi \right\} = \begin{cases} 1 & \text{if } n = 0 \\ 0 & \text{if } n \neq 0 \end{cases}$$

and

$$\mathcal{F}_c\{F(x,s)\} = \int_0^1 F(\xi,s)\cos n\pi\xi\, d\xi$$

Thus, equation (4-39) became

$$\bar{V}_{(n,s)} = \frac{1}{s+n^2\pi^2}\left\{-J(s) + G(s)\cos n\pi + \int_0^1 (1)\cos n\pi\xi\, d\xi + \int_0^1 F(\xi,s)\cos n\pi\xi\, d\xi\right\} \tag{4-41}$$

Now the inverse of the Finite Fourier Cosine Transform is given by

$$v(x,s) = \bar{V}(0,s) + 2\sum_{n=1}^{\infty}\bar{V}(n,s)\cos n\pi x \tag{4-42}$$

thus

$$v(x,s) = \frac{1}{s}\left[-J(s) + G(s) + \int_0^1 F(\xi,s)d\xi\right]$$

$$+ 2\sum_{n=1}^{\infty}\frac{\cos n\pi x}{s+n^2\pi^2}\left[-J(s) + G(s)\cos n\pi + \int_0^1 F(\xi,s)\cos n\pi\xi\, d\xi\right] \tag{4-43}$$

Next the inverse Laplace transform was applied which lead to

$$V(x,t) = 1 + \int_0^t\left[-J(u) + G(u) + \int_0^1 F(\xi,u)d\xi\right]du$$

$$+ 2\sum_{n=1}^{\infty}\cos n\pi x\left[\int_0^t\left\{\left[-J(u) + \cos n\pi\, G(u) + \int_0^1 F(\xi,u)\cos n\pi\xi\, d\xi\right]\right.\right.$$

$$\left.\left. e^{-n^2\pi^2(t-u)}\right\}du\right] \tag{4-44}$$

Regrouping terms (4-44) became

$$V(x,t) = 1 - \int_0^t\left\{1+2\sum_{n=1}^{\infty}e^{-n^2\pi^2(t-u)}\cos n\pi x\right\}J(u)\, du$$

$$+ \int_0^t\left\{1+2\sum_{n=1}^{\infty}e^{-n^2\pi^2(t-u)}\cos n\pi\cos n\pi x\right\}G(u)\, du$$

$$+ \int_0^1\int_0^t\left\{1+2\sum_{n=1}^{\infty}e^{-n^2\pi^2(t-u)}\cos n\pi x\cos n\pi\xi\right\}F(\xi,u)du\, d\xi \tag{4-45}$$

Next, use was made of the trigometric identies

$$\text{Cos } n\pi = (-1)^n$$

and

$$\text{Cos } (x \pm y) = \text{Cos } x \text{ Cos } y \mp \text{Sin } x \text{ Sin } y$$

which reduced (4-45) to

$$V(x,t) = 1 - \int_0^t \left[1+2\sum_{n=1}^{\infty} e^{-n^2\pi^2(t-u)} \text{Cos } n\pi x\right] J(u)\, du$$

$$+ \int_0^t \left[1+2\sum_{n=1}^{\infty} (-1)^n e^{-n^2\pi^2(t-u)} \text{Cos } n\pi x\right] G(u)\, du$$

$$+ \int_0^1 \int_0^t \left\{\left[1+2\sum_{n=1}^{\infty} e^{-n^2\pi^2(t-u)}\right]\left\{\text{Cos}[n\pi(x-\xi)] + \text{Cos}[n\pi(x+\xi)]\right\}\right\} F(\xi,u)\, du\, d\xi \quad (4\text{-}46)$$

Equation (4-46) was then simplified, symbolically at least, by the introduction of the definition of two of the Theta functions

$$\theta_3(\zeta,\tau) \equiv 1+2\sum_{n=1}^{\infty} e^{-n^2\pi^2\tau} \text{Cos } (2n\pi\zeta) \quad (4\text{-}47)$$

and

$$\theta_4(\zeta,\tau) \equiv 1+2\sum_{n=1}^{\infty} (-1)^n e^{-n^2\pi^2\tau} \text{Cos } (2n\pi\zeta). \quad (4\text{-}48)$$

An additional bit of notation, K, was introduced where

$$K(\eta,\zeta,\tau) \equiv \frac{1}{2}\left\{\theta_3\left(\frac{\eta+\zeta}{2}, \tau\right) + \theta_3\left(\frac{\eta-\zeta}{2}, \tau\right)\right\} \quad (4\text{-}49)$$

Finally equation (4-46) became

$$V(x,t) = 1 - \int_0^t \theta_3\left(\frac{x}{2}, t-u\right) J(u)\, du + \int_0^t \theta_4\left(\frac{x}{2}, t-u\right) G(u)\, du$$

$$+ \int_0^1 \int_0^t K(x,\xi,t-u)\, F(\xi,u)\, du\, d\xi \quad (4\text{-}50)$$

Due to the symmetry of the convolution integral, an equivalent form of equation (4-50) was obtained

$$V(x,t) = 1 - \int_0^t J(t-u)\theta_3\left(\frac{x}{2},u\right) du + \int_0^t G(t-u)\, \theta_4\left(\frac{x}{2}, u\right) du$$

$$+ \int_0^1 \int_0^t F(\xi,t-u)\, K(x,\xi,u)\, du\, d\xi \quad (4\text{-}51)$$

Since J(t) given by

$$J(t) = h\left[V^4(o,t) - V_c^4(t)\right]$$

involved $V^4(o,t)$ it was judged desirable to solve for V(o,t) first, such equations (4-50) and (4-51) become simple quadratures provided $V_c(t)$ and F(x,t) are prescribed functions. This was accomplished by substituting x = 0 into either equations (4-50) or (4-51). Utilizing the symmetry of

$$K(o,\xi,t) = \theta_3\left(\frac{\xi}{2}, t\right)$$

thus equations (4-50) and (4-51) were reduced to

$$V(o,t) = 1 - \int_0^t \theta_3(o,t-u)\, J(u)\, du + \int_0^t \theta_4(o,t-u) G(u)\, du$$

$$+ \int_0^t \int_0^1 \theta_3\left(\frac{\xi}{2}, t-u\right) F(\xi,u)\, d\xi\, du \quad (4\text{-}52)$$

Within the scope of this contract, F(x,t) was taken to be zero and the resulting solution did not incorporate the internal generation term. The resulting computer program could, however, be modified to include this effect.

The solutions and the resulting computer program was pursued based upon the following restrictions:

1. F(x,t) = 0
2. H = $-c_1$ (a constant)
3. $V_c^4(t) = c_2$ (a constant)
4. G(t) = c_3 (a constant)

[illegible] first restriction would require considerable modification of the existing computer program, but is well within the capability of the present analysis. The last three restrictions are such that minor program changes would allow the present computer program to adequately handle them.

The resulting equations which were solved are as follows:

$$V(o,t) = 1 + c_1 \int_o^t \theta_3(o,t-u)\{V^4(o,u) - c_2\}du + c_3 \int_o^t \theta_4(o,u)du \qquad (4-53)$$

and

$$V(x,t) = 1 + c_1 \int_o^t \theta_3(\tfrac{x}{2},t-u)\{V^4(o,u) - c_2\}du + c_3 \int_o^t \theta_4(\tfrac{x}{2},u)du \qquad (4-54)$$

Notice that (4-53) is a non-linear integral equation (in V(o,t)) of the Volterra type which is essentially an initial valued problem.

4. NUMERICAL SOLUTION

Equations (4-53) and (4-54) were then solved numerically utilizing a technique developed by Brannen and Raymond,* which enables one to obtain non-iterative solutions to a family of functional equations of the type

$$y(t) = Q(t;y) \qquad (4-55)$$

This works particularly well in a case such as equation (4-53) where Q(t;y) includes an integral of the Volterra type. Their method consist of constructing a polygonal approximation for the function y(t).

Before further discussion of the solution, detail consideration of some of the basic problems involved in the solution of equation (4-55) is beneficial. Consider the case where y(t) has been constructed from t = 0

* "Non-Iterative Solutions to Functional Equations," by J. P. Brannen and R. E. Raymond, accepted for publication in "Computing."

to $t = t_1 - \Delta t$ by a polygonal approximation as shown below.

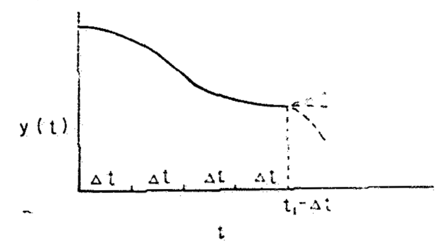

[illegible]

Now in order to find $y(t_1)$, a value of t_1 must be [illegible]. In addition, let z* represent the desired solution, thus

$$y(t_1) = z^* \quad [illegible]$$

The solution to the problem may be represented graphically as illustrated below

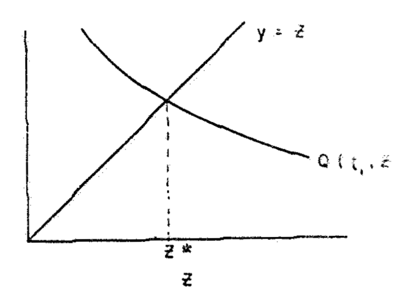

FIG. 4-1[illegible]

Where the two equations

$$y(t_1) = z \quad vs. \quad [illegible] \qquad (4-[illegible])$$

that

$$Q(t_1, z) \quad \text{vs.} \quad z \qquad (4\text{-}5)(4)$$

are plotted. The ordinate of these equations, z^*, represents the desired solution.

The fixed point, z^*, of the functional $q(t_1, z)$ may be sought in a number of ways. One of the most widely used methods known in the heat transfer literature is that of iteration. The iteration of $q(t_1, z)$ will not in general yield information concerning the location of z^*, however, it may, under certain conditions, converge to z^* when iteration is utilized. Consider the following example given by Isaacson and Haywood.

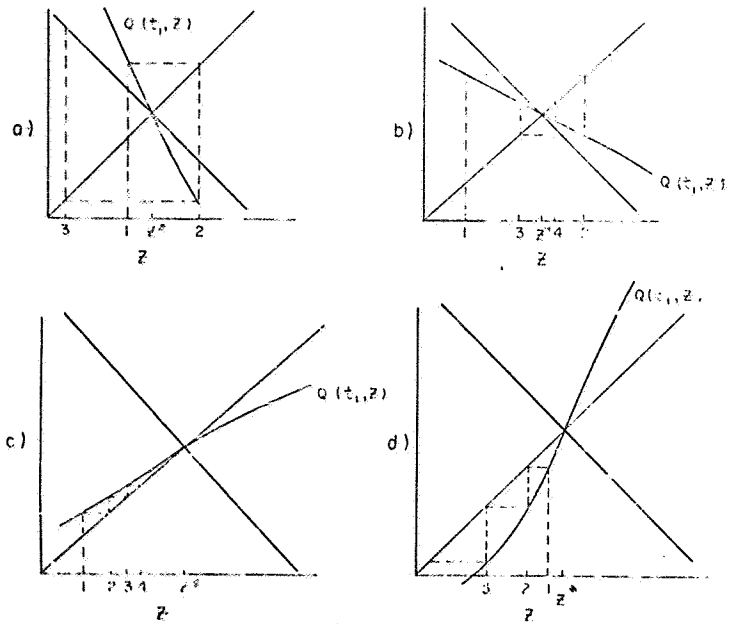

FIG. 4-5

Figure 4- [illegible] the [illegible] the first [illegible] of [illegible] curves (1) [illegible] possible [illegible] indication [illegible] these are the [illegible] the thing [illegible] the [illegible]

Returning [illegible] solution [illegible]

1. [illegible] and identify [illegible] increases. [illegible] of the solution is [illegible]

An initial [illegible] $(z_0 - q(t_1, z_0))$ is negative, [illegible] zero, then [illegible], is taken to

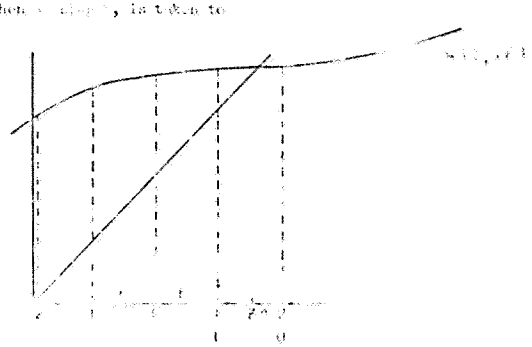

$z_1 = z_o \pm E$, the test

$$\left(\left(z_o - E\right) - Q\left(t_1, \left(z_o - E\right)\right)\right)$$

and

$$\left(\left(z_o + E\right) - Q\left(t_1, \left(z_o + E\right)\right)\right)$$

are then made and compared, if they have the same sign then another step, E, is taken and the test repeated, this process continues until the test yields two values of opposite sign. The solution is then bounded, the upper and lower bounds may be set, and the type of crossing identified.

2. Phase 2 consists of locating the fixed point z^* and is carried out by the portion of the program LOCATE, as shown in Fig. 4-16.

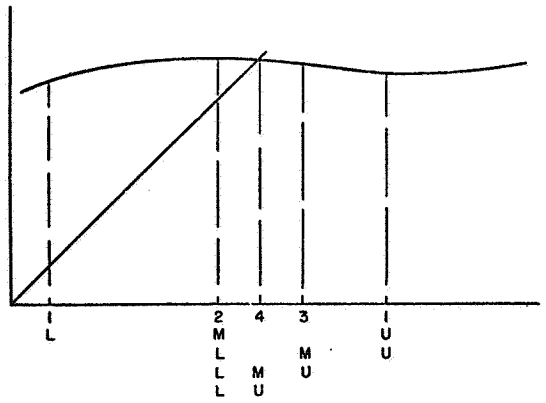

FIG. 4-16

The points 1 represent the upper and lower bounds as obtained from IDENT. The mid-point is then taken and the test

$$\left(z_\varepsilon - Q(t_1, z_2)\right)$$

is made and compared with test for points 1, and a new upper or lower bound is then established. The midpoint of z_1, z_2 is then z_3 and a new test is made to establish a new upper or lower bound. The bifurcation continues until the upper and lower bounds differ by some specified amount. The midpoint is then taken to be fixed point of $Q(t_1, z^*)$ and it is then possible to march forward by Δt and repeat the procedure.

One of the basic requirements for the application of the method of Brannen and Haymond was that $Q(t,y)$ be a computable functional. In this particular problem, $\theta_3(0,t)$ and $\theta_4(\frac{1}{2}, t)$ are undefined as t approaches zero, thus a modification of the basic method was required. This was solved by use of the periodicity of θ_3 and θ_4 along with a small time approximation of θ_3.

From equations (4.47) and (4-48) it may be readily seen that

$$\theta_3(\zeta, \tau) = \theta_4(\zeta + \tfrac{1}{2}, \tau)$$

Thus

$$\theta_3(0, t) = \theta_4(\tfrac{1}{2}, t) \qquad (4\text{-}58)$$

Equivalent forms of equations (4-47) and (4-48) may be written in terms of exponentials from which small time approximations are readily obtained. These equivalent equations are

$$\theta_3(\zeta, \tau) = \frac{1}{\sqrt{\pi\tau}} \sum_{n=-\infty}^{n=\infty} e^{-(\zeta+n)^2 1/\tau}$$

$$\theta_4(\zeta, \tau) = \frac{1}{\sqrt{\pi\tau}} \sum_{n=-\infty}^{n=\infty} e^{-(\zeta+n+\frac{1}{2})^2 1/\tau} \qquad (4\text{-}59)$$

The above forms were used in the computer program to generate θ_3 and θ_4

as well as to obtain a small time approximation for θ_3. Notice that $\theta_3(0,t)$ may be written as

$$\theta_3(0,t) = \frac{1}{\sqrt{\pi t}}\left\{1 + 2\sum_{n=1}^{\infty} e^{-\frac{n^2}{t}}\right\} \qquad (4\text{-}60)$$

and using the limit

$$\lim_{t\to 0} e^{-\frac{n^2}{t}} = \lim_{t\to 0} \frac{1}{e^{n^2/t}} = \frac{1}{e^{\infty}} = 0$$

Thus for small t, the approximation

$$\theta_3(0,t) \simeq \frac{1}{\sqrt{\pi t}} \qquad (4\text{-}61)$$

was utilized. This allowed for the representation of equation (4-53) by an approximate integral plus a polygon. This was accomplished as follows: Beginning with (4-53)

$$V(0,t) = 1 + C_1 \int_0^t \theta_3(0,t-u)\{V^4(0,u) - C_2\}du + C_3 \int_0^t \theta_4(0,u)du \qquad (4.62)$$

Assuming

1. $\theta_3(0,t) = \frac{1}{\sqrt{\pi t}}$ $\quad 0 \le t \le \epsilon$
2. $V(0,t) = V(0,t_1)$ $\quad t_1 - \epsilon \le t \le t_1$

where ϵ is a very small value of t. Then V(0,t) becomes

$$V(0,t) = 1 + C_1 \int_0^{t-\epsilon} \theta_3(0,t-u)\{V^4(0,u) - C_2\}du + C_1\{V^4(0,t) - C_2\} \int_{t-\epsilon}^{t} \frac{du}{\sqrt{\pi(t-u)}} + C_3 \int_0^t \theta_4(0,u)du \qquad (4\text{-}63)$$

Now

$$\int_{t-\epsilon}^{t} \frac{du}{\sqrt{\pi(t-u)}} = 2\sqrt{\frac{\epsilon}{\pi}} \qquad (4\text{-}64)$$

Thus

$$V(0,t) = 1 + 2C_1\{V^4(0,t) - C_2\}\sqrt{\frac{\epsilon}{\pi}} + C_1 \int_0^{t-\epsilon} \theta_3(0,t-u)\{V^3(0,u) - C_2\}du + C_3 \int_0^t \theta_4(0,u)du \qquad (4\text{-}65)$$

The last two terms were then represented by a trapezoidal rule as the simplest form of a polygon representation. The remainder of the solution then followed the procedure of Brannen and Haymond as previously described.

Once V(0,t) was known, equation (4-54) was thus reduced to a simple quadrature for all values of x less than one, however, when x equals one, $\theta_4(\frac{1}{2},t)$ displays a singularity at t equal zero, and thus a similar procedure to that outlined above was required. Equation (4-54) was then reduced to the following:

$$V(1,t) = 1 + 2C_3\sqrt{\frac{\epsilon}{\pi}} + C_3 \int_{\epsilon}^{t} \theta_4(\tfrac{1}{2},u)du + C_1 \int_0^t \theta_3(\tfrac{1}{2},t-u)\{V^4(0,u) - C_2\}du \qquad (4\text{-}66)$$

Here, as before, the last two terms were then represented by the trapezoidal rule representation of an integral.

NOMENCLATURE

A	Cross-sectional area
B	Proportionality factor for radiation transfer
C	Specific heat
E	Step size
F	$\frac{\overset{\circ}{q}(\bar{x},\bar{t})L^2}{k\,T_o}$ dimensionless heat generation
F_{dx-A_j}	Radiation shape factor from area dx to area A_j
$\mathcal{G}$	Overall exchange factor for non-black
H	$\frac{LT_o^3\,\sigma}{k}$ dimensionless radiation
G	Irradiation - incident radiant flux per unit area per unit time; also $\frac{q(L,\bar{t})L}{k\,A\,T_o}$ dimensionless solar flux
J	Radiosity - radiant flux leaving a surface per unit area per unit time; also $H(V^4(0,t) - V_e^4(t))$
k	Thermal conductivity
L	Length of rod or length of conduction path
N_c	$\frac{\sigma T_1^3 L^2}{k\,t^1}$ conduction parameter
q	Solar flux
$\overset{\circ}{q}$	Heat generation
t	$\frac{\alpha\bar{t}}{L^2}$ dimensionless time
$\bar{t}$	Time
t^1	Thickness of experiment package
T	Absolute temperature
T_e	Absolute temperature of environment
T_o	Initial absolute temperature
u	displacement of a point measured from its position at $T = T_o$
V	$\frac{T}{T_o}$ dimensionless temperature
x	$\frac{\bar{x}}{L}$ dimensionless length

$\bar{x}$	Axial coordinate
α	Thermal diffusivity
α_r	Absorbtivity
α_T	Coefficient of thermal expansion
$\bar{\alpha}_T$	Average coefficient of thermal expansion
ϵ	emissivity
ϵ_x	thermal strain in the $\bar{x}$ direction
ρ	mass density; reflectivity
σ	Stefan-Boltzmann constant